JOURNAL OF CAVE AND KARST STUDIES

June 2026
Volume 88, Number 1-2
ISSN 1090-6924
A Publication of the National Speleological Society

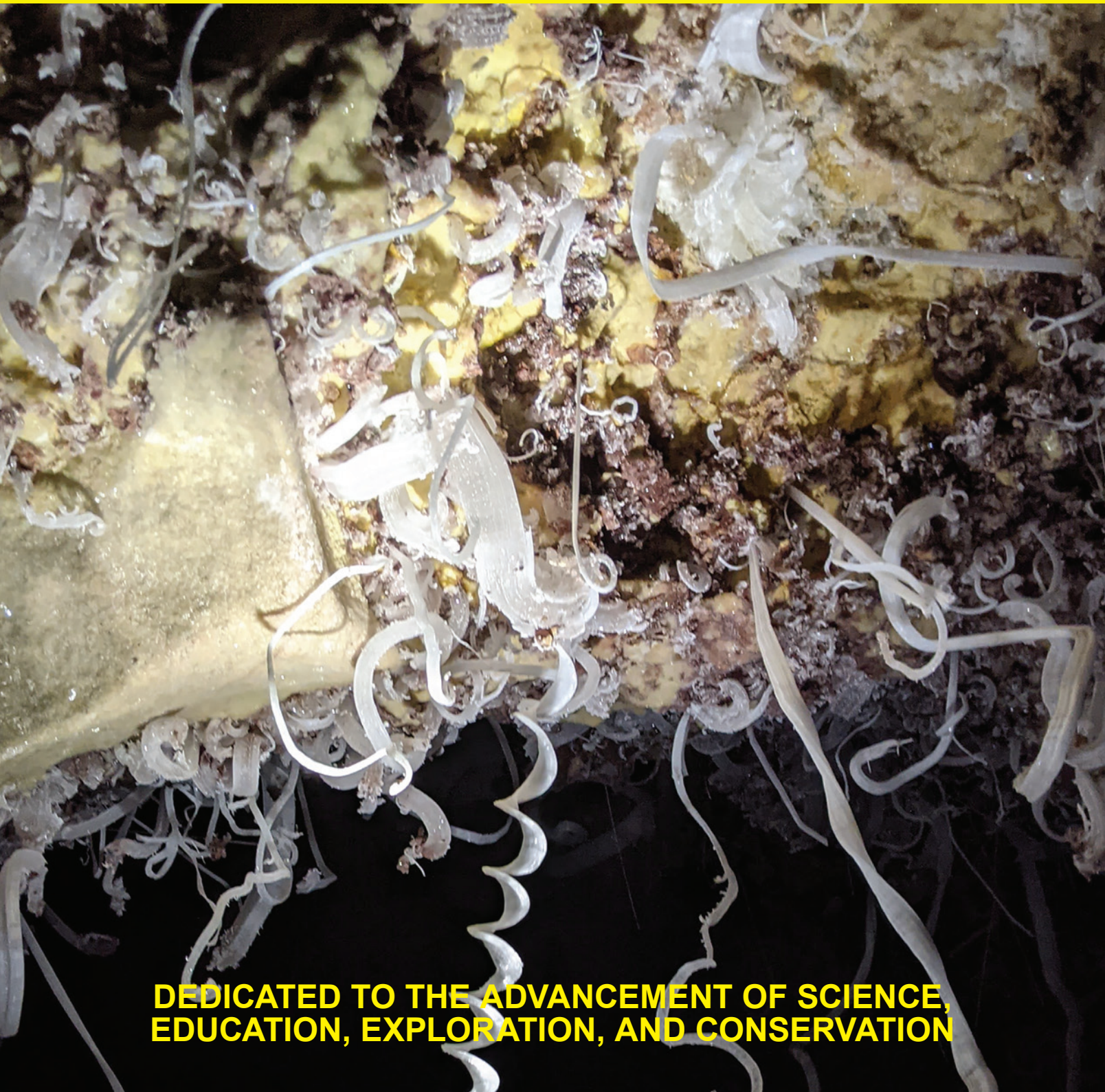

DEDICATED TO THE ADVANCEMENT OF SCIENCE, EDUCATION, EXPLORATION, AND CONSERVATION

Published By
The National Speleological Society

http://caves.org/pub/journal

Office
6001 Pulaski Pike NW
Huntsville, AL 35810 USA
Tel:256-852-1300
nss@caves.org

Editor-in-Chief
Malcolm S. Field
Washington, DC
703-347-8601
field.malcolm1@gmail.com

Production Editor
Scott A. Engel
Knoxville, TN
225-281-3914
sengel@caves.org

The *Journal of Cave and Karst Studies* , ISSN 1090-6924, CPM Number #40065056, is a multi-disciplinary, refereed journal published four times a year by the National Speleological Society. The *Journal* is available by open access on its website, or check the website for current print subscription rates. Back issues are available from the NSS office.

POSTMASTER: send address changes to the National Speleological Society Office listed above.

The Journal of Cave and Karst Studies is covered by the following ISI Thomson Services Science Citation Index Expanded, ISI Alerting Services, and Current Contents/Physical, Chemical, and Earth Sciences.

Front Cover: A corkscrew-shaped gypsum flower (approximately 25 cm long) extruding from a breccia layer in the Bopper Cave System. Photo by Sierra Heimel.

Sierra Heimel, Benjamin Tobin, and Georgina Lukoczki. Multi-phase hypogene speleogenesis: The Bopper Cave System, Grand Canyon, USA. *Journal of Cave and Karst Studies*, v. 88, nos. 1/2, p. 1-18. DOI: 10.4311/2025ES0114

MULTI-PHASE HYPOGENE SPELEOGENESIS: THE BOPPER CAVE SYSTEM, GRAND CANYON, USA

Sierra Heimel[1,2,C], Benjamin Tobin[2,3], and Georgina Lukoczki[2]

Abstract

The Bopper Cave System (BCS) in the Grand Canyon, USA, offers a unique case study in multi-phase hypogene speleogenesis. The BCS, discovered in 2006, presents distinct features differing from other hypogene caves regionally yet sharing similarities with sulfuric acid caves globally. We hypothesize that the formation of the BCS involves multiple hypogene fluids varying in origin, composition, and timing. Field observations and mineralogical analyses support this, revealing four stages of speleogenesis: dissolution of the network maze cave (likely by CO_2-rich waters), fluctuation in the water table and subsequent fluid chemistry change resulting in deposition of Fe–Mn oxides, lowering of the water table and subsequent speleogenetic (replacement) gypsum rind deposition and speleogen development (likely by SO_4-rich waters), and a transition to vadose conditions followed by secondary sulfate and carbonate deposition. These stages, driven by shifting hydrogeologic conditions, have resulted in the diverse morphology and mineralogy observed in the BCS. Our findings, when added to regional cave development models, suggest localized variability in speleogenetic processes driven by hypogene fluids that led to the formation of the BCS. This study underscores the complexity of hypogene speleogenesis and the need for more nuanced models to account for spatial and temporal variability in fluid chemistry.

INTRODUCTION

In the United States, the understanding of hypogene speleogenesis has grown as studies have begun applying the concept of speleogenesis to karst regions across diverse physiographic provinces (Hill, 1990; Palmer et al., 2016). As recognition of the widespread influence of hypogene processes on karst systems has evolved, the broader need to document hypogene fluid behaviors and complexities in karst literature has become more evident (DuChene et al., 2017; Gulley and Polk, 2017; Tennyson et al., 2017; Burgess, 2021; Hose et al., 2021).

While the dominant models in hypogene speleogenesis describe cave formation via fluids rich in sulfate (SO_4) (De Waele et al., 2024) or carbon dioxide (CO_2) (Spötl et al., 2016), these models often assume a single, stable fluid source throughout the cave-forming process. This simplification may overlook the dynamic and potentially variable nature of fluid contributions over time, including shifts in geochemical composition, tectonic processes, or hydrological connectivity. As a result, such models might not fully capture the complexity of subsurface environments, where fluids derived from different sources, each with distinct chemical signatures, can alternate or interact with bedrock in deep confined aquifers, influencing dissolution patterns and overprinting mineral deposits in more intricate ways than previously accounted for. Previous studies of Grand Canyon hypogene caves included smaller caves, which were likely dissected components of larger systems unknown at the time (Polyak et al., 2008). The Bopper Cave System (BCS) allows for the study of a large and more complete cave system.

This focus on a singular fluid origin overlooks the dynamic nature of fluid interactions across spatial and temporal scales, which has been well-documented in geologic research outside karst environments (e.g., Bucher and Stober, 2010; Pegler et al., 2014). Research has demonstrated that the spatial and temporal heterogeneity of speleogenetic fluids is intrinsically linked to regionally variable tectonic processes, highlighting how shifts in geological dynamics influence fluid migration and chemistry over time (Huntoon, 1996). Such variability, observed from diagenesis to present-day hydrological patterns, underscores the complexity inherent in cave development (Klimchouk et al., 2017) and challenges the assumption of uniform fluid sources in hypogene systems. Notably, research from the Colorado Plateau physiographic region has emphasized the complexity of tectonic evolution in the region and the interaction of multiple fluids with differing chemistries moving through confined aquifers and permeable strata over time (Wenrich and Sutphin, 1989; Huntoon, 1996; Crossey et al., 2006).

Despite significant advancements in the identification and interpretation of hypogene cave systems over the last half century, critical gaps remain in understanding the role of these varying fluid chemistries in cave development, especially as they relate to regionally variable tectonic processes. Only recently in the karst literature have spatially and temporally

[1]National Park Service, Oregon Caves National Monument and Preserve, 21000 Caves Hwy, Cave Junction, OR 97523
[2]Kentucky Geological Survey, University of Kentucky, 310 Columbia Ave., Lexington, KY 40506
[3]National Cave and Karst Research Institute, New Mexico Tech, Carlsbad, NM 88220
[C]Corresponding author: sierra_heimel@nps.gov.

heterogeneous fluids been considered to play a major role in speleogenesis (Columbu et al., 2021). This is particularly applicable within hypogene systems with polygenetic origins, inactive hypogene caves, or those obscured by secondary epigenetic features, which often complicate interpretations (Farrant and Harrison, 2017; Klimchouk et al., 2017; Spötl et al., 2017).

Previous hypogene speleogenesis models have suggested a relatively uniform speleogenetic framework dominated by CO_2-rich fluids for hypogenic karst in the Grand Canyon. Observations from the BCS, an inactive hypogene cave in the Grand Canyon, suggest that this model is incomplete. Using evidence from cave mineralogy and morphologic features, we assess the hypothesis that hypogene speleogenesis in the Grand Canyon reflects spatial and temporal heterogeneity in the origin and composition of hypogene fluids and processes.

STUDY SITE

The Grand Canyon of northwestern Arizona is located on the western edge of the Colorado Plateau physiographic region of the United States (Fig. 1), a tectonically active region characterized by thick continental crust (Karlstrom et al., 2022). The term hypogene speleogenesis was first applied to the phreatic caves in the Grand Canyon by Hill and Polyak (2010) and was also the first mention of hypogene speleogenesis on the Colorado Plateau. Huntoon (2000a) referred to these caves as artesian. The BCS was discovered in 2006 and was recognized as an inactive hypogene cave with unique minerals and cave formations that had never been described in hypogene caves before (Tobin et al., 2021).

Geologic Setting

The Grand Canyon showcases over 1.6 billion years of geological history, most of which is exposed by stratigraphic units from the lower Proterozoic Vishnu Basement Rocks to the upper Permian Kaibab Formation. Key stratigraphic units include the Cambrian Tapeats Sandstone and Bright Angel Shale, which represent the base of the Paleozoic section and indicate ancient marine environments. These are overlain by the regionally important carbonate sequence of the Redwall–Muav (RM) aquifer, comprising the Cambrian Muav Limestone, the Devonian Temple Butte Formation, and the Mississippian Redwall Limestone (Huntoon, 1974). The sedimentary units were deposited in shallow marine and fluvial environments, which laid the groundwork for fluid interactions influencing the formation of the region's extensive cave systems (Kent and Rawson, 1980). The stratigraphic units above the Redwall Limestone comprise a suite of sedimentary layers, representing a variety of marine and terrestrial environments deposited through the end of the Paleozoic era.

The tectonic evolution of the Colorado Plateau has dramatically influenced its geology and hydrology. The uplift of the Mogollon Highlands during the Triassic period redirected fluid pathways and altered the chemistry of infiltrating waters (Huntoon, 1996). Uplift during the Laramide Orogeny, approximately 60 million years ago, elevated the landscape and modified groundwater flow patterns. Uplift of the Colorado Plateau is debated and poorly constrained, but it is generally described as occurring in three phases since the Cretaceous, with rates increasing through time (Roberts et al., 2012). Incision rates of the Colorado River in the Grand Canyon are used to estimate uplift and indicate steady long-term incision that varies spatially from east to west, consistent with migrating mantle buoyancy and uplift from Neogene volcanism (Roberts et al., 2012; Crow et al., 2014).

Moreover, the volcanic history of the Grand Canyon region is marked by episodes of volcanic activity that have contributed to its geological complexity. Quaternary volcanic features, including composite lava dams, indicate recent volcanic processes occurring in the Grand Canyon region (Crow et al., 2008). Today, evidence of neotectonic activity and mantle-derived gases can be seen in the geochemical signatures of modern springs (Crossey et al., 2009). Breccia pipes, which are vertical, cylindrical features formed from the collapse of overlying sediments into the underlying Redwall Limestone, serve as crucial conduits for both hydrothermal fluids and groundwater and were likely mineralized by fluids that interacted with eroding volcanic and Precambrian crystalline rocks in the Triassic Mogollon highlands to the south (Wenrich and Sutphin, 1989).

The combined impact of tectonic uplift and volcanic activity has led to varied spatial and temporal fluid contributions within the Colorado Plateau. This interaction of diverse hydrochemical processes has resulted in a heterogeneous distribution of hypogene fluid contributions to the groundwater, which, in turn, plays a significant role in cave development. The variability in fluid sources and compositions, profoundly influenced by tectonic forces and volcanic activity, underscores the intricate relationships shaping the karst systems of the Grand Canyon.

Karst Development in the Grand Canyon

During the late Mississippian, a regionally widespread karst developed in the newly emergent Redwall Limestone (McKee and Gutschick, 1969; Beus, 1990). Since its formation, this karst has been infilled with sediments, breccias, and cements and is recognized today as a paleokarst system. The Redwall Limestone was reportedly buried to a maximum depth of 5 km (Karlstrom et al., 2014) approximately 250 million years ago and remained deeply buried from the end of the Paleozoic through the beginning of the Cenozoic (Sylvia, 1985). Fractures and faults from the Laramide Orogeny,

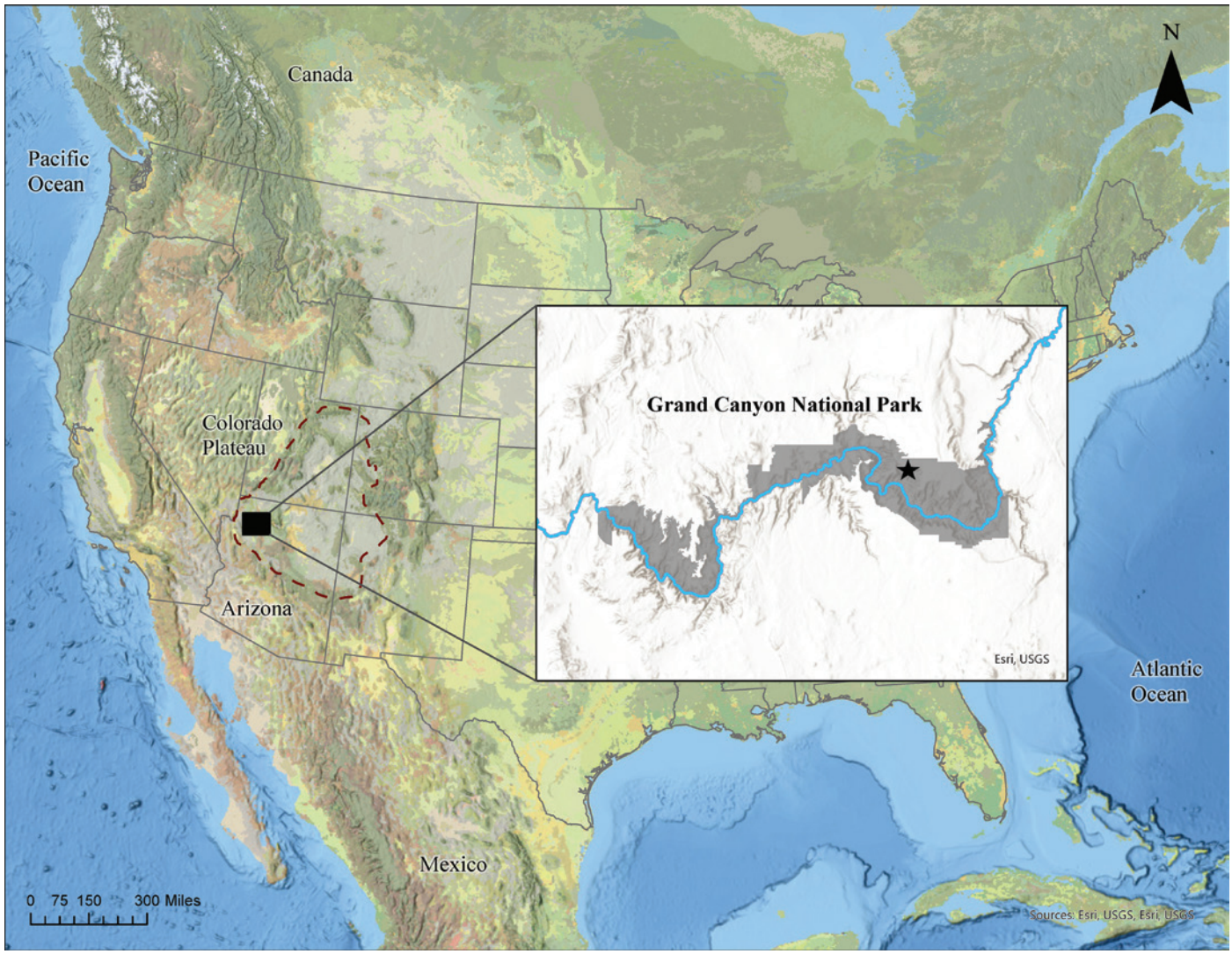

Figure 1. Location of the Bopper Cave System (star) and Grand Canyon National Park (dark gray) within the greater context of the Colorado Plateau, USA.

which uplifted the region approximately 60 million years ago to its current elevation, play a significant role in enhancing permeability within the RM aquifer, especially in the Redwall Limestone (Blakey and Ranney, 2008). Well before the establishment of the BCS, large-scale faults displaced the Redwall Limestone by hundreds of meters, creating zones of increased permeability and cavern development in areas of groundwater circulation (Huntoon, 1974). Recent studies highlight the importance of preferential dissolution of the dolomitic facies in the Mooney Falls Member of the Redwall Limestone, which leads to increased porosity, permeability, and large groundwater storage potential (Dohm, 2017; Heimel, 2019).

Today, an extensive karst system exists in the Redwall and Muav Limestones, with over 500 caves documented and 150 km of surveyed cave passage (Tobin et al., 2021). There are two distinct morphologies of caves in the Grand Canyon: confined (phreatic origin) and unconfined (vadose origin) caves (Huntoon, 2000b). Confined caves were formed in the phreatic zone, below the water table, and are generally found in the Mooney Falls member of the Redwall Limestone (Fig. 2) (McKee, 1963). Prior to the incision of the Grand Canyon and a related drop in the water table, these caves were fully saturated and developed into 2- and 3-dimensional maze caves with generally low hydraulic gradients (Palmer, 1975; Hill and Polyak, 2010) that tend to follow regional structural patterns (Heimel and Tobin, 2022). Unconfined caves have formed since the incision of the canyon and are fed by recharge from precipitation on the rims of the canyon (Jones, 2017). These caves are typically simpler in morphology with steeper hydraulic gradients than confined caves and are often associated with major springs in the canyon (Huntoon, 2000b). Both confined and unconfined systems are associated with regional faults (Tobin et al., 2021).

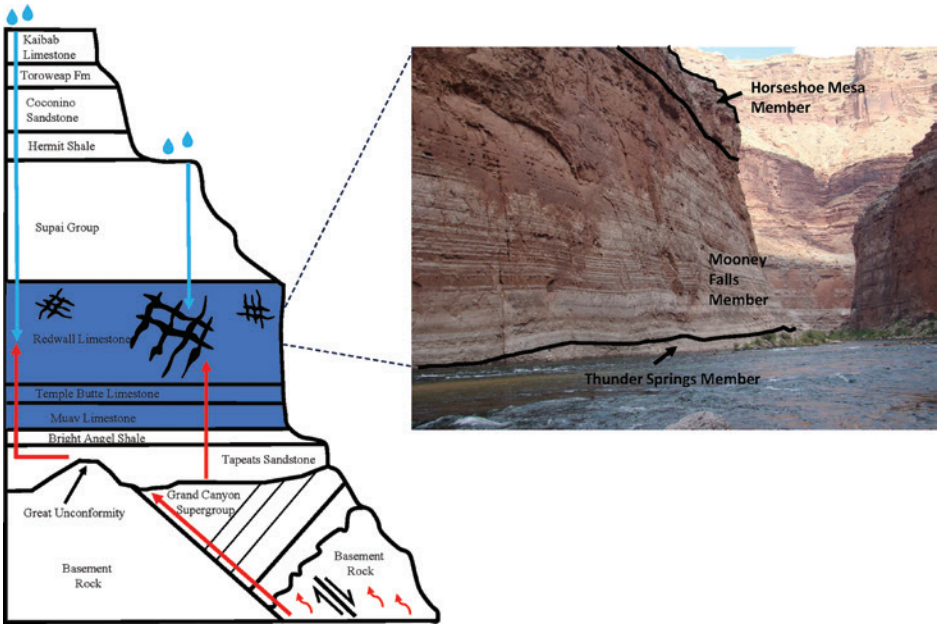

Figure 2. Stratigraphic and speleogenetic setting for cave development in the Redwall–Muav aquifer (shown in dark blue) of the Grand Canyon. Faults and fractures serve as conduits for fluid migration. Epigenic fluids (blue arrows) migrate downward from the rims of the Grand Canyon, and hypogenic fluids (red arrows) migrate upward from deep sources. The inset image is a photograph modified from Dohm (2017) showing the exposed members of the Redwall Limestone in the eastern Grand Canyon; from bottom to top: the Thunder Springs Member at river level, the dolomite-banded Mooney Falls Member, and the overlying Horseshoe Mesa Member. The Mooney Falls Member is approximately 96 m thick in this part of Grand Canyon.

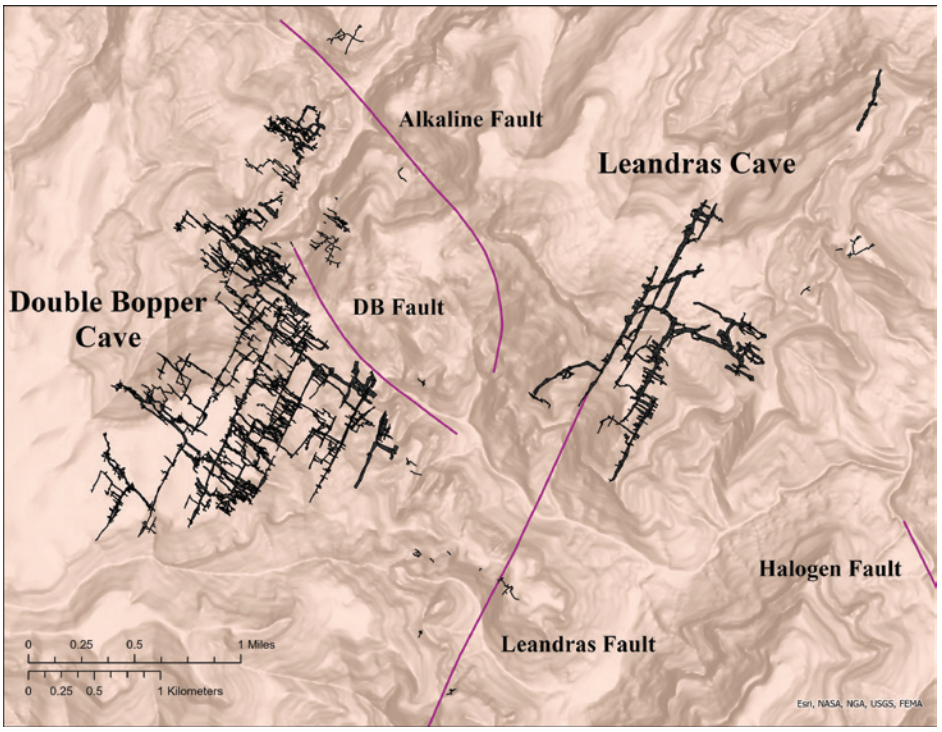

Figure 3. Map of the Bopper Cave System (BCS), including Double Bopper Cave and Leandras Cave along with many other smaller caves (names not shown) that comprise the BCS. Faults are shown in purple.

The Bopper Cave System

The BCS is located in a remote alcove in the upper reaches of the Redwall Limestone on the Kaibab Plateau. The BCS is composed of several distinct caves, including large caves such as Double Bopper and Leandras Caves in addition to many smaller caves (Fig. 3). These caves are crosscut and separated by major side canyons that indicate the caves were once connected before the incision of the Grand Canyon bisected the BCS. The primary cave of focus for this study is Double Bopper. With over 64 km (40 mi) of mapped passage, Double Bopper is the longest cave in the Grand Canyon and, as of 2026, the 13th longest cave in the United States.

The BCS is not associated with modern water flow and is a hypogene network maze cave with a high density of caves and large natural cave entrances (Tobin et al., 2021; Heimel and Tobin, 2022). Passages do not converge as tributaries but instead branch outward from fracture networks (Fig. 3). The network maze of passages in the BCS includes both spongework-type and rectilinear passages as defined by Palmer (1991). The BCS has a large horizontal extent, and the sizes of cave passages vary widely, ranging from tens of meters in diameter to passage widths impassable by humans. The largest passages in the BCS are in the Leandras portion of the BCS and along the trace of the Double Bopper Fault in Double Bopper Cave, with the largest passages having widths over 38 m and lengths of up to 1 km. The smallest passages in the BCS are located at the distal ends of Double Bopper Cave, with large passages narrowing to eventually become too tight for human exploration. Many of the large rooms are zones of breakdown and collapse, with less breakdown present in smaller passages.

The BCS displays no spatial relationship with surface topography on the Kaibab Plateau of the North Rim of the Grand Canyon but has important relationships with the local

fracture network and surrounding faults (Heimel and Tobin, 2022). The joint-controlled nature of the cave system is likely a result of tectonic forces and erosional unloading of overburden (Mandl, 2005; Klimchouk, 2009). Thus, the BCS has developed within a complex structural setting with well-developed fracture networks in the Redwall Limestone and four major documented faults proximal to the BCS: the Halogen, Alkaline, Leandras, and Double Bopper Faults (Fig. 3). The Halogen Fault is a high angle normal fault 15 km long with 6–24 m of offset (Billingsley and Hampton, 2000) located over a kilometer away from the BCS, the Leandras fault is a high angle normal fault 4 km long (Billingsley and Hampton, 2000) that intersects major passages of the BCS, the Double Bopper fault sits adjacent to terminating passages in the BCS, and the Alkaline Fault is located between the Leandras and Double Bopper Caves and sits adjacent to smaller caves in the BCS. Passage size statistically decreases with increasing distance from the Halogen and Leandras faults, suggesting their role as conduits for aggressive hypogene fluids that enhanced dissolution near the faults, while the inverse relationship with the Double Bopper fault suggests it acted as a barrier to speleogenetic fluids (Heimel and Tobin, 2022). These relationships, however, are complex, and additional controls such as fracture permeability and lithologic variability also influence passage size. Additionally, there are smaller faults expressed and documented more recently from within the BCS, such as the Green Door Fault (Heimel, 2022) (Fig. 4).

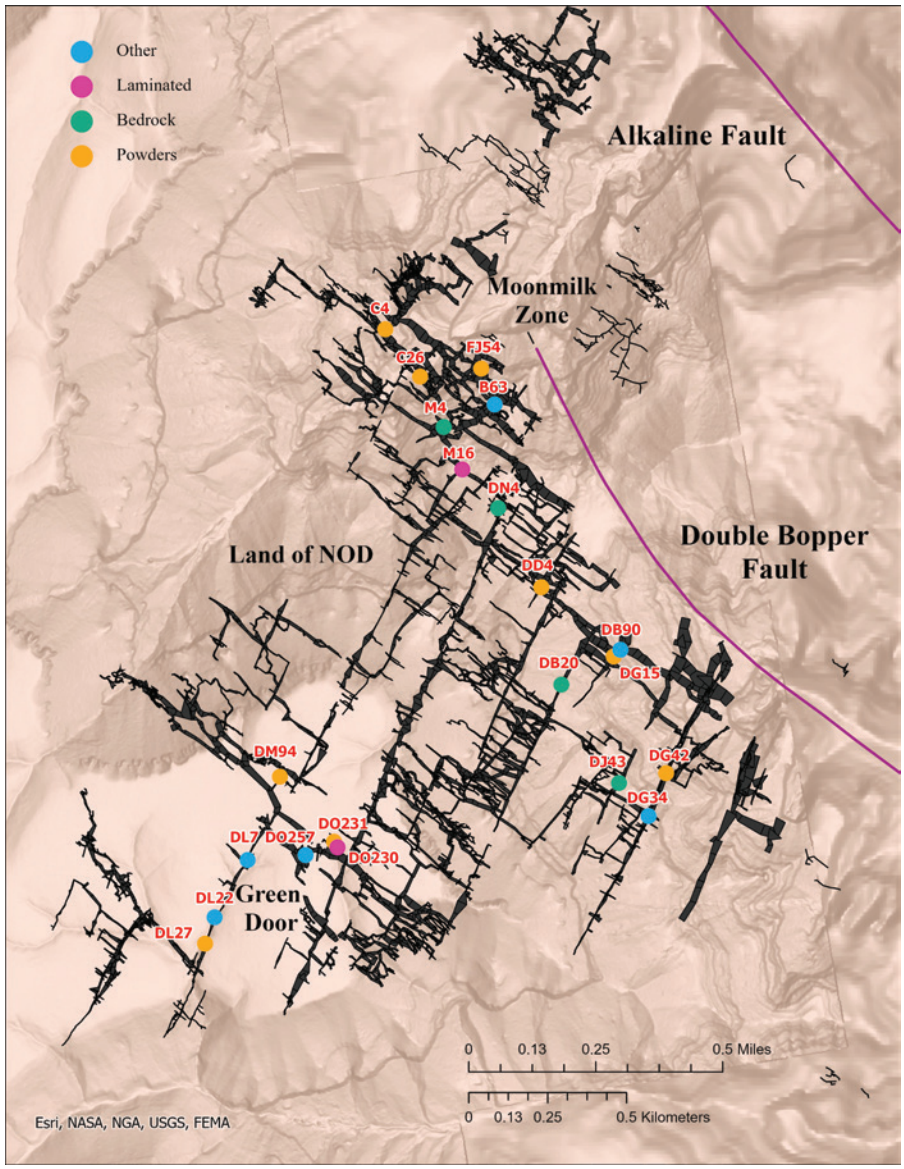

Figure 4. Sampling locations for X-ray diffraction analysis in the Double Bopper portion of the Bopper Cave System. The colored circles represent the types of samples analyzed: powdered deposits are orange, bedrock samples are green, laminated deposits are pink, and samples that do not fall into the preceding categories are labeled as "other" and are marked with blue. Three zones mentioned in the text include the Land of NOD, a.k.a Noxious Orange Dust, the Green Door (located at station DO257), and the Moonmilk Zone.

METHODS

Field Observations

We documented geologic field observations to describe the occurrence and types of cave morphologies, speleogens, sediments, secondary deposits, and cave-related structural features. Secondary deposits refer to speleothems and sediments formed after the initial dissolution of the cave system. For each identified feature, we recorded descriptive characteristics and spatial locations using a combination of notes and photographs. For spatial reference, we documented features' locations to the nearest cave survey station. We used photographs to document the scales of features, though some features were photographed occurring in the ceiling of the cave and have no scale.

Sample Collection

Our team spent 4 days underground from October 26 through 29, 2021, collecting 13 bedrock and 85 secondary deposit samples. The collection locations of secondary deposits, intended for broad spatial coverage within the cave, were determined by our travel routes. We selected previously unidentified mineral specimens based on documentation from previous cave resource inventory surveys conducted by citizen scientists. These notes detailed the colors and morphologies of unidentified minerals relative to specific cave survey stations. In our sampling approach, we focused on obtaining at least one specimen of each type of unidentified mineral. To minimize impact to the cave, mineral and speleothem samples were limited to those that had fallen to the cave floor whenever possible.

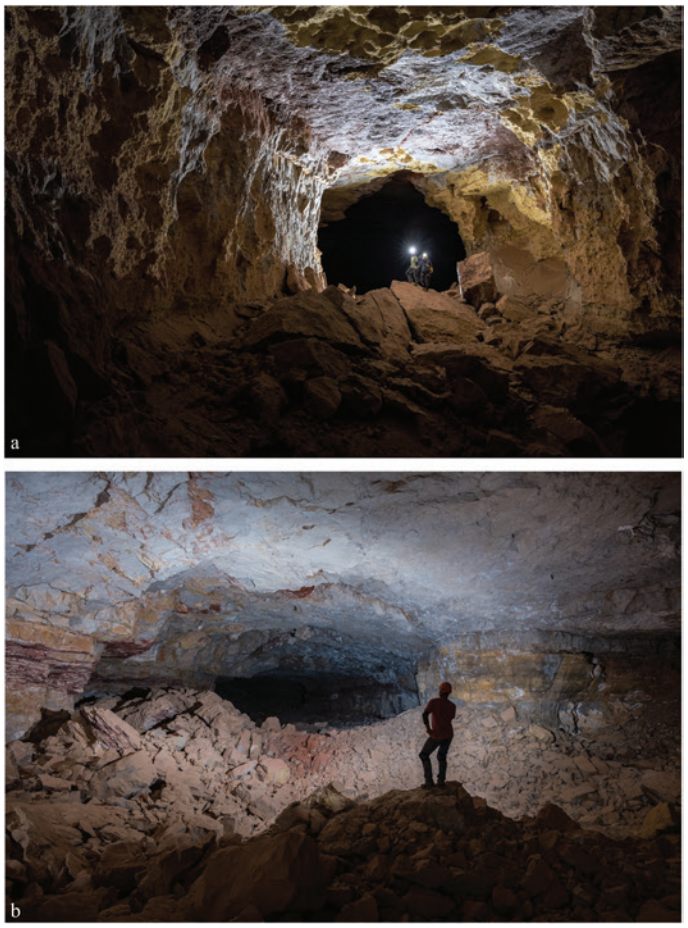

Figure 5. (a) Circular passage morphology with post-speleogenetic breakdown and collapse. Caver in the center of the photo for scale. Photo by Stephen Eginoire. (b) Lens-shaped morphology with post-speleogenetic breakdown and collapse. Prominent iron-red, stratiform, block-like breccia on the left side of the photo. The extent of the breakdown is unknown. Photo by James Hunter.

X-Ray Diffraction

Of the nearly 100 samples we collected, 22 were analyzed for mineral composition (Fig. 4) by powder X-ray diffraction (XRD) using a Bruker D8 DISCOVER equipped with a Bruker scintillation counter detector with CuKα radiation (X-ray tube operated at 40 kV and 40 mA) at the Kentucky Geological Survey, University of Kentucky. Data were collected in the angular range of 2°–70° 2θ with a 0.02° step size and <1 s counting time per step. We identified mineral phases using the Bruker DIFFRAC.EVA software version 5.2 with powder diffraction database version PDF 2-2021.

RESULTS

Morphology

The BCS exhibits a variety of phreatic morphologies, including large lens-shaped and circular passages (Fig. 5). Extensive post-speleogenetic breakdown and collapse are evident in large passages, obscuring the lower half of the cave passages. This may conceal rift-shaped floors, which are a common morphology associated with hypogene speleogenesis. Passages in the BCS are generally horizontal, with an average dip of 2° to the south, matching the regional dip of the Mooney Falls Member of the Redwall Limestone. Smaller cave passages and passages in close proximity to faults are irregular in shape. The vertical extent of the cave reaches 30 m due to one fissure passage in Double Bopper that breaches down into the Thunder Springs Member of the Redwall Limestone. This is the only reported occurrence of cave development in the chert-banded Thunder Springs Member in Grand Canyon. Morphologies typical of vadose caves, such as shafts, canyons, or dome and pit complexes, have not been documented in Double Bopper.

Speleogens

Speleogens found in the BCS consist of cupolas, air scallops, solution domes, pendants, ceiling half tubes, and acid pool basins with rillenkarren. Variously sized cupolas dot the ceiling and adjacent walls in many passages and do not follow visible fractures (Fig. 6). Air scallops are micro cupolas and are abundant in the BCS. Pendants are found in the BCS in many locations and are likely either breccia or other insoluble bedrock residues left behind after selective dissolution in the cave passage (Fig. 7). Ceiling half tubes are not as common as phreatic tubes in the BCS but are seen at several locations (Fig. 8). Solution domes are larger than cupolas and are found in the ceiling of many larger passages in the BCS, with some ceiling domes reaching over 15 m high (Fig. 9). Wall channels with rillenkarren are found in isolated locations and may represent relic acid pool basins with rillenkarren marking the top edge of a pool in the BCS. There are no speleogens typical of vadose caves documented in the BCS, such as solution scallops or anastomoses.

Secondary Deposits and Speleothems

Colorful secondary deposits are abundant throughout the cave and include a diverse range of speleothems and sediments. These deposits consist of various minerals, including sulfates, carbonates, Fe–Mn oxides, a phosphate mineral, and quartz (Table 1).

The largest passages in the cave are associated with the main entrance series near the Double Bopper Fault and are predominantly filled with buff-colored breakdown boulders. Stalagmites and stalactites have only been documented in the BCS proximal to this fault. Moving away from the Double Bopper Fault, passages become drier and coated in gypsum occurring as corkscrew-shaped “flowers,” “swords,” “chandeliers,” “grass,” and “hair” (Figs. 10–12, DG34 and DB90 in Table 1). In those areas of the BCS where the cave walls are not decorated with secondary deposits or

Figure 6. Extensive cupola and air scallop development on the "pocketed" cave walls in a fissure passage. Photo by Stephen Eginoire.

Figure 7. A large, isolated ceiling pendant speleogen impregnated with Fe–Mn oxides. Photo by James Hunter.

Figure 8. Ceiling half tube in a lens-shaped passage with gypsum flowers extruding from the walls and ceiling. Photo by Stephen Eginoire.

Figure 9. Vertical ceiling dome with cupola and air scallops outlining the dome. Photo by Stephen Eginoire.

speleothems, the bedrock is highly friable and bleached white with hues of orange and red (Fig. 14). Laterally continuous breccia layers are common in the BCS and consist of brecciated blocks of limestone embedded in yellow and red clays (Figs. 10 and 11). Gypsum also preferentially extrudes from some of these breccia layers, often highlighting alternating layers of the bedrock (Fig. 11).

Table 1. Description and mineralogy of samples analyzed by X-ray diffraction.

Sample ID	Sample Type	Sample Description	Minerals Identified
C4	Powder	Brown powder	Goethite—Fe(OH)O
C26	Powder	White powder	Hydromagnesite—$Mg_5(CO_3)_4(OH)_2{\cdot}4H_2O$
DM94	Powder	Orange powder	Hematite—Fe_2O_3
DO231	Powder	Black powder	Manganese oxide—Mn_2O_3
B63	Other	Green translucent coating around boxwork	Gypsum—$CaSO_4{\cdot}2H_2O$, brushite—$CaPO_3(OH){\cdot}2H_2O$
DL27-1	Powder	White powder	Thenardite—Na_2SO_4
DD4	Powder	Yellow powder	Jarosite—$KFe_3(SO_4)_2(OH)_6$, natrojarosite—$NaFe_3(SO_4)_2(OH)_6$
DL22-2	Other	Gypsum foam	Gypsum
DL7	Other	Flower on gypsum foam	Gypsum
DG34	Other	Yellow nodule	Gypsum, calcite—$CaCO_3$, epsomite—$MgSO_4{\cdot}7H_2O$
DG42-1	Powder	Yellow-brown powder	Quartz—SiO_2, gypsum
M4	Bedrock	Purple fine-grained laminated sedimentary rock	Quartz, hematite
DB90-2	Other	Gypsum foam and coating	Anhydrite—$CaSO_4$, quartz
DO257-1	Other	Green-blue botryoidal mineral	Malachite—$Cu_2CO_3(OH)_2$, calcite
DG15	Powder	Yellow powder	Gypsum, jarosite
DB20-3	Bedrock	Red bedrock limestone	Calcite, quartz
DO257	Other	Gypsum foam	Calcite, gypsum
FJ54	Powder	White powder	Epsomite, mirabilite—$Na_2SO_4{\cdot}10H_2O$
DJ43	Bedrock	Crystalized bedrock	Gypsum, dolomite—$CaMg(CO_3)_2$
DO230	Laminated	Brown-yellow powder	Goethite
M16-2	Laminated	Red powder	Hematite
DN4	Bedrock	Green fine-grained bedrock sedimentary rock	Dolomite, calcite

Throughout the cave there are also crusts, rinds, and powder deposits. Crusts occur as coatings up to a few centimeters thick around the rims on breakdown rocks, bedrock, and other secondary deposits. Crusts are typically white and were identified as gypsum and dolomite. Massive, somewhat botryoidal white rinds of 5–10 cm thickness coat the walls, floor, and ceiling in the BCS and were identified as gypsum (DB90-2, Table 1). A small but vibrant green-yellow crusty nodule was observed in one locality in the cave and was identified as epsomite (DG34, Table 1 and Fig. 12).

The sampled powders are fine-grained, porous, lightweight, varied in color, and found as piles or layers on the floor. Piles of white powder are common near gypsum speleothems in the BCS and were identified as thenardite, epsomite, and mirabilite (FJ54 and DL27-1, Table 1). Bright yellow piles of powder found coating a cluster of red breakdown blocks on the floor were identified as jarosite and natrojarosite (DD4, Table 1). The source of this deposit appears to be a 5 cm diameter mineralized zone in the ceiling. Another pile of yellow-brown powder was identified as quartz and gypsum (DG42-1, Table 1). One cave passage, designated as the Moonmilk Zone (Fig. 4), spans approximately 15 m in width and 40 m in length and was found to be blanketed with a 25–30 cm thick layer of white powder, identified as hydromagnesite (C26, Table 1). The source of this deposit appears to be an irregular fracture network of white mineralized veins in the ceiling directly above this passage.

The central portions of the BCS, furthest from entrances and near the center of the network maze cave, display increasing amounts of red, orange, yellow, brown, and black consolidated powders, identified as hematite, goethite, and manganese oxides hereinafter referred to as Fe–Mn oxides (C4, DM94, DO230, DO231, M16-2 in Table 1). Fe and Mn oxides are found primarily in lightweight deposits up to 25 cm thick on the floors and as porous, multicolored coatings on walls and breakdown. Some of the powders form semi-rectangular or circular blocks, and some are laminated (Fig. 13). Disturbance of the consolidated powders results in aerosolization of the fine sediments, thus a section of the BCS is satirically named “The Land of NOD,” a.k.a Noxious Orange Dust. There are some passages where the Fe–Mn oxides and sulfate deposits have peeled away from the cave walls, exposing the friable and bleached bedrock (Fig. 14). A green clayey-looking material was also documented in the exposed bedrock in this section of the cave, which was identified as dolomite and calcite (DN4, Table 1).

Figure 10. A corkscrew-shaped gypsum flower (approximately 25 cm long) extruding from a breccia layer in the Bopper Cave System. Photo by Sierra Heimel.

Figure 11. Gypsum flowers preferentially extruding from horizontal breccia layers in the Mooney Falls Member. Photo by Dave Bunnell.

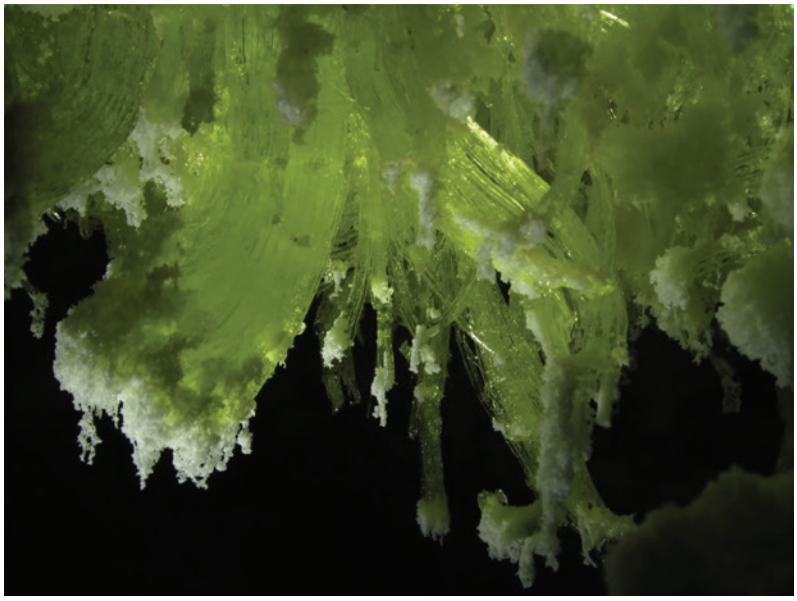

Figure 12. Light green sulfate minerals, likely a combination of epsomite and gypsum. Photo by Paul Burger.

Passages near the Green Door zone (Fig. 4) occur along an unmapped fault. A zone of mineralization with botryoidal green and blue minerals is found here. A sample collected here was identified as malachite (DO257-1 in Table 1 and Fig. 15). Azurite is commonly found with malachite and is likely the blue mineral found in association with malachite but was not differentiated by our XRD analysis. The malachite mineralization was found in association with massive calcite and Fe–Mn oxides in the fault plane. Large, approximately 10 cm long scalenohedral dogtooth calcite spar crystals were found in a cavity in the Green Door zone but not in the fault plane (Fig. 16). Mammillary calcite formations have not been documented in Double Bopper; however, Leandras is documented to contain localized mammillary formations.

The most unique secondary deposits found in the BCS are lightweight, froth- or foam-like deposits made up of gypsum, calcite, and anhydrite (sample DL22-2, Table 1) and are henceforth referred to as gypsum foam. These deposits are found in abundance on the walls and floors of select portions of the BCS. Gypsum foam is extremely delicate; however, a hard secondary coating or encasing was observed around a gypsum foam sample, and this coating was identified as quartz with XRD (Fig. 17). A soft green coating on a gypsum foam sample was identified as brushite (sample B63 in Table 1).

DISCUSSION

The wide variety of speleogens, speleothems, and secondary cave deposits observed in the BCS suggests a complex origin, likely resulting from multiple fluids moving through the Redwall Limestone at different times, dissolving the

Figure 13. Autochthonous cave sediments composed of bright yellow, fine-grained, laminated Fe-oxide sediments. Photo by Sierra Heimel.

Figure 14. An exposed section of bleached and friable bedrock (orange and yellow) underneath a layer of Fe–Mn oxides (brown and black) underneath a botryoidal white gypsum rind. Photo by Sierra Heimel.

Figure 15. Botryoidal malachite and calcite mineralization found near the Green Door mineralized fault zone. Photo by Sierra Heimel.

bedrock and depositing hypogene speleothems in the process. Our observations suggest four distinct stages of speleogenetic development that led to the formation of the BCS (Table 2). Consequently, we propose a modified model of hypogene cave development in the Grand Canyon, building on the previous work by Polyak et al. (2017).

Stage 1 of speleogenesis commenced sometime prior to 4 million years ago, predating the incision of the Grand Canyon, when the Redwall Limestone existed within the deep phreatic zone of the ancient RM aquifer (Polyak et al., 2008) (Table 2, Stage 1). We interpret that the horizontal tube passages in the BCS were formed deep in the ancient RM aquifer during a time when hypogene fluid contributions were present. The spatial patterns of maze caves suggest they were created through the simultaneous widening of passages in low-gradient environments (Klimchouk and Ford, 2000; Klimchouk, 2012). Additionally, the spatial patterns of passage size decreasing in relation to distance from faults suggest that large contributions of hypogene fluids may have been episodically sourced from nearby faults, flowing at low gradients toward Double Bopper Cave, further aiding passage development (Heimel and Tobin, 2022). During this initial phase, acidic hypogene fluids altered the cave walls, bleaching and corroding them to a friable texture at depths of several tens of centimeters. These fluids were likely rich in carbonic acid, as previously proposed (Hill and Polyak, 2010), evidenced by locally preserved dogtooth calcite spar mineralization. The presence of this large euhedral dogtooth calcite spar suggests that it could have formed 500 ± 250 m beneath the water table in the deep phreatic zone, where the transition from supercritical to subcritical CO_2 drives both limestone dissolution and calcite precipitation (Decker et al., 2016) with respect to depth, temperature, and the solubility of $CaCO_3$ during the descent of the potentiometric surface as the cave shifts from the solutional zone into the depositional zone (Hill and Polyak, 2010).

Following the initial dissolution processes, *Stage 2* initiated as the water chemistry of the fluids in the conduits changed with the gradual lowering and fluctuation of the potentiometric surface in the ancient RM aquifer (Table 2, Stage 2). This transition is evidenced by the presence of large quantities of Fe–Mn oxides coating the bleached and altered bedrock, along with laminated Fe–Mn oxides in the BCS. Hematite, an iron oxide mineral commonly deposited in caves from thermal waters and under oxidizing conditions, may convert into goethite (Hill and Forti, 1997). Iron and manganese oxides and hydroxides serve as redox indicators (Levy, 2007), favoring transport in fluids in their reduced form at low pH and Eh, and precipitating as Fe–Mn oxides when these variables increase (Palmer and Palmer, 2012). Fluctuations in the pH and Eh of the ancient RM aquifer, likely influenced by changes in the potentiometric surface

Figure 16. Scalenohedral dogtooth calcite spar near the Green Door zone. Photo by Sierra Heimel.

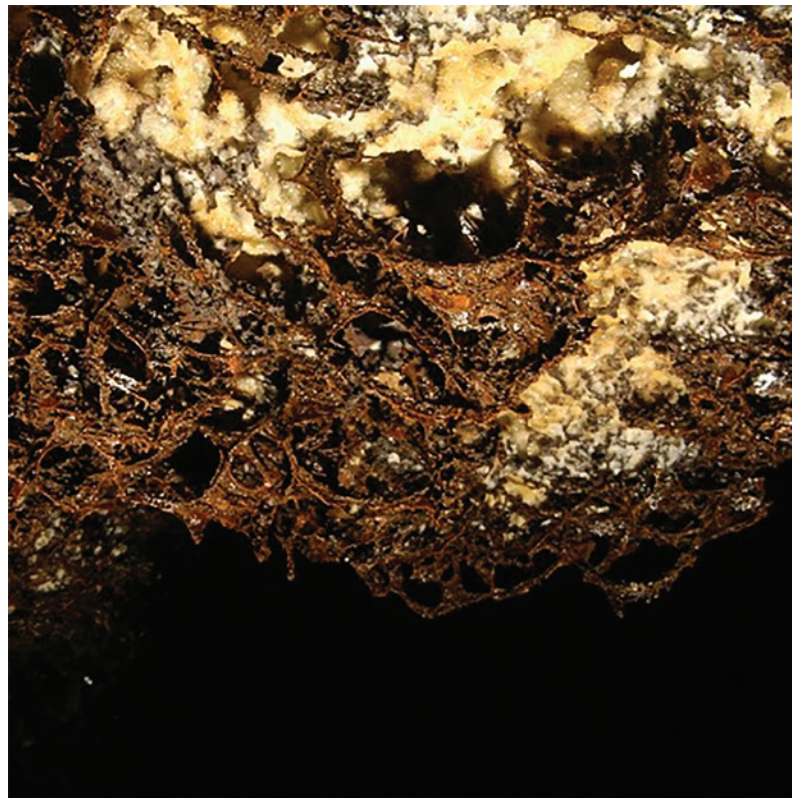

Figure 17. Gypsum foam, made up of anhydrite, gypsum, and quartz (see text for further details). Photo by Stephen Eginoire.

and limestone dissolution, could have led to rising pH levels, promoting the subsequent precipitation of previously soluble iron and manganese as Fe–Mn oxide minerals (Palmer and Palmer, 2012). However, Fe–Mn oxides can also precipitate without a change in pH, particularly when aided by microbial processes (Carmichael et al., 2013). The fine-grained and laminated nature of these sediments indicates that they settled slowly out of the water column in a low-energy environment. The formation of goethite and hematite Liesegang banding likely occurred during Stage 2, with bands representing precipitation lines of iron-rich minerals along groundwater chemical interfaces. These processes are typically the result of numerous precipitation events over long periods of time, with moving groundwater under oxic conditions (Wells et al., 2003).

Additional evidence for Stage 2 is observed in the co-occurrence of Fe–Mn oxides with malachite deposits at the Green Door fault plane, which likely served as a significant fluid pathway. Malachite is typically found in the oxidized upper zones of copper sulfide deposits (Melchiorre and Enders, 2003), where copper-bearing minerals are exposed to groundwater and hydrothermal fluids (Hill and Polyak, 2010). The most likely source of copper in the BCS region is from copper sulfide deposits in breccia pipes (Wenrich, 1985). The carbonate component is likely acquired from CO_2 dissolved in groundwater due to the dissolution of the Paleozoic carbonate bedrock. Therefore, the formation of

Table 2. Speleogenetic stages of the Bopper Cave System.

Stage	Description	Evidence
Stage 1	Initial phreatic conditions with carbonic acid hypogene fluid contributions and early dissolution of limestone.	Abundance of horizontal tube passages, bleached bedrock, and dogtooth calcite.
Stage 2	Changes in water chemistry, rise in pH, and precipitation of Fe–Mn oxides.	Coating and laminations of Fe–Mn oxides, malachite deposit in fault.
Stage 3	Transition to sulfate-dominated fluids, leading to sulfuric acid speleogenesis dominated by dissolution and the formation of replacement gypsum.	Presence of speleogenetic gypsum rinds, distinctive cupolas, air scallops, solution domes, and other features.
Stage 4	Evaporative vadose conditions resulting from water table incision, leading to the deposition of sulfate minerals.	Prolific gypsum deposits, hydromagnesite, and other evaporite minerals.

Table 3. Comparison of conceptual models for hypogene speleogenesis in the Grand Canyon.

Aspect	Polyak et al. (2017) Conceptual Model	BCS Conceptual Model (This Study)
Speleogenetic agents	Dominantly CO_2-rich hypogene fluids; H_2S considered a minor contributor based on limited gypsum abundance.	Multiple hypogene fluids, including CO_2, H_2S, and Cu-rich fluids; sulfuric acid plays a major role during at least one speleogenetic phase.
Role of sulfuric acid speleogenesis (SAS)	Secondary or limited; inferred from a limited gypsum rind and sulfate deposits.	Abundant and locally dominant, evidenced by common gypsum rinds and sulfate mineral assemblages.
Fluid types	Deep-seated hypogene fluids linked to magmatic and/or tectonic activity.	Diverse types of hypogene fluids, including magmatic, tectonic, copper-bearing fluids; contribution of various fluid types varies spatially.
Hydrologic controls	Regional water table fluctuations control dissolution and mineral paragenesis.	Water table position important; episodic interplay with fault-controlled flow paths creates locally unique geochemical conditions and mineral paragenesis.
Predicted speleogenetic sequence	Fe and Mn oxides → calcite spar linings → mammillary calcite → folia → cave rafts → gypsum rinds.	Incomplete or altered sequence with potential overprinting; Fe and Mn oxides → calcite spar linings → mammillary calcite → overprinting and dissolution of most calcite → gypsum rinds → secondary sulfate deposits.
Calcite spar linings	Common and widespread in phreatic passages; used as indicators of formation depth.	Largely absent, suggesting depth estimates based on spar may not apply universally.
Mammillary calcite	Common component of the hypogene mineral assemblage.	Limited or absent in major portions of the BCS.
Gypsum occurrence	Present mainly as late-stage rinds.	Abundant and diverse gypsum formations, indicating sustained sulfuric acid influence.
Cave size vs. completeness of sequence	Larger caves are more likely to preserve the full sequence of hypogene subevents.	The largest cave in the Grand Canyon yet lacks the full predicted sequence.
Conceptual implication	Hypogene caves broadly follow a common evolutionary pathway in the Grand Canyon.	Hypogene speleogenesis is highly heterogeneous; no single model or sequence applies to all Grand Canyon caves.

malachite at the Green Door fault plane likely arises from groundwater interacting with these copper sulfides, migrating upward through the fault structure, and redepositing them as malachite near faults. Although Stage 2 provides suitable conditions for malachite formation, it is also feasible for malachite to precipitate during later stages of speleogenesis as fluid migration patterns evolve, highlighting the complex interactions between geochemical processes and mineral deposition in the Grand Canyon.

Stage 3 (Table 2, Stage 3) subaqueous and subaerial processes took place in a mixed phreatic and vadose environment when the potentiometric surface was at the level of the BCS following a transition to sulfate (SO_4)-dominated fluids at some point, likely prior to the onset of Stage 3, as indicated by the formation of sulfuric acid speleogens (replacement gypsum) in the subaerial zone, just above the water table (Polyak et al., 2017). Speleogenetic (replacement gypsum), a direct product of hypogene processes in the Grand Canyon (Hill and Polyak, 2010), results from the dissolution of limestone by sulfuric acid, accompanied by gypsum co-precipitation (Polyak and Provencio, 2001). Unlike evaporative gypsum, speleogenetic (replacement gypsum) forms thick rinds that are denser and more massive. Observations of massive white rinds, 5–10 cm thick, in combination with XRD analyses, suggest that sample DJ43 contains this type of gypsum, which is common throughout the BCS. This process would have occurred as H_2S migrated upward from deep sources along faults and fractures, interacting with oxygenated water near the BCS subaerial zone, thus producing sulfuric acid and vapor. The resulting sulfate accumulation, along with the calcium from the limestone, would cause gypsum to precipitate on cave surfaces (Palmer, 2007). The sulfuric vapors likely generated buoyant convection currents, with condensation corrosion inducing localized dissolution at the water table interface, resulting in distinctive features such as cupolas, air scallops, solution domes, pendants, ceiling half tubes, and wall channels with rillenkarren (Figs. 6–9). These speleogens are not structurally controlled and do not follow joints or fractures, a trait shared with other large hypogene systems (Galdenzi et al., 2014; De Waele et al., 2024). Some hypogene caves have documented these speleogens forming above structurally controlled feeders (De Waele et al., 2016), but definitive feeders have not been identified in the BCS.

During *Stage 4* (Table 2, Stage 4), as the Colorado River incised the Grand Canyon, the potentiometric surface of the ancient RM aquifer dropped below the level of the BCS, transitioning the cave environment to an entirely evaporative vadose system. This shift resulted in decreased pressure on the cave walls, leading to significant collapse and breakdown of larger conduits. Additional breakdown may also be due to gypsum crystal wedging (White and White, 2003; Gásquez et al., 2019). In this environment, residual sulfate-bearing fluids were stored in the pore spaces of the altered bedrock, facilitating the precipitation of various sulfate minerals, including prolific gypsum deposits, gypsum foam, and

additional varieties such as epsomite, thenardite, mirabilite, jarosite, and natrojarosite (Figs. 14–16). Gypsum flowers, common speleothems, exhibit unique curved or spiral forms driven by episodic variations in $CaSO_4$ solution flow rate and concentration during fibrous or prismatic crystal growth (Ghergari and Onac, 1995). The unusual gypsum foam, not previously documented in other cave systems, displays vibrant colors that may be caused by small amounts of Fe–Mn oxide coatings; however, these oxides were not detected by powder XRD. Epsomite appears as bright green-yellow nodules, whereas mirabilite and thenardite are white powders. These are highly soluble sulfate minerals that are common in sulfuric acid caves and are sensitive to humidity and temperature, with mirabilite altering to thenardite upon exposure to dry air (Hill and Forti, 1997). Sodium and magnesium may have been sourced from evaporite deposits interbedded with gypsum and dolomite in the Toroweap Formation located above the Redwall Limestone (Sorauf and Billingsley, 1991) or, alternatively, could have been sourced from Precambrian felsic igneous and metamorphic rocks located below the Redwall Limestone (Brown et al., 1979; Ilg et al., 1996). Magnesium may have additionally been sourced from interbedded dolomite in the Mooney Falls Member of the Redwall Limestone (Dohm, 2017).

Additionally, other less common minerals, such as jarosite and natrojarosite, precipitated after sulfate-rich waters ceased following the drop in the potentiometric surface, further evidencing this evaporative stage of speleogenesis. These hydroxysulfate minerals, forming in sulfuric acid-rich environments (Kawano and Tomita, 2001), can form directly from the interaction of H_2SO_4 with K, Al, and Fe clays (Polyak and Provencio, 2001; D'Angeli et al., 2018) or can originate from pyrite oxidation or sulfate-rich solutions found in other caves (Hill and Forti, 1997; Audra et al., 2013). The sodium in natrojarosite may derive from halite-bearing Precambrian sedimentary rocks or from igneous rocks with Na-varieties of feldspar (Karlstrom et al., 2012), while potassium sources could include Precambrian sedimentary rocks and clays from the Cambrian Bright Angel Shale (Baldwin et al., 2004). Furthermore, both potassium and sodium are common in breccia pipes with concentrations above average for host formations (Wenrich, 1985). We interpret that the formation of the hydromagnesite deposits also occurred during Stage 4, likely resulting from the dissolution of dolomitic rocks (Hill and Forti, 1997). As groundwater interacts with dolomitic rocks, the Mg/Ca ratio rises, allowing magnesium-rich minerals such as hydromagnesite and magnesite to form (Columbu et al., 2021). Lastly, brushite, a hydrated calcium phosphate, can form via the alteration of bat guano (e.g., Marincea et al., 2004; Audra et al., 2019). The presence of thousands of mummified bats is a unique feature of the BCS (Mead et al., 2021; Chambers et al., 2024), potentially explaining the presence of brushite in this cave system.

APPROXIMATE AGE AND TIMING OF THE BCS STAGES

The BCS currently sits 6.6 km away and 940 m above the Colorado River and is a relict feature of the ancient RM aquifer, which existed before the formation of the Grand Canyon, adding complexity to our understanding of its speleogenetic history. New numerical modeling using multivariate statistical analysis by Ashjari et al. (2024) estimates that it could have taken between 4 and 10 million years for the BCS to develop at depth beneath the water table, which would coincide with the timing of our stages 1 and 2.

Previous hypogene speleogenesis models for Grand Canyon caves have provided important information on the canyon's age and evolution, specifically by Polyak et al. (2008), who dated mammillary formations in Leandras, indicating that the water table was at the elevation of the BCS around 3.5 ± 1.2 Ma. This timeframe suggests that the first two stages of BCS speleogenesis occurred in the phreatic zone before 3.5 ± 1.2 Ma, which is broadly in alignment with the timing inferred from Ashjari et al. (2024), while the third stage began after the water table descended to the level of the BCS.

Modern incision rates from the eastern Grand Canyon of 160 m/Ma (Crow et al., 2014) are temporally stable but spatially variable and indicate it could have taken approximately 5.9 Ma for the water table to drop from the elevation of the BCS to its current level, suggesting that stages 3 and 4 took place during the last 5.9 Ma. However, based on the variable nature of incision rates in the Grand Canyon region, in addition to the U/Pb dates of mammillary formations in Leandras (Polyak et al., 2008), we conclude that stages 3 and 4 likely happened over the past ~4.7 Ma. The stage 4 processes were initiated when the water table dropped completely below the level of the BCS when incision and denudation carved side canyons around the BCS, creating multiple new entrances exposed on opposite sides of canyons, suggesting that previously these would have been throughgoing cave passages that are now crosscut by side canyons. Chambers et al. (2024) radiocarbon dated 67 well-preserved bat specimens from the BCS and found that ages range from modern to >45,800 cal BP, near the practical upper limit of radiocarbon dating; this indicates that the caves were accessible to bats (and therefore open to the surface) for at least ~46 ka. Although stage 4 was likely initiated much earlier than the radiocarbon window, the >45,800 cal BP result provides a minimum age constraint on stage 4 initiation.

HYPOGENE FLUID HETEROGENEITY AND MULTI-PHASE SPELEOGENESIS IN THE GRAND CANYON

The formation of the BCS reflects a complex interplay of tectonic evolution, hydrogeological conditions, and the migration of chemically diverse hypogene fluids. The existing conceptual model for hypogene cave formation in the

Grand Canyon developed by Polyak et al. (2017) provides a valuable framework in which caves formed primarily through the ascent of CO_2-rich fluids under deep phreatic conditions, with sulfuric acid playing a minor role. In this model, speleogenetic byproducts record an ordered sequence of subevents related to regional water table fluctuations and episodic tectonic or magmatic activity.

The BCS shares key elements of this framework, notably the hypogene origin linked to deep-seated fluid ascent in relation to the position of the descending water table. Early phreatic dissolution in the BCS likely occurred under CO_2-rich conditions at depth, consistent with hypogene cave development elsewhere in the Grand Canyon. However, the mineralogical record of the BCS indicates important departures from the existing conceptual model (Table 3).

Most notably, the BCS contains abundant sulfate minerals, including extensive speleogenetic gypsum rinds, indicating that sulfuric acid likely played a major role during one of the later phases of cave development. This contrasts with many previously documented hypogene caves in the Grand Canyon, where limited gypsum abundance suggested a minor role of H_2S. The dominance of sulfate minerals in addition to copper mineralization in the BCS highlights substantial spatial variability in hypogene fluid chemistry across the Grand Canyon.

Additional divergence is evident in the speleogenetic byproducts and secondary mineral deposits preserved in the BCS. Although Polyak et al. (2017) described a progression that includes cave dissolution, Fe and Mn oxides, calcite spar linings, mammillary calcite, folia, cave rafts, and late-stage gypsum rinds, the BCS exhibits some components of this suite, but others have not been identified to date. Calcite spar linings are largely absent (other than locally preserved spar near the Green Door Fault zone), mammillary calcite formations are limited in Leandras and not documented in Double Bopper, and folia and cave rafts are not widely documented, despite the BCS being the largest cave system in the Grand Canyon. Instead, sulfate deposits dominate the secondary mineral assemblage, indicating an altered or incomplete speleogenetic sequence with the potential for overprinting.

The absence of widespread calcite spar linings also bears on estimates of speleogenetic depth. Previous estimates placing cave spar formation at approximately 500 ± 250 m below the water table are based on observations from the unconfined karst system of the Guadalupe Mountains (Decker et al., 2016). In contrast, hypogene cave development in the Grand Canyon likely occurred under initially confined conditions, followed by progressive water table lowering with transition to an unconfined system. As a result, depth estimates derived from unconfined settings may not be directly transferable, and more site-specific hydrogeologic and geochemical modeling is required to constrain speleogenetic depths in the Grand Canyon.

These observations indicate that hypogene speleogenesis in the Grand Canyon is controlled not only by the position of the water table and the contribution of hypogene fluids but also by the pronounced spatial and temporal heterogeneity in fluid sources and migration pathways via faults. Building on the framework of Polyak et al. (2017), our model emphasizes that multiple hypogene fluids of varying origins can mix and react in complex, location-dependent ways, as the evolving fault and fracture network at BCS taps distinct reservoirs and flow paths during magmatic and tectonic events. The BCS demonstrates that no single speleogenetic sequence applies regionally, underscoring the need for a more flexible conceptual model for hypogene cave development in the Grand Canyon.

CONCLUSIONS

The formation of the BCS occurred through the complex interplay of geological and hydrological processes over millions of years. Initially, acidic hypogene fluids circulated through the Redwall Limestone in the deep phreatic zone, dissolving bedrock and creating horizontal passageways. As the environment evolved, fluctuating potentiometric surfaces and changing water chemistries led to the deposition of various minerals, including iron and manganese oxides. The transition to an unconfined evaporative vadose system further contributed to the mineral diversity within the cave, producing speleothems such as gypsum flowers and unique gypsum foam. Subsequent mineral formations, including stalagmites, stalactites, and phosphates from bat guano, reflect the ongoing modern vadose processes within the cave system. This multistage speleogenesis highlights the dynamic interactions between groundwater movement, mineral precipitation, and the geological framework of the Grand Canyon region, ultimately shaping the BCS into the complex cave observed today.

The BCS, recognized as hosting the two largest caves in the Grand Canyon, offers compelling new evidence that broadens existing models of hypogene speleogenesis in the region (Polyak et al., 2017). Our research highlights the influential role of both regional-scale processes and localized geochemical variability in driving cave formation. A key contribution of this study is the emphasis on multifluid interaction in the speleogenesis of the BCS. The cave's development was shaped by the interplay between various hypogenic fluids, specifically carbonic acid, sulfuric acid, and copper-bearing fluids, contributing to remarkable mineralogical diversity, including distinct deposits of malachite, gypsum, and jarosite.

Moreover, our findings underscore the critical importance of recognizing the heterogeneous sources of origin for these fluids in hypogene speleogenesis. The observed variability in fluid contributions is essential for understanding the mechanisms behind mineral deposition and cave morphology, as localized geochemical conditions can greatly

influence the variety of unique features within the BCS, setting it apart from other hypogene systems documented in the Grand Canyon. Finally, this study calls for a more integrated approach to hypogene karst research that considers the episodic, regionally variable, and multifluid nature of speleogenesis. Future investigations should prioritize exploring the interplay of multiple fluids and their evolving roles in shaping cave formation processes. This novel understanding of the spatial and temporal heterogeneity of groundwater fluids observed in the BCS not only contributes unique insights to karst literature but also serves as a vital component in advancing our understanding of hypogene caves in both contemporary and ancient systems.

ACKNOWLEDGMENTS

This work is the culmination of over a decade's worth of exploration from numerous citizen scientists in the caving community who have dedicated enormous efforts to map and document the unique resources in the Bopper Cave System. Sample collection was completed with help from James Hunter, Garrison Loope, and Jason Ballensky. Several photographers granted permission for use of their spectacular photos, including Stephen Eginoire, James Hunter, Paul Burger, and Dave Bunnell. We also thank Dr. Joe De Waele, Dr. Augusto Auler, and an anonymous reviewer for the *Journal of Cave and Karst Studies* for their thoughtful, constructive feedback and insightful suggestions that helped improve this manuscript and highlighted directions for future research. This research was conducted under NPS permit GRCA-2021-SCI-0014.

AUTHOR CONTRIBUTION STATEMENT

BT proposed and received funding for the study. SH and BT finalized the study design. SH, BT, and GL collected the samples. SH analyzed the data and wrote the manuscript. BT and GL assisted with interpretation and editing of the manuscript.

REFERENCES

Ashjari, J., Tobin, B., Fryar, A.E., and Ashjari, Z., 2024, Numerical modeling of development of Leandras and Double Bopper Caves, Grand Canyon, USA: Hydrogeology Journal, v. 32, no. 6, p. 1751–1768, https://doi.org/10.1007/s10040-024-02812-z.

Audra, P., Gázquez, F., Rull, F., Bigot, J.-Y., and Camus, H., 2013, Hypogene sulfuric acid speleogenesis and rare sulfate minerals (Fibroferrite, Jarosite subgroup) Baume Galiniere Cave (Alpes-de-Haute-Provence, France), *in* Filippi, M., and Bosák, P., eds., Proceedings of the International Congress of Speleology, 16th, Brno, Czech Republic: Volume 3: Praha, Czech Republic, Czech Speleological Society, p. 432–436.

Audra, P., De Waele, J., Bentaleb, I., Chroňáková, A., Krištůfek, V., D'Angeli, I., Carbone, C., Madonia, G., Vattano, M., Scopelliti, G., Cailhol, D., Vanara, N., Temovski, M., Bigot, J., Nobecourt, J.-C., Galli, E., Rull, F., and Sanz-Arranz, A., 2019, Guano-related phosphate-rich minerals in European caves: International Journal of Speleology, v. 48, no. 1, p. 75–105.

Baldwin, C.T., Strother, P.K., Beck, J.H., and Rose, E., 2004, Palaeoecology of the Bright Angel Shale in the eastern Grand Canyon, Arizona, USA, incorporating sedimentological, ichnological and palynological data, *in* McIlroy, D., ed., *The Application of Ichnology to Palaeoenvironmental and Stratigraphic Analysis*: London, Geological Society, Special Publication 228, p. 213–236, https://doi.org/10.1144/GSL.SP.2004.228.01.11.

Billingsley, G.H., and Hampton, H.M., 2000, Geologip map of the Grand Canyon 30′ x 60′ quadrangle, Coconino and Mohave counties, northwestern Arizona: U.S. Geological Survey Geologic Investigation Series I-2688, version 1.0, scale 1:100,000, p. 15, http://pubs.usgs.gov/imap/i-2688.

Beus, S.S., 1990, Redwall Limestone and Surprise Canyon Formation, *in* Beus, S.S., and Morales, M., eds., *Grand Canyon Geology*: New York, Oxford University Press, p. 119–145.

Blakey, R.C., and Ranney, W., 2008, *Ancient Landscapes of the Colorado Plateau*: Grand Canyon Village, AZ, Grand Canyon Association, p. 156.

Brown, E.H., Babcock, R.S., Clark, M.D., and Livingston, D.E., 1979, Geology of the older Precambrian rocks of the Grand Canyon: Part I: Petrology and structure of the Vishnu Complex: Precambrian Research, v. 8, no. 3–4, p. 219–241, https://doi.org/10.1016/0301-9268(79)90030-5.

Bucher, K., and Stober, I., 2010, Fluids in the upper continental crust: Geofluids, v. 10, no. 1–2, p. 241–253, https://doi.org/10.1111/j.1468-8123.2010.00279.x.

Burgess, S.A., 2021, Sulfur systematics and carbonate diagenesis in the Mitchell Plateau, Indiana [Master's thesis]: Bloomington, Indiana University, 149 p.

Carmichael, M.J., Carmichael, S.K., Santelli, C.M., Strom, A., and Bräuer, S.L., 2013, Mn(II)-oxidizing bacteria are abundant and environmentally relevant members of ferromanganese deposits in caves of the upper Tennessee river basin: Geomicrobiology Journal, v. 30, no. 9, p. 779–800, https://doi.org/10.1080/01490451.2013.769651.

Chambers, C.L., Thomas, S., Santucci, V.L., Oswald, H., and Ballensky, J., 2024, Ancient bat remains illustrate the role of caves as habitat anchors in the temporally dynamic landscape of the Grand Canyon: Parks Stewardship Forum, v. 40, no. 1, p. 39–52, https://doi.org/10.5070/P540162920.

Columbu, A., Audra, P., Gázquez, F., D'Angeli, I.M., Bigot, J.-Y., Koltai, G., Chiesa, R., Yu, T.-L., Hu, H.-M., Shen, C.-C., Carbone, C., Heresanu, V., Nobécourt, J.-C., and De Waele, J., 2021, A hypogenic cave system with late-stage condensation-corrosion and epigenic overprinting (Toirano, Liguria, Italy): Geomorphology, v. 376, p. 107561, https://doi.org/10.1016/j.geomorph.2020.107561.

Crossey, L.J., Fischer, T.P., Patchett, P.J., Karlstrom, K.E., Hilton, D.R., Newell, D.L., Huntoon, P., Reynolds, A.C., and de Leeuw, G.A.M., 2006, Dissected hydrologic system at the Grand Canyon: Interaction between deeply derived fluids and plateau aquifer waters in modern springs and travertine: Geology, v. 34, no. 1, p. 25–28, https://doi.org/10.1130/G22057.1.

Crossey, L.J., Karlstrom, K.E., Springer, A.E., Newell, D., Hilton, D.R., and Fischer, T., 2009, Degassing of mantle-derived CO_2 and He from springs in the Southern Colorado Plateau region-Neotectonic Connections and implications for groundwater systems: Geological Society of America Bulletin, v. 121, no. 7–8, p. 1034–1053, https://doi.org/10.1130/B26394.1.

Crow, R., Karlstrom, K.E., McIntosh, W., Peters, L., and Dunbar, N., 2008, History of quaternary volcanism and lava dams in Western Grand Canyon based on lidar analysis,^{40}Ar/^{39}Ar dating, and field studies: Implications for flow stratigraphy, timing of volcanic events, and lava dams: Geosphere, v. 4, no. 1, p. 183–206, https://doi.org/10.1130/GES00133.1.

Crow, R., Karlstrom, K., Darling, A., Crossey, L., Polyak, V., Granger, D., Asmerom, Y., and Schmandt, B., 2014, Steady incision of Grand Canyon at the million year timeframe: A case for mantle-driven differential uplift: Earth and Planetary Science Letters, v. 397, p. 159–173, https://doi.org/10.1016/j.epsl.2014.04.020.

D'Angeli, I., Carbone, C., Nagostinis, M., Parise, M., Vattano, M., Madonia, G., and De Waele, J., 2018, New insights on secondary minerals from Italian sulfuric acid caves: International Journal of Speleology, v. 47, no. 3, p. 271–291.

De Waele, J., Audra, P., Madonia, G., Vattano, M., Plan, L., D'Angeli, I.M., Bigot, J., and Nobécourt, J-C., 2016, Sulfuric acid speleogenesis (SAS) close to the water table: Examples from southern France, Austria, and Sicily: Geomorphology, v. 253, 452–467, https://doi.org/10.1016/j.geomorph.2015.10.019.

De Waele, J., D'Angeli, I.M., Audra, P., Plan, L., and Palmer, A.N., 2024, Sulfuric acid caves of the world: A review: Earth-Science Reviews, v. 250, p. 104693, https://doi.org/10.1016/j.earscirev.2024.104693.

Decker, D.D., Polyak, V.J., and Asmerom, Y., 2016, A supercritical CO_2 hypogene speleogenesis model: The origin of spar caves and cave spar in the Guadalupe Mountains, USA, *in* Chavez, T., and Reehling, P., eds., *Proceedings of DeepKarst 2016*: Carlsbad, NM, April 11–14: National Cave and Karst Research Institute, p. 21–25.

Dohm, P.W., 2017, A sequence stratigraphic analysis of the Mooney Falls Member of the Redwall Limestone [Bachelor's thesis]: Durango, Fort Lewis College, 45 p.

DuChene, H.R., Palmer, A.N., Palmer, M.V., Michael Queen, J., Polyak, V.J., Decker, D.D., Hill, C.A., Spilde, M., Burger, P.A., Kirkland, D.W., and Boston, P., 2017, Hypogene speleogenesis in the Guadalupe Mountains, New Mexico and Texas, USA, *in* Klimchouk, A., Palmer, A.N., De Waele, J., Auler, A.S., and Audra, P., eds., *Hypogene Karst Regions and Caves of the World*: Cham, Springer, p. 511–530, https://doi.org/10.1007/978-3-319-53348-3_31.

Farrant, A.R., and Harrison, T., 2017, Hypogenic caves in the UK, *in* Klimchouk, A., Palmer, A.N., De Waele, J., Auler, A.S., and Audra, P., eds., *Hypogene Karst Regions and Caves of the World*: Cham, Springer, p. 43–60, https://doi.org/10.1007/978-3-319-53348-3_2.

Galdenzi, S., Jones, D.S., and Macalady, J.L., 2014, Condensation corrosion: Measurements and geomorphic evidence in the Frasassi caves, *in* Klimchouk, A., Sasowsky, I.D., Mylroie, J., Engel, S.A., and Engel, A.S., eds., *Hypogene Cave Morphologies*: Karst Waters Institute, Inc., Leesburg, VA, Karst Waters Institute Special Publication 18, Karst Waters Institute, Inc., p. 44–46.

Gásquez, F., Calaforra, J.M., Evans, N.P., Turchyn, A.V., Rull, F., Medina, J., Ros, A., Llamusi, J.L., Sanchez, J.A.R., and Hodell, D.A., 2019, Physical weathering of carbonate host-rock by precipitation of soluble salts in caves: A case study in El Oron-Arco Cave (Region of Murcia, SE Spain): Chemical Geology, v. 521, p. 1–11, https://doi.org/10.1016/j.chemgeo.2019.05.010.

Ghergari, L., and Onac, B.-P., 1995, The crystallogenesis of gypsum flowers: Cave and Karst Science, v. 22, no. 3, p. 119–122.

Gulley, J.D., and Polk, J.S., 2017, Hypogene karst influences in the Upper Floridan aquifer, *in* Klimchouk, A., Palmer, A.N., De Waele, J., Auler, A.S., and Audra, P., eds., *Hypogene Karst Regions and Caves of the World*: Cham, Springer, p. 745–755, https://doi.org/10.1007/978-3-319-53348-3_50.

Heimel, S., 2019, Matrix porosity controls on karst morphology in the Mooney Falls Member of the Redwall Limestone of the Grand Canyon [Bachelor's thesis]: Durango, Fort Lewis College, 25 p., https://doi.org/10.13140/RG.2.2.16292.35206.

Heimel, S., 2022, Hypogene speleogenesis in the Grand Canyon: Observational, mineralogical, and geochemical investigations from the Bopper Cave System [Master's thesis]: Lexington, University of Kentucky, 105 p, https://doi.org/10.13023/etd.2023.025.

Heimel, S.M., and Tobin, B.W., 2022, Geospatial applications of cave resource data to better understand epikarst and unsaturated zone groundwater flow path development: Geosciences, v. 12, no. 2, p. 47, https://doi.org/10.3390/geosciences12020047.

Hill, C.A., 1990, Sulfuric acid speleogenesis of Carlsbad Cavern and its relationship to hydrocarbons, Delaware basin, New Mexico and Texas: American Association of Petroleum Geologists Bulletin, v. 74, no. 11, p. 1685–1694.https://doi.org/10.1306/0C9B2565-1710-11D7-8645000102C1865D.

Hill, C.A., and Forti, P., 1997, *Cave Minerals of the World* (2nd edition): Huntsville, AL, National Speleological Society, p. 463.

Hill, C.A., and Polyak, V.J., 2010, Karst hydrology of Grand Canyon, Arizona, USA: Journal of Hydrology, v. 390, no. 3–4, p. 169–181, https://doi.org/10.1016/j.jhydrol.2010.06.040.

Hose, L.D., DuChene, H.R., Jones, D., Baker, G.M., Havlena, Z., Sweetkind, D., and Powell, D., 2021, Hypogenic karst of the Great Basin, *in* Florsheim, J., Koeberl, C., McKay, M.P., and Riggs, N., eds., *Field Excursions from the 2021 GSA Section Meetings: Geological Society of America Field Guide 61*: Boulder, CO, The Geological Society of America (GSA), p. 77–114, https://doi.org/10.1130/2020.0061(05).

Huntoon, P.W., 1974, The karstic groundwater basins of the Kaibab Plateau, Arizona: Water Resources Research, v. 10, no. 3, p. 579–590, https://doi.org/10.1029/WR010i003p00579.

Huntoon, P.W., 1996, Large-basin ground water circulation and paleo-reconstruction of circulation leading to uranium mineralization in Grand Canyon breccia pipes, Arizona: The Mountain Geologist, v. 33, no. 3, p. 71–84.

Huntoon, P.W., 2000a, *Karstification Associated with Groundwater Circulation Through the Redwall Artesian Aquifer*: Grand Canyon, AR, National Speleological Society.

Huntoon, P.W., 2000b, Variability of karstic permeability between unconfined and confined aquifers, Grand Canyon region, Arizona: Environmental and Engineering Geoscience, v. 6, no. 2, p. 155–170, https://doi.org/10.2113/gseegeosci.6.2.155.

Ilg, B.R., Karlstrom, K.E., Hawkins, D.P., and Williams, M.L., 1996, Tectonic evolution of Paleoproterozoic rocks in the Grand Canyon: Insights into middle-crustal processes: Geological Society of America Bulletin, v. 108, no. 9, p. 1149–1166, https://doi.org/10.1130/0016-7606(1996)108≤1149:TEOPRI≥2.3.CO;2.

Jones, C.J.R., 2017, Characterization of the Redwall–Muav aquifer of the Grand Canyon and Kaibab Plateau, Arizona, based on Roaring Springs hydrograph analysis [Master's thesis]: Flagstaff, Northern Arizona University, 151 p.

Karlstrom, K.E., Timmons, J.M., and Crossey, L.J., 2012, Introduction to Grand Canyon geology, *in* Timmons, M.J., and Karlstrom, K.E., eds., *Grand Canyon Geology: Two Billion Years of Earth's History*: Boulder, CO, Geological Society of America, https://doi.org/10.1130/2012.2489(00).

Karlstrom, K.E., Lee, J.P., Kelley, S.A., Crow, R.S., Crossey, L.J., Young, R.A., Lazear, G., Beard, L.S., Ricketts, J.W., Fox, M., and Shuster, D.L., 2014, Formation of the Grand Canyon 5 to 6 million years ago through integration of older palaeocanyons: Nature Geoscience, v. 7, no. 3, p. 239–244, https://doi.org/10.1038/ngeo2065.

Karlstrom, K.E., Wilgus, J., Thacker, J.O., Schmandt, B., Coblentz, D., and Albonico, M., 2022, Tectonics of the Colorado Plateau and its margins: Annual Review of Earth and Planetary Sciences, v. 50, no. 1, p. 295–322, https://doi.org/10.1146/annurev-earth-032320-111432.

Kawano, M., and Tomita, K., 2001, Geochemical modeling of bacterially induced mineralization of Schwertmannite and Jarosite in sulfuric acid spring water: American Mineralogist, v. 86, no. 10, p. 1156–1165, https://doi.org/10.2138/am-2001-1005.

Kent, W.N., and Rawson, R.R., 1980, Depositional environments of the Mississippian Redwall Limestone in northeastern Arizona, *in* Fouch, T.D., and Magathan, E.R., eds., *Proceedings, Rocky Mountain Paleogeography Symposium, 1st*: Denver, CO, Society of Economic Paleontologists and Mineralogists, Rocky Mountain Section, p. 101–109.

Klimchouk, A., and Ford, D., 2000, Lithologies and structural controls of dissolutional cave development, *in* Bottrell, S.H., Gunn, J., Lowe, D.J., Klimchouk, A.B., Ford, D.C., Palmer, A.N., and Dreybrodt, W., eds., *Speleogenesis: Evolution of Karst Aquifers*: Huntsville, AL, National Speleological Society, p. 54–64.

Klimchouk, A., 2009, Morphogenesis of hypogenic caves: Geomorphology, v. 106, no. 1–2, p. 100–117, https://doi.org/10.1016/j.geomorph.2008.09.013.

Klimchouk, A., 2012, Speleogenesis, hypogenic, *in* White, W.B., and Culver, D.C., eds., *Encyclopedia of Caves* (2nd edition): Waltham, MA, Academic Press, p. 748–765, https://doi.org/10.1016/B978-0-12-383832-2.00110-9.

Klimchouk, A., Palmer, A.N., De Waele, J., Auler, A.S., and Audra, P., eds., 2017, *Hypogene Karst Regions and Caves of the World*: Cham, Springer, p. 911, https://doi.org/10.1007/978-3-319-53348-3.

Levy, D.B., 2007, Oxidation-reduction chemistry of Lechuguilla Cave seepage: Journal of Cave and Karst Studies, v. 69, no. 3, p. 351–358.

Mandl, G., 2005, *Rock Joints: The Mechanical Genesis*: Berlin, Springer, p. 230, https://doi.org/10.1007/b137623.

Marincea, S., Dumitraş, D.-G., Diaconu, G., and Bilal, E., 2004, Hydroxylapatite, brushite and ardealite in the bat guano deposit from Peştera Mare de la Mereşti, Perşani Mountains, Romania, Neues Jahrbuch fur Mineralogie Monatshefte, v. 10, p. 464–488.

McKee, E.D., 1963, Nomenclature for lithologic subdivisions of the Mississippian Redwall Limestone, Arizona: U.S. Geological Survey Professional Paper 475-C, p. C21–C22, https://doi.org/10.3133/pp475C.

McKee, E.D., and Gutschick, R.C., 1969, History of the Redwall Limestone of northern Arizona: Geological Society of America Memoir, v. 114, p. 726, https://doi.org/10.1130/MEM114-p1.

Mead, J.I., Tweet, J.S., Santucci, V.L., Tobin, B., Chambers, C.L., Thomas, S.C., and Carpenter, M.C., 2021, Pleistocene/Holocene cave fossils from Grand Canyon National Park-Ice Age (Pleistocene) flora, fauna, environments, and climate of the Grand Canyon, Arizona, *in* Santucci, V.L., and Tweet, J.S., eds., *Grand Canyon National Park Centennial Paleontological Resource Inventory—A Century of Fossil Discovery and Research*: Utah Geological Association Special Publication 1, p. 221–240.

Melchiorre, E.B., and Enders, M.S., 2003, Stable isotope geochemistry of copper carbonates at the Northwest Extension Deposit, Morenci District, Arizona: Implications for conditions of supergene oxidation and related mineralization: Economic Geology, v. 98, no. 3, p. 607–621, https://doi.org/10.2113/98.3.607.

Palmer, A.N., 1975, The Origin of Maze Caves: NSS Bulletin, v. 37, no. 3, p. 57–76.

Palmer, A.N., 1991, Origin and morphology of limestone caves: Geological Society of America Bulletin, v. 103, no. 1, p. 1–21, https://doi.org/10.1130/0016-7606(1991)103<0001:OAMOLC>2.3.CO;2.

Palmer, A.N., 2007, *Cave Geology*: Dayton, Ohio, Cave Books, 454 p.

Palmer, A.N., Palmer, M.V., and Paces, J.B., 2016, Geologic history of the Black Hills caves, South Dakota, *in* Feinberg, J.M., Gao, Y., and Alexander, E.C., eds., *Caves and Karst Across Time*: Geological Society of America Special Paper 516, p. 87–101, https://doi.org/10.1130/2015.2516(07).

Palmer, M.V., and Palmer, A.N., 2012, Petrographic and isotopic evidence for late-stage processes in sulfuric acid caves of the Guadalupe Mountains, New Mexico, USA: International Journal of Speleology, v. 41, no. 2, p. 231–250, https://doi.org/10.5038/1827-806X.41.2.10.

Pegler, S.S., Huppert, H.E., and Neufeld, J.A., 2014, Fluid migration between confined aquifers: Journal of Fluid Mechanics, v. 757, p. 330–353, https://doi.org/10.1017/jfm.2014.469.

Polyak, V., Hill, C., and Asmerom, Y., 2008, Age and evolution of the Grand Canyon revealed by U–Pb dating of water table-type speleothems: Science, v. 319, no. 5868, p. 1377–1380, https://doi.org/10.1126/science.1151248.

Polyak, V.J., Hill, C.A., Asmerom, Y., and Decker, D.D., 2017, A conceptual model for hypogene speleogenesis in Grand Canyon, Arizona, *in* Klimchouk, A., Palmer, A.N., De Waele, J., Auler, A.S., and Audra, P., eds., *Hypogene Karst Regions and Caves of the World*: Cham, Springer, p. 555–564, https://doi.org/10.1007/978-3-319-53348-3_34.

Polyak, V.P., and Provencio, P., 2001, By-product materials related to H_2S-H_2SO_4 influenced speleogenesis of Carlsbad, Lechuguilla, and other caves of the Guadalupe Mountains, New Mexico: Journal of Cave and Karst Studies, v. 63, no. 1, p. 23–32.

Roberts, G.G., White, N.J., Martin-Brandis, G.L., and Crosby, A.G., 2012, An uplift history of the Colorado Plateau and its surroundings from inverse modeling of longitudinal river profiles: Tectonics, v. 31, no. 4, p. 27, https://doi.org/10.1029/2012TC003107.

Sorauf, J.E., and Billingsley, G.H., 1991, Members of the Toroweap and Kaibab Formations, Lower Permian, northern Arizona and southwestern Utah: The Mountain Geologist, v. 28, no. 1, p. 9–24.

Spötl, C., Desch, A., Dublyansky, Y., Plan, L., and Mangini, A., 2016, Hypogene speleogenesis in dolomite host rock by CO_2 rich fluids, Kozak Cave (southern Austria): Geomorphology, v. 255, p. 39–48, https://doi.org/10.1016/j.geomorph.2015.12.001.

Spötl, C., Plan, L., and Dublyansky, Y., 2017, Hypogene karst in Austria, *in* Klimchouk, A., Palmer, A.N., De Waele, J., Auler, A.S., and Audra, P., eds., *Hypogene Karst Regions and Caves of the World*: Cham, Springer, p. 113–126, https://doi.org/10.1007/978-3-319-53348-3_6.

Sylvia, D.A., 1985, Depositional, diagenetic, and subsidence history of the Redwall Limestone, Grand Canyon National Park, Arizona [Master's thesis]: Tucson, University of Arizona, 265 p.

Tennyson, R., Brahana, V., Polyak, V.J., Potra, A., Covington, M., Asmerom, Y., Terry, J., Pollock, E., and Decker, D.D., 2017, Hypogene speleogenesis in the southern Ozark uplands, mid-continental United States, *in* Klimchouk, A., Palmer, A.N., De Waele, J., Auler, A.S., and Audra, P., eds., *Hypogene Karst Regions and Caves of the World*: Cham, Springer, p. 663–676, https://doi.org/10.1007/978-3-319-53348-3_43.

Tobin, B.W., Springer, A.E., Ballensky, J., and Armstrong, A., 2021, Cave and karst of the Grand Canyon World Heritage Site: Zeitschrift Für Geomorphologie, v. 62, no. 3, p. 125–144, https://doi.org/10.1127/zfg_suppl/2021/0693.

Wells, N.A., Waugh, D.A., and Foos, A.M., 2003, Some notes and hypotheses concerning iron and iron remobilization features in the Sharon Formation (Summit County, Ohio), *in* Foos, A.M., ed., *Pennsylvanian Sharon Formation, Past and Present: Sedimentology, Hydrogeology, and Historical and Environmental Significance: Ohio Division of Geological Survey Guidebook* 18: Columbus, OH, Department of Natural Resources, Division of Geological Survey, p. 33–37.

Wenrich, K.J., 1985, Mineralization of breccia pipes in northern Arizona: Economic Geology, v. 80, no. 6, p. 1722–1735, https://doi.org/10.2113/gsecongeo.80.6.1722.
Wenrich, K.J., and Sutphin, H.B., 1989, *Lithotectonic setting necessary for formation of a uranium-rich, solution-collapse Breccia-Pipe Province, Grand Canyon Region*: Arizona, U.S. Geological Survey Open-File Report 89-0173.
White, W.B., and White, E.L., 2003, Gypsum wedging and cavern breakdown: Studies in the Mammoth Cave System, Kentucky: Journal of Cave and Karst Studies, v. 65, no. 1, p. 43–52.

Mélida Gutiérrez, Claudia P. Colmenero-Chacón, and Kevin Mickus. Monitoring shallow groundwater quality in the Springfield Plateau of Missouri via Karst springs. *Journal of Cave and Karst Studies,* v. 88, nos. 1/2 p. 19-28. DOI:10.4311/2025ES0101

MONITORING SHALLOW GROUNDWATER QUALITY IN THE SPRINGFIELD PLATEAU OF MISSOURI VIA KARST SPRINGS

Mélida Gutiérrez[1,C], Claudia P. Colmenero-Chacón[1], and Kevin Mickus[1]

Abstract

Shallow groundwater plays an ever-important role in determining surface water quality and stream ecology. Since shallow groundwater is so readily affected by contaminants produced by human activities, its discharge to surface water may contribute to stream contamination; therefore, its monitoring is critical for protecting water resources. Seven rural karst springs from an area utilized for cattle grazing and pastureland in southwest Missouri, USA, were monitored for a year. Shallow wells in the vicinity of the sampled springs, plus two urban springs, were included to appraise the effect of land use on water quality. The study focused on NO_3−N and Cl as indicators of pollution. The results show (a) a specific pattern of concentrations for each spring and the season in which the concentration of pollutants peaked, (b) the underlying Ozark Aquifer was not significantly affected by leakage from the Springfield Plateau aquifer, and (c) compared with the urban springs, the rural springs had about the same NO_3−N content but less Cl. Two rural springs reached concentrations above 4 mg/L NO_3−N during the spring months, a concentration that may lead to eutrophication. The area experienced an abnormally dry period during this study, for which the results represent baseline conditions and the springs' response to an expected effect (longer droughts) of climate change.

INTRODUCTION

Compared to shallow aquifers, deep aquifers are commonly preferred as a drinking water source because they commonly have a better water quality that results from being farther from surface-derived human contamination (agricultural, sewage, and industrial), a distance that also allows for natural self-cleaning processes to take place (Zheng et al., 2005; Li et al., 2021). The longer and more tortuous path of groundwater as it moves to deeper parts of the aquifer cleanses contaminants by filtration as well as by chemical and biological processes (Gorelick and Zheng, 2015; Hare et al., 2021). Thus, shallow aquifers are less frequently used for drinking purposes and, therefore, monitored less.

Recent advances in the study of near-surface water processes and their association with the decline and degradation of water resources, such as the worldwide decline in the flow of streams and springs (Weissinger et al., 2016; Ranjan and Pandey, 2019; Currell and Katz, 2022) and degraded groundwater and stream water quality (MacDonald et al., 2016; Hare et al., 2021), have renewed the attention to shallow groundwater systems and the role these systems play in surface water quality and stream ecology (Lewandowski et al., 2020; Hare et al., 2021). Degradation of the water quality of streams has manifested predominantly in regions impacted by agricultural (Boumaiza et al., 2022; Jia and Qian, 2025) or urban pollution (Popp et al., 2024).

Shallow aquifers readily reflect changes in land use and are more vulnerable to pollution (Knierim et al., 2015; Lewandowski et al., 2020; Hare et al., 2021, Li et al., 2021). For example, changing forested land to agricultural land can cause induced groundwater recharge but also an increase in salinity due to the leaching of surface salts, fertilizer, and other surface contaminants (Scanlon et al., 2007; Bouselsal and Saibi, 2022). The degradation of water quality is becoming a critical problem in many different groundwater systems worldwide, such as semi-arid areas and overexploited aquifers (Bouselsal and Saibi, 2022). Currently, there are few environments where water resources are not threatened (Currell and Katz, 2022). Karst areas are also highly vulnerable to groundwater contamination due to groundwater flowing through large fractures and cave systems without natural filtration (Kresic, 2013; Maas et al., 2019, Tobin et al., 2021). Hence, the monitoring of shallow aquifers is important for the potential input of contaminants to their receiving streams and/or deeper aquifers and for the future availability of water resources (Weissinger et al., 2016; Lewandowski et al., 2020; Ferencz et al., 2022; Currell and Katz, 2022).

In non-industrialized areas, groundwater contamination commonly comes from human activities, including sewage, septic tanks, and urban runoff. This contamination can be toxic and long-lasting when persistent chemicals such as pharmaceuticals and pesticides are present (Adamski, 1997; Pope et al., 2009; MacDonald et al., 2016). As the contaminants present in sewage and agricultural waste can be many, consisting of one or more different solutes, a particular chemical is commonly utilized as an indicator. The choice of an indicator depends on the type of pollution expected in a particular region. Chemical compounds commonly utilized as indicators of agricultural and human-related contamination include nitrate (NO_3), total dissolved solids (TDS), and chloride (Cl). These chemical compounds are good water

[1]School of Earth, Environment and Sustainability, Missouri State University, Springfield, MI 65897
[C]Corresponding author: mgutierrez@missouristate.edu.

quality indicators because they are present in measurable concentrations, relatively soluble, stable under oxic conditions, and are associated with pollutants such as pesticides, pharmaceuticals, and organic micropollutants (Panno and Kelly, 2004).

Nitrate is a soluble, stable component under oxidizing conditions and has been labeled an anthropogenic contaminant because of its association with agricultural and domestic wastes (Jia and Qian, 2025). The nitrogen (N) cycle is complex; in agricultural areas, N can take various forms depending on the redox conditions. Under oxidizing conditions, it is mainly present as nitrate (NO_3^-), and under reduced conditions, NO_3^- is reduced to nitrite (NO_2^-), N_2O gas (nitrous oxide), and dinitrogen gas (N_2). Sources of N include the irrigation returns of overfertilized fields (either from synthetic N-fertilizers or manure), septic tank effluents, and treated and non-treated wastewater (Boumaiza et al., 2022; Hamlin et al., 2022). Nitrate is either expressed as NO_3 or the nitrogen in nitrate (NO_3−N). The U.S. Environmental Protection Agency drinking water guideline for nitrate is 10 mg/L NO_3−N (44.3 mg/L NO_3) (USEPA, 2012). However, recent research has found that even smaller concentrations, e.g., 4.0 mg/L NO_3−N may cause eutrophication of downstream water bodies and, if chronically ingested, serious health problems, including various types of cancers, hypothyroidism, and birth defects (García-Torres et al., 2022; Hamlin et al., 2022).

The impact of shallow groundwater input on stream quality has become an increasing concern after degradation in the quality of streams in various parts of the world became evident (MacDonald et al., 2016; Hare et al., 2021; Popp et al., 2024). A thorough monitoring of shallow groundwater quality and the various pathways that groundwater takes toward its receiving stream has been increasingly studied (Cey et al., 1998; Zheng et al., 2005; Hare et al., 2021). For example, streams carrying a large load of nutrients (especially NO_3 as it is the limiting factor for growth in ocean water) can cause ocean dead zones (Tagne and Dowling, 2020). Monitoring and the implementation of strategies to reduce the level of contaminants (e.g., nutrients) is needed, even at the small watershed scale (Tagne and Dowling, 2020). Water quality of the Springfield Plateau aquifer, a shallow carbonate aquifer, is reported here based on the monitoring of several karst springs (Fig. 1).

Seven rural and two urban karst springs discharging from the Springfield Plateau aquifer of southwest Missouri (Figs. 2 and 3) were monitored in 2023. Karst springs represent the hydrological connection between groundwater and surface water, and their water quality reflects the various activities occurring at the surface (Knierim et al., 2015; Katz, 2020; Currell and Katz, 2022). The land around the studied rural springs is used for pastureland and cattle grazing; six springs are in Lawrence County and one in the rural part of Greene County (Figs. 2 and 3). Lawrence County contains the largest number of cattle in Missouri (USDA, 2025). Tall fescue grass, the common pasture grass grown to feed the cattle, has a requirement of 195 kg per ha of N-fertilizer (4–5 lbs. per 1,000 ft^2) (Sleper and West, 1996). Because of the large number of cattle, the N-fertilization applied, and the abundant septic tanks, N-contamination in the unconfined Springfield Plateau aquifer was suspected, and to test this hypothesis, the water quality was monitored via springs for 1 year.

Monitoring the water quality of springs over time, especially NO_3−N concentrations, will indicate how much contamination is present in the Springfield Plateau aquifer, its seasonal variation, and the difference in water quality between urban and rural springs. The results can be compared to previous regional water studies conducted in this region to determine if water quality has changed from 1993 to 1995 (Adamski, 2000) to the present.

METHODS

Study Area

The study area is located within Lawrence and Greene counties in the Springfield Plateau region of southwest Missouri, USA (Fig. 2). The Springfield Plateau consists mostly of Mississippian and Ordovician carbonate rocks with minor amounts of clastic sedimentary

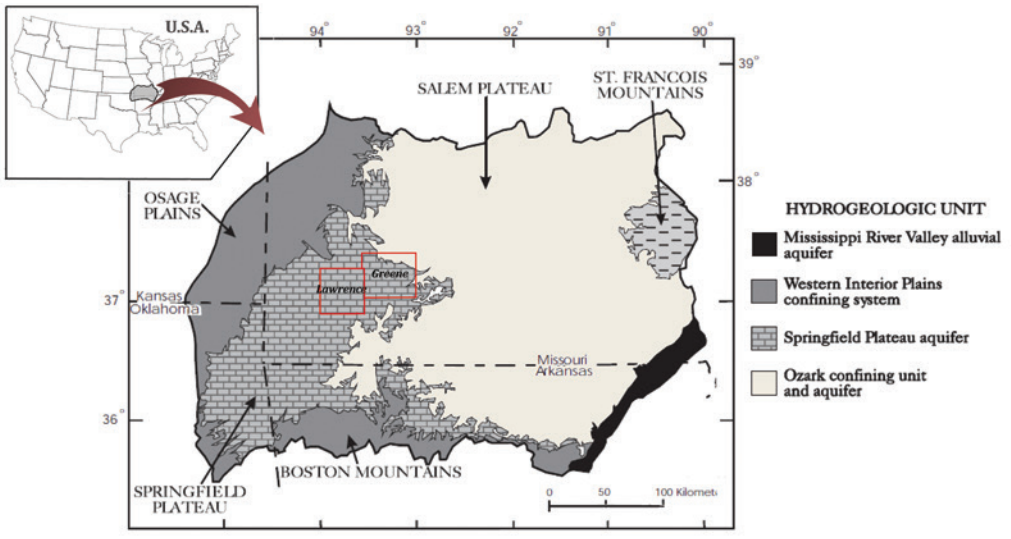

Figure 1. Hydrogeologic units and the various physiographic provinces (e.g., Springfield Plateau, Salem Plateau) that make up the Ozark Plateau physiographic province (modified from Adamski, 1997). Red boxes are Lawrence and Greene counties.

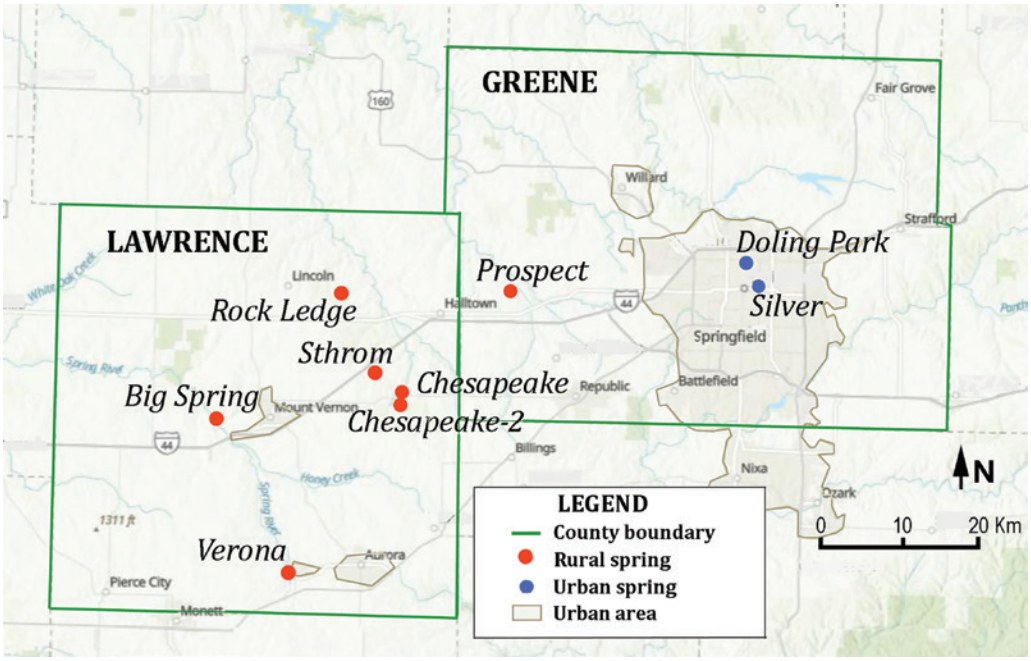

Figure 2. Location of sampled springs within Lawrence and Greene counties (Source: MODNR).

Figure 3. (a) Chesapeake Spring in Lawrence County and (b) Silver Spring in Springfield, Missouri, as examples of a rural and an urban spring, respectively. Photos by the authors.

units that are exposed in southwest Missouri and northwest Arkansas and extend into parts of Oklahoma and Kansas. The Mississippian-aged limestones comprise the Springfield Plateau aquifer, an unconfined aquifer with an average thickness of 30–60 m (Adamski, 2000; Clark et al., 2019). The Springfield Plateau aquifer varies in thickness, with an average of 60 m within the study area (Clark et al., 2019), and it is separated from the underlying Ozark aquifer by a thin (0–13 m) Ozark confining layer. The Ozark confining layer is absent in some areas.

The Burlington–Keokuk limestone of Mississippian age is a highly karstified rock that covers most of the study area, although the underlying Ordovician dolostone outcrops in a few locations in the northeast corner of Greene County and along the Chesapeake fault in Lawrence County (Fig. 4). This dolostone is the top of several carbonate rocks that form the Ozark aquifer.

Karstic aquifers are prone to contamination because of the secondary porosity formed after dissolution enlarges the fractures in carbonate rocks, facilitating the passage of contaminants to deeper parts of the aquifer. Despite this predisposition to contamination, few water quality studies have been conducted of the Springfield Plateau aquifer, with the notable exceptions of the studies by Imes and Davis (1990), Adamski and Pugh (1996), and Adamski (2000). One possible reason for it being less studied is that the Springfield Plateau aquifer is not a major source of drinking water, as the underlying Ozark aquifer is the major drinking water source for the region and has received more attention as a result (Pope et al., 2009; Kingsbury, 2020).

In this study, the water quality of seven rural springs and two urban springs is reported, as well as their seasonal variation and their response to the abnormally dry period experienced in the region during the summer and fall of 2023. The analysis focuses on the contaminants expected from the land use as pastureland and cattle grazing, namely NO_3–N and Cl concentrations, although all major ions and TDS were analyzed. The response of the springs to rain events was included by comparing water quality to the cumulative precipitation data from 3 days prior to sample collection reported by the nearest weather station (NWS, 2024).

In addition to the monitoring of the rural springs, a few private shallow (hand pump) wells located within 1 km of a studied spring were sampled once to detect possible NO_3–N leakage from the Springfield Plateau aquifer. Because the wells were hand-pumped, they are likely about 10 m (25–35 feet) deep and are tapped to the Springfield Plateau aquifer or to the top of the Ozark aquifer. The locations of the sampled wells are shown in Figure 4. The two sampled urban springs, Doling Park Spring and Silver Spring, discharge from the Springfield Plateau aquifer and are used to compare between rural and urban land use effects.

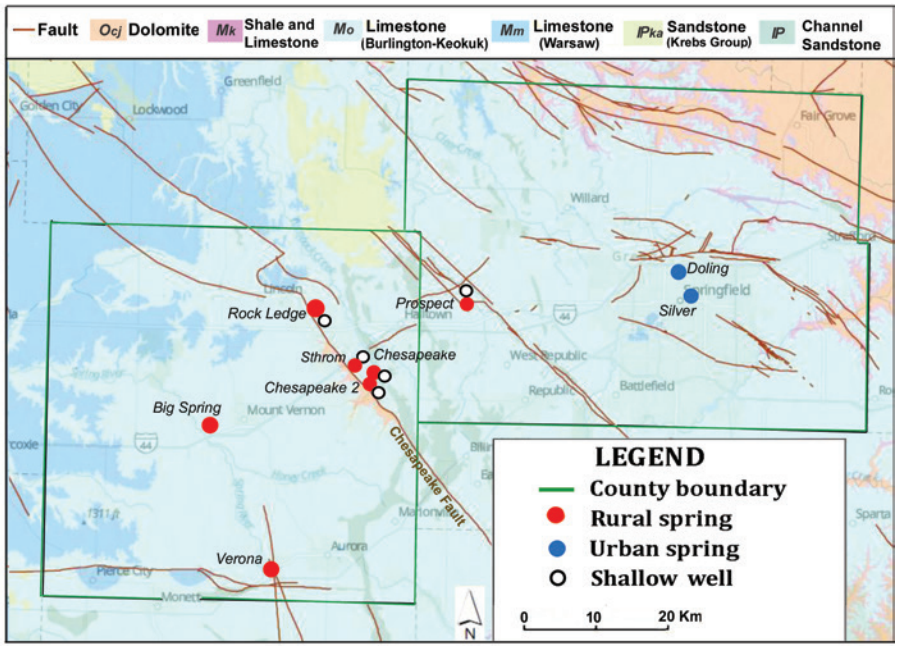

Figure 4. Geology of the study area and location of the sampled wells (Source: MODNR).

Sampling and Analyses

From the rural springs sampled, all but one had a name. The spring with no name will be referred here as Chesapeake 2 since it is near the Chesapeake Spring (see Fig. 2). The springs were sampled approximately monthly for 1 year, and their water quality analyzed according to standard guidelines and protocols (Clesceri et al., 1998). The urban springs were sampled at about the same times (within 2 days) as the rural springs. Samples were collected using acid-washed 1-L plastic bottles filled three times with samples and discarding the first two volumes of the sample. This sampling procedure was also followed for hand-pumped wells.

Samples were kept refrigerated after collection, and the pH and alkalinity were determined as soon as the samples arrived at the Water Laboratory at Missouri State University. The pH was determined by a Fisher Scientific pH meter and the alkalinity by titration with HCl 0.01 M. NO_3−N was determined by colorimetry using a Hach DR3900 Spectrophotometer and reagents for a 0.23–13.50 mg/L NO_3−N concentration range. Total and calcium (Ca) hardness were determined by titration with EDTA 0.005 M, from which Ca and magnesium (Mg) concentrations were calculated. Chloride concentrations were determined by the argentometric method, and sulfate (SO_4^{2-}) by the turbidimetric method (Clesceri et al., 1998). Sodium (Na) concentrations were determined using a PerkinElmer AAnalyst 300 Atomic Absorption Spectrometer. Potassium (K), present in small concentrations (0.9 mg/L K; Adamski, 2000), was estimated from the Mg content after correlation with regional water quality data. Pope et al. (2009) found the closest association of K to be with Mg. Detailed analysis procedures can be found in Colmenero-Chacón (2024).

Quality Assurance/Quality Control

Sampling bottles and glassware were acid-washed and rinsed with double-distilled water. Analyses were conducted using high-grade chemical reagents, and all analytical determinations followed standard procedures (Clesceri et al., 1998). Instruments (pH meter and turbidity meter) were calibrated daily. Replicates and blanks were run approximately every eighth sample, and the methods were tested by determining the concentrations of standard solutions (NO_3−N and SO_4) approximately every 15 samples. All blanks and standard solution calibrations were within the expected levels of below detection for blanks and within <1% error for standard solutions. In contrast, replicates had a small variation depending on the parameter. Chloride concentrations of replicates varied the most as the titrimetric method becomes less accurate at low concentrations. All other parameters had better replicability (<10% deviation), and the best was obtained for NO_3−N, with a variation among duplicates of ±0.01 ppm. The ionic balance (EB%) had an average of 1.83% and a maximum of 10%. A few samples surpassing 10% EB were discarded from the statistical results.

RESULTS AND DISCUSSION

The precipitation in 2023 was referred to by a drought monitor (NIDIS, 2024) as “abnormally low rain,” for which the springs are considered to have reached base level at the end of the summer. Visual inspection of the spring flow during sample collection indicated a relatively unchanged flow at some springs (Big Spring, Verona, and Chesapeake), whereas other springs (Rock Ledge) dried up by late summer, or their flow was significantly diminished (Prospect, Sthrom, and Chesapeake 2). The differences in the flows were assumed to reflect the size of a spring’s draining basin, and this characteristic presumably affected the water quality of a particular spring as well.

The water quality results are listed in Table 1. The Spearman correlation coefficients between the major ions and precipitation are shown in Table 2.

Interestingly, the NO_3−N concentrations did not correlate with any of the other parameters, whereas most of the other solutes (SO_4, Cl, Na, and TDS) correlated among themselves. As expected, Ca, HCO_3, and TDS concentrations had a strong inverse correlation with precipitation.

Table 1. Water quality data of rural springs in southwest Missouri and cumulative precipitation amounts for 3 days before sampling.

Sampling Date, 2023	pH	Alkalinity (mg/L $CaCO_3$)	HCO_3 (mg/L)	NO_3−N (mg/L)	Cl (mg/L)	SO_4 (mg/L)	Ca (mg/L)	Mg (mg/L)	Na (mg/L)	K (mg/L)	TDS (mg/L)	3-Day Precip., (in)
Prospect Spring												
Mar. 12	7.56	184	112	2.63	6.4	3.3	58.4	3.4	6.1	0.4	193	0.220
Apr. 02	7.55	180	110	2.47	5.7	0.7	63.2	10.7	7.4	1.2	201	0.850
May 07	7.64	240	146	2.85	11.0	4.7	92.0	3.9	8.6	0.4	270	0.000
Aug. 26	7.82	256	156	2.63	7.8	4.6	76.0	8.8	6.4	1.0	263	0.000
Sep. 30	7.86	236	144	2.36	9.9	7.0	78.4	11.2	7.5	1.2	262	0.000
Nov. 04	7.92	224	137	2.35	6.4	3.4	74.4	16.0	7.8	1.8	249	0.000
Nov. 25	8.20	228	139	2.40	5.7	2.5	76.8	15.1	8.2	1.7	251	0.000
Rock Ledge Spring												
Apr. 02	7.33	176	107	2.46	5.0	4.9	60.8	9.2	5.7	1.0	196	0.850
May 07	7.25	212	129	2.10	7.1	7.2	66.4	1.5	6.1	0.2	221	0.000
Aug. 26	7.46	256	156	2.74	9.9	2.1	77.6	9.2	4.4	1.0	263	0.000
Sep. 30	7.39	212	129	2.18	9.2	2.0	68.0	12.2	3.9	1.3	228	0.000
Sthrom Spring												
Mar. 12	7.01	180	110	2.69	1.4	2.8	61.6	4.9	5.1	0.5	189	0.220
Apr. 02	7.01	180	110	2.28	2.1	3.4	64.0	7.3	7.9	0.8	198	0.850
May 07	7.01	180	110	2.19	5.3	3.3	67.2	4.4	6.0	0.5	199	0.000
Aug. 26	7.18	299	182	2.95	7.8	3.3	87.2	5.3	5.4	0.6	295	0.000
Sep. 30	7.38	232	142	2.71	8.5	2.0	87.2	10.2	6.8	1.1	260	0.000
Nov. 04	7.32	240	146	2.95	12.8	5.9	91.2	16.0	10.0	1.8	286	0.000
Dec. 11	7.41	244	149	2.92	12.1	5.5	97.6	10.7	10.4	1.2	289	0.000
Chesapeake Spring												
Mar. 12	6.91	176	107	3.65	<0.7	2.3	54.4	12.2	5.2	1.3	186	0.220
Apr. 02	6.97	180	110	3.40	5.4	2.0	55.2	14.6	6.1	1.6	197	0.850
May 07	6.89	150	92	3.12	2.1	2.0	50.4	11.7	5.3	1.3	167	0.000
Aug. 26	7.26	200	122	2.97	8.5	2.6	56.8	14.1	4.0	1.6	212	0.000
Sep. 30	7.18	188	115	2.90	5.7	0.8	53.6	19.0	3.4	2.1	201	0.000
Nov. 04	7.27	200	122	3.25	4.3	2.8	85.6	15.1	6.3	1.7	240	0.000
Dec. 11	7.34	240	146	3.30	6.4	0.9	86.4	17.5	6.2	1.9	268	0.000
Chesapeake 2												
Mar. 12	7.14	176	107	1.73	<0.7	2.0	40.0	9.7	3.0	1.1	165	0.220
Apr. 02	7.16	152	93	1.30	2.1	1.0	40.0	13.6	4.2	1.5	156	0.850
May 07	7.15	156	95	1.05	<0.7	0.8	44.0	12.2	2.9	1.3	157	0.000
Aug. 26	7.24	214	131	1.40	<0.7	2.5	60.8	10.7	2.3	1.2	209	0.000
Sep. 30	7.24	196	120	1.29	4.3	2.9	59.2	17.5	2.0	1.9	207	0.000
Nov. 04	7.38	252	154	1.38	5.0	2.6	88.0	17.5	2.8	1.9	272	0.000
Dec. 11	7.45	252	154	1.44	3.6	0.6	80.0	24.8	2.8	2.8	268	0.000
Big Spring												
Apr. 02	6.87	156	95	4.18	0.7	5.1	60.0	6.8	6.1	0.8	179	0.850
May 07	6.93	156	95	3.88	11.4	3.0	56.0	9.7	5.7	1.1	186	0.000
Aug. 26	7.07	212	129	3.32	9.2	4.2	71.2	1.9	5.6	0.2	226	0.000

Continued

Table 1. *Continued*

Sep. 30	7.13	184	112	3.84	7.1	5.2	65.6	7.3	4.8	0.8	207	0.000
Nov. 04	7.07	176	107	3.49	12.8	5.9	70.4	14.1	8.0	1.6	223	0.000
Dec. 11	7.20	188	115	4.10	7.1	1.1	69.6	11.2	8.4	1.2	217	0.000
Verona Spring												
Mar. 12	6.85	108	66	5.77	<0.7	3.9	45.6	4.9	5.1	0.5	132	0.220
Apr. 02	6.85	108	66	6.09	<0.7	5.2	40.0	8.7	7.2	1.0	134	0.850
May 07	6.73	212	129	4.35	9.9	4.9	48.8	4.4	4.8	0.5	207	0.000
Aug. 26	7.01	172	105	3.42	5.0	4.0	65.6	3.9	4.2	0.4	192	0.000
Sep. 30	6.96	168	102	3.65	7.1	4.3	60.0	6.3	3.8	0.7	189	0.000
Nov. 04	7.09	164	100	2.74	7.1	4.0	63.2	23.3	6.5	2.6	208	0.000
Dec. 11	7.91	200	122	3.89	7.8	1.0	68.0	8.3	5.7	0.9	218	0.000

Table 2. Spearman correlation (ρ) among rural springs, with significant correlation ($p < 0.05$) in bold.

	HCO_3	NO_3–N	Cl	SO_4	Ca	Mg	Na	TDS	Precip.
HCO_3	1.00	−0.17	**0.53**	0.18	**0.86**	0.20	0.18	**0.96**	**−0.77**
NO_3–N		1.00	0.30	0.31	−0.06	−0.24	0.30	0.11	0.10
Cl			1.00	**0.43**	**0.57**	−0.13	**0.47**	**0.61**	−0.35
SO_4				1.00	**0.38**	**−0.49**	**0.54**	0.25	−0.07
Ca					1.00	−0.01	**0.47**	**0.93**	**−0.53**
Mg						1.00	−0.28	0.22	**−0.40**
Na							1.00	0.31	0.12
TDS								1.00	**−0.70**
Precip.									1.00

Note: Precip. = cumulative precipitation amounts for the 3 days before sampling date.

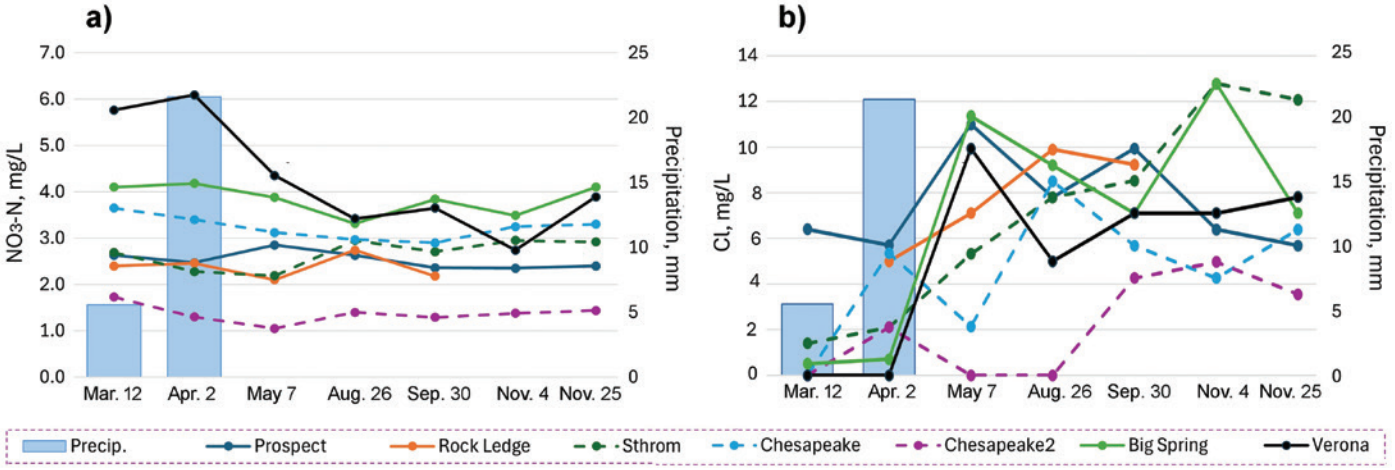

Figure 5. Concentration patterns of (a) NO_3–N and (b) Cl as a function of time for each of the seven rural springs.

The concentrations of the two parameters of interest (NO_3–N and Cl) are plotted in Figure 5 to better visualize their variation with respect to time. Figure 5 shows that each spring had its own pattern of water quality, but the response of each spring to the lack of precipitation differed; while the NO_3–N concentrations became more constant at a lower concentration, Cl concentrations increased with time.

Fescue grass is generally fertilized during the mid-spring months, which may explain that the highest NO_3–N concentrations were observed in late spring, after which the concentrations stayed at a lower level (from 1.5 mg/L NO_3–N for Chesapeake 2 Spring to 4.1 mg/L NO_3–N for Big Spring). All the rural springs had a relatively low NO_3–N concentration, which suggests that the human activities on the surface (cattle farming and pastureland) follow best practices and cause little impact on the Springfield Plateau aquifer in the vicinity of the sampled springs. The highest NO_3–N concentrations,

up to 5.9 mg/L NO_3−N, were detected during the late spring months at the Verona and Big springs, both located in the western part of the study area and near the headwaters of the Spring River (Fig. 2), but all other parameters were low. These high NO_3−N concentrations may have resulted from the septic tank leaching fields of nearby farms, and their presence attests to the susceptibility of contamination of karst regions. The behavior of Cl was to gradually increase with time, which may be, at least in part, a concentration effect, as there was a long period of little to no precipitation.

Concentrations of NO_3−N reached a peak in the spring, and an increase of Cl in the fall and early winter was also reported in another cattle-grazing area within the Springfield Plateau in the nearby Polk County, where, unlike this study, precipitation in 2022 was abundant during spring and summer (Gomez and Gutiérrez, 2022).

To visually compare the results between the rural and urban springs, chemical concentrations of four rural springs (Sthrom, Chesapeake, Big Spring, and Verona) were plotted together with the two urban springs (Doling Park and Silver, in red), as shown in Figure 6. The NO_3−N concentrations of the urban springs had similar concentrations and responses to precipitation than the rural springs. In contrast, Cl concentrations of the urban springs were higher and more erratic than those of the rural springs.

The water quality of the springs within Lawrence County was compared with other studies within the Springfield Plateau aquifer, as shown in Table 3. The NO_3−N concentrations showed little change from 1993 to 1995 (Adamski, 2000) to the present. In contrast, a large difference exists between NO_3−N values obtained in this study and those reported for nearby unconfined carbonate aquifers of Iowa and Illinois (Table 3). The consistently low concentrations of the above chemicals within the springs of the Springfield Plateau are likely a result of rainfall comprising the recharge, a short residence time due to the large fractures in the karstified rock, and a sustainable operation of pastureland and cattle grazing activities. In contrast, increased concentrations of the same chemicals within the karst areas in Illinois and Iowa are likely the result of lateral flows contributing to aquifer recharge in addition to precipitation as well as leakage from agricultural activities that include growing a variety of row crops (Maas et al., 2019; Schilling et al., 2019).

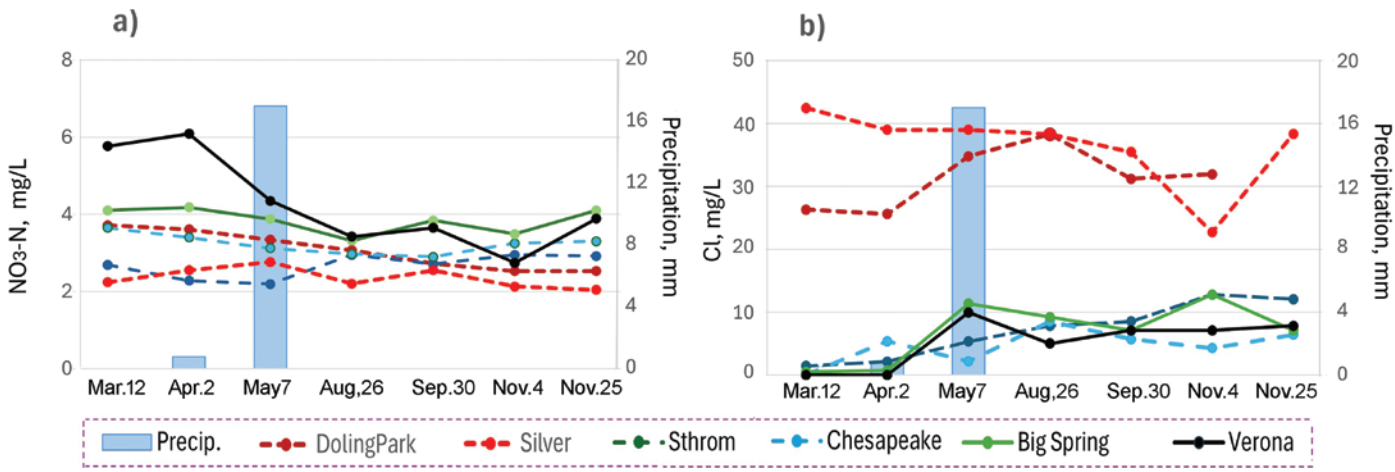

Figure 6. Concentrations of (a) NO_3−N and (b) Cl for selected urban and rural springs. Urban springs (Doling Park, Silver) are shown in red.

Table 3. Summary of water quality studies on karst springs within the Springfield Plateau aquifer and nearby carbonate aquifers.

	NO_3−N (mg/L)			Cl (mg/L)			
No. Springs	**Min.**	**Ave.**	**Max.**	**Min.**	**Ave.**	**Max.**	**References**
Springfield Plateau Aquifer							
7	1.05	2.91	6.09	<0.7	5.92	12.8	This study
61 (+50 wells)	<0.05	1.90	25.00	0.9	5.90	220	Adamski (2000)
1	0.6	2.27	5.70	1.0	5.60	15.0	Knierim et al. (2015)
5	0.05	1.39	6.00	0.5	11.70	67.5	Gomez and Gutiérrez (2022)
1	2.74	4.07	4.79	n.a.	n.a.	n.a.	Peterson et al. (2002)
Other Carbonate Aquifers (Illinois, Iowa)							
5	2.92	15.53	30.10	5.4	18.63	26.7	Maas et al. (2019)
2	3.64	14.69	22.12	n.a.	n.a.	n.a.	Schilling et al. (2019)

n.a. = not available.

Table 4. Water quality of springs in the study area (average values) and its nearby hand-pumped well.

	No. samples		NO_3−N (mg/L)		Cl (mg/L)		TDS (mg/L)	
	Spring	Well	Spring	Well	Spring	Well	Spring	Well
Prospect	7	1	2.53	0.56	7.6	2.1	238	172
Rock Ledge	4	1	2.46	0.31	8.0	5.7	229	346
Sthrom	7	1	2.62	0.04	7.0	6.4	237	289
Chesapeake	7	1	2.90	0.92	4.0	<0.7	214	269
Chesapeake 2	7	1	2.88	0.80	4.1	0.7	208	224

Because the Ozark confining layer may be very thin and fractured, the potential leakage of contaminants from the Springfield Plateau aquifer to the underlying Ozark aquifer was tested by comparing the water quality concentration data (NO_3−N, Cl, and TDS) between each of the five springs in the study area and water collected from hand-pumped wells near (within 1 km) each spring. The shallow wells, since they are hand-pumped wells, typically draw water from 8 to 11 m (25–35 feet) deep and thus collect water from the Springfield Plateau aquifer. The wells were selected based on the availability to collect a sample, as they were private wells. The water quality results are listed in Table 4.

The concentrations, as shown in Table 4, show a sharp decrease in NO_3−N concentrations in the well water compared to that of the spring water, a less pronounced decrease in Cl concentrations, and a small increase in TDS. The TDS increase is expected because of the increased dissolution that results from a longer water–carbonate rock contact. The drought conditions during the sampling period suggest that these values are possibly the most concentrated values encountered in these springs, and that once precipitation returns to normal conditions, concentrations will decrease because of dilution.

Overall, and although the water quality of each spring was unique, all the springs complied with drinking water quality guidelines, thus there is little concern for contamination of the underlying aquifer with leakage from the Springfield Plateau aquifer. However, this conclusion may change if the Springfield Plateau aquifer becomes contaminated in the future, which is possible due to expanding housing development in the region as well as changes in precipitation due to climate change. Continued monitoring of water quality is recommended to keep both the Springfield Plateau and Ozark aquifers safe from contamination.

CONCLUSIONS

Despite the prevalence of agricultural (pastureland) land use and the large number of cattle in the study area in southwest Missouri, the water quality of the Springfield Plateau aquifer complies with drinking quality guidelines of the contaminants of interest, 10 mg/L NO_3−N and 250 mg/L Cl (USEPA, 2012). The results suggest that the number of cattle and farming activities has little to no negative impact on the water quality of the Springfield Plateau and Ozark aquifers in Lawrence County. Only two of the seven monitored springs showed NO_3−N concentrations above 4.0 mg/L, an unenforced limit to prevent eutrophication and ocean dead zones. Chloride concentrations remained low in rural springs, with values up to 12.8 mg/L, and higher but modest Cl concentrations (up to 42 mg/L) were observed in urban springs.

Despite being relatively close to each other, each spring possessed its own pattern of concentrations in response to seasonal changes in precipitation and farming activities such as fertilization application. Seasonal variations showed an increase in NO_3−N concentrations in late spring and in Cl concentrations in late fall. Oddly, NO_3−N values did not correlate with other water parameters nor with precipitation, whereas the other parameters (Ca, Mg, Na, Cl, and SO_4) were associated with each other as well as with precipitation. The low concentrations of contaminants suggest that even if the Springfield Plateau aquifer were to leak into the underlying aquifer, contamination is not a concerning issue at this time, as even though the region was experiencing a drought and water was concentrated with solutes, these remained at low concentrations. A water quality baseline for the Springfield Plateau aquifer in Lawrence County, Missouri, was obtained.

ACKNOWLEDGMENTS

This study was partially funded by the Graduate College of Missouri State University. The authors also acknowledge the National Science Foundation 1828069 CHE grant that awarded Missouri State University the Inductively Coupled Plasma Mass Spectrometer system utilized in this study.

REFERENCES

Adamski, J.C., and Pugh, A.L., 1996, Occurrence of pesticides in ground water of the Ozark Plateaus Province: JAWRA Journal of the American Water Resources Association, v. 32, no. 1, p. 97–105.

Adamski, J.C., 1997, Nutrients and pesticides in ground water of the Ozark Plateaus in Arkansas, Kansas, Missouri, and Oklahoma, Arkansas, Little Rock: USGS Water-Resources Investigations Report 96-4313, 34 p.

Adamski, J., 2000, Geochemistry of the Springfield Plateau aquifer of the Ozark Plateaus Province in Arkansas, Kansas, Missouri and Oklahoma, USA: Hydrological Processes, v. 14, no. 5, p. 849–866.

Boumaiza, L., Walter, J., Chesnaux, R., Huneau, F., Garel, É., Erostate, M., Johannesson, K.H., Vystavna, Y., Bougherira, N., Bordeleau, G., Stotler, R.L., Blarasin, M., Gutiérrez, M., Knöller, K., and Stumpp, C., 2022, Multi-tracer approach to understand nitrate contamination and groundwater-surface water interactions in the Mediterranean coastal area of Guerbes-Senhadja, Algeria: Journal of Contaminant Hydrology, v. 251, p. 104098, https://doi.org/10.1016/j.jconhyd.2022.104098.

Bouselsal, B., and Saibi, H., 2022, Evaluation of groundwater quality and hydrochemical characteristics in the shallow aquifer of El-Oued region (Algerian Sahara): Groundwater for Sustainable Development, v. 17, p. 100747, https://doi.org/10.1016/j.gsd.2022.100747.

Cey, E.E., Rudolph, D.L., Parkin, G.W., and Aravena, R., 1998, Quantifying groundwater discharge to a small perennial stream in southern Ontario, Canada: Journal of Hydrology, v. 210, no. 1–4, p. 21–37.

Clark, B.R., Duncan, L.L., and Knierim, K.J., 2019, Groundwater availability in the Ozark Plateaus aquifer system: U.S. Geological Survey Professional Paper 1854, 82 pp, https://doi.org/10.3133/pp1854.

Clesceri, L.S., Greenberg, A.E., and Eaton, A.D., 1998, Standard Methods for the Examination of Water and Wastewater, 20th ed.: Washington, DC, American Public Health Association, American Water Works Association, Water Environmental Federation, 1,325 pp.

Colmenero-Chacón, C.P., 2024, Water quality of a karstic shallow aquifer in Greene and Lawrence counties, Missouri [M.S. thesis]: Missouri State University, 127 pp.

Currell, M.J., and Katz, B.G., 2022, *Threats to Springs in a Changing World: Science and Policies for Protection*, Vol. 275: John Wiley and Sons.

Ferencz, B., Dawidek, J., and Bronowicka-Mielniczuk, U., 2022, Alteration of yield and springs number as an indicator of climate changes. Case study of Eastern Poland: Ecological Indicators, v. 138, p. 108798, https://doi.org/10.1016/j.ecolind.2022.108798.

García-Torres, E., Pérez-Morales, R., González-Zamora, A., and Calleros-Rincón, E.Y., 2022, Subclinical hypothyroidism in families due to chronic consumption of nitrate-contaminated water in rural areas with intensive livestock and agricultural practices in Durango, Mexico: Water, v. 14, no. 3, p. 282, https://doi.org/10.3390/w14030282.

Gomez, R., and Gutiérrez, M., 2022, Water quality monitoring of five karst springs within a pastureland in southwest Polk County, Missouri: Environmental & Engineering Geoscience, v. 28, p. 387–396, https://doi.org/10.2113/EEG-D-21-00115.

Gorelick, S.M., and Zheng, C., 2015, Global change and the groundwater management challenge: Water Resources Research, v. 51, no. 5, p. 3031–3051, https://doi.org/10.1002/2014WR016825.

Hamlin, Q., Martin, S., Kendall, A., and Hyndman, D., 2022, Examining relationships between groundwater nitrate concentrations in drinking water and landscape characteristics to understand health risks: GeoHealth, v. 6, no. 5, p. e2021GH000524, https://doi.org/10.1029/2021GH000524.

Hare, D.K., Helton, A.M., Johnson, Z.C., Lane, J.W., and Briggs, M.A., 2021, Continental-scale analysis of shallow and deep groundwater contributions to streams: Nature Communications, v. 12, no. 1, p. 1450, https://doi.org/10.1038/s41467-021-21651-0.

Imes, J.L., and Davis, J.V., 1990, Water type and concentration of dissolved solids, chloride, and sulfate in water from the Springfield Plateau aquifer in Missouri, Arkansas, Kansas, and Oklahoma: U.S. Geological Survey Hydrologic Investigations Atlas HA-711-L, 2 Sheets, https://doi.org/10.3133/ha711L.

Jia, H., and Qian, H., 2025, Groundwater nitrate response to hydrogeological conditions and socioeconomic load in an agriculture dominated area: Scientific Reports, v. 15, no. 1, p. 1315, https://doi.org/10.1038/s41598-024-84318-y.

Katz, B.G., 2020, Nitrate contamination in springs, in Katz, B.G., ed., *Nitrogen Overload: Environmental Degradation, Ramifications and Economic Costs*, New York, John Wiley and Sons: American Geophysical Union Geophysical Monograph 250, 155–174 pp.

Kingsbury, J.A., 2020, Groundwater quality in the Ozarks Plateaus Aquifer Systems, Central United States: USGS Fact Sheet 2019-3057, https://doi.org/10.3133/fs20193057.

Kresic, N., 2013, *Water in Karst. Management, Vulnerability, and Restoration*: McGraw Hill, 708 p.

Knierim, K.J., Hays, P.D., and Bowman, D., 2015, Quantifying the variability in *Escherichia coli* (*E. coli*) throughout storm events at a karst spring in northwestern Arkansas, United States: Environmental Earth Sciences, v. 74, no. 6, p. 4607–4623, https://doi.org/10.1007/s12665-015-4416-5.

Lewandowski, J., Meinikmann, K., and Krause, S., 2020, Groundwater–surface water interactions: Recent advances and interdisciplinary challenges: Water, v. 12, no. 1, p. 296, https://doi.org/10.3390/w12010296.

Li, P., Karunanidhi, D., Subramani, T., and Srinivasamoorthy, K., 2021, Sources and consequences of groundwater contamination: Archives of Environmental Contamination and Toxicology, v. 80, no. 1, p. 1–10, https://doi.org/10.1007/s00244-020-00805-z.

Maas, B., Peterson, E.W., Honings, J., Oberhelman, A., Oware, P., Rusthoven, I., and Watson, A., 2019, Differentiation of surface water and groundwater in a karst system using anthropogenic signatures: Geosciences, v. 9, no. 4, p. 148, https://doi.org/10.3390/geosciences9040148.

MacDonald, A.M., Bonsor, H.C., Ahmed, K.M., Burgess, W.G., Basharat, M., Calow, R.C., Dixit, A., Foster, S.S.D., Gopal, K., Lapworth, D.J., Lark, R.M., Moench, M., Mukherjee, A., Rao, M.S., Shamsudduha, M., Smith, L., Taylor, R.G., Tucker, J., van Steenbergen, F., and Yadav, S.K., 2016, Groundwater quality and depletion in the Indo-Gangetic Basin mapped from *in situ* observations: Nature Geoscience, v. 9, no. 10, p. 762–766, https://doi.org/10.1038/NGEO2791.

MODNR Missouri Department of Natural Resources GEOSTRAT: https://dnr.mo.gov/land-geology/maps-data-research/geosciences-technical-resource-assessment-tool-geostrat (accessed May, 2025).

National Integrated Drought Information System, NIDIS: https://www.drought.gov/data-maps-tools/us-drought-monitor (accessed December 1, 2024).

National Weather Service (NWS), 2024, Springfield, Missouri: https://www.weather.gov/sgf/ (accessed December 1, 2024).

Panno, S.V., and Kelly, W.R., 2004, Nitrate and herbicide loading in two groundwater basins of Illinois' sinkhole plain: Journal of Hydrology, v. 290, no. 3–4, p. 229–242, https://doi.org/10.1016/j.hydrol.2003.12.017.

Peterson, E.W., Davis, R.K., Brahana, J.V., and Orndorff, H.A., 2002, Movement of nitrate through regolith covered karst terrane, NW Arkansas: Journal of Hydrology, v. 256, no. 1–2, p. 35–47.

Pope, L.M., Mehl, H.E., and Coiner, R., 2009, Quality characteristics of ground water in the Ozark aquifer of northwestern Arkansas, southeastern Kansas, southwestern Missouri, and northeastern Oklahoma, 2006–07: U.S. Geological Survey Scientific Investigations Report 2009-5093, 60 p.

Popp, A.L., Weatherl, R., Moeck, C., Hollender, J., and Schirmer, M., 2024, Assessing hydrology, biogeochemistry, and organic micropollutants in an urban stream-aquifer system: An interdisciplinary data set: Journal of Geophysical Research: Biogeosciences, v. 129, no. 1, p. e2023JG007827, https://doi.org/10.1029/2023JG007827.

Ranjan, P., and Pandey, P.K., 2019, Reviving, development and protection of springs to increase water security in the Himalayan region, in Proceedings of 5th International Conference on Computers and Management Skills (ICCM) 2019: Computer Science Research Network, pp. 25–29. ISSN: 1556-5068

Scanlon, B.R., Jolly, I., Sophocleous, M., and Zhang, L., 2007, Global impacts of conversions from natural to agricultural ecosystems on water resources: quantity versus quality: Water Resources Research, v. 43, no. 3, p. 3, https://doi.org/10.1029/2006WR005486.

Schilling, K.E., Jones, C.S., Clark, R.J., Libra, R.D., Liang, X., and Zhang, Y., 2019, Contrasting NO_3−N concentration patterns at two karst springs in Iowa (USA): Insights on aquifer nitrogen storage and delivery: Hydrogeology Journal, v. 27, no. 4, p. 1389–1400, https://doi.org/10.007/s10040-019-01935-y.

Sleper, D.A., and West, C.P., 1996, Tall fescue: Cool-Season Forage Grasses, v. 34, p. 471–502, https://doi.org/10.2134/agronmonogr34.c15.

Tagne, G.V., and Dowling, C., 2020, Land-use controls on nutrient loads in aquifers draining agricultural and mixed-use karstic watersheds: Environmental Monitoring and Assessment, v. 192, no. 3, p. 168, https://doi.org/10.1007/s10661-020-8126-4.

Tobin, B.W., Polk, J.S., Arpin, S.M., Shelley, A., and Taylor, C., 2021, A conceptual model of epikarst processes across sites, seasons, and storm events: Journal of Hydrology, v. 596, p. 125692, https://doi.org/10.1016/j.jhydrol.2020.125692.

U.S. Department of Agriculture: https://www.nass.usda.gov/Statistics_by_State/Missouri/Publications/County_Estimates/index.php (accessed 31 January, 2025).

U.S. Environmental Protection Agency: *2012 Edition of the Drinking Water Standards and Health Advisories*: Washington, Office of Water: www.epa.gov/dwstandardsregulations/drinking-water-standards-and-health-advisory-tables (accessed 3 May, 2025).

Weissinger, R., Philippi, T.E., and Thoma, D., 2016, Linking climate to changing discharge at springs in Arches National Park, Utah, USA: Ecosphere, v. 7, no. 10, p. e01491, https://doi.org/10.1002/ecs2.1491.

Zheng, Y., van Geen, A., Stute, M., Dhar, R., Mo, Z., Cheng, Z., Horneman, A., Gavrieli, I., Simpson, H.J., Versteeg, R., Steckler, M., Grazioli-Venier, A., Goodbred, S., Shahnewaz, M., Shamsudduha, M., Hoque, M.A., and Ahmed, K.M., 2005, Geochemical and hydrogeological contrasts between shallow and deeper aquifers in two villages of Araihazar, Bangladesh: Implications for deeper aquifers as drinking water sources: Geochimica et Cosmochimica Acta, v. 69, no. 22, p. 5203–5218, https://doi.org/10.1016/j.gca.2005.06.001.

Sanjeef Kumr Subramaniam, Nur Muhammad Taufiq-Makmor, Tan Weng Hui, Mohammed Rizman-Idid, Hasmahzaiti Omar, Abiramy Krishnan, and Siti Aisyah Alias. Environmental DNA metabarcoding of fungi associated with bat guano in Wang Burma Cave (Perlis, Peninsular Malaysia). Journal of Cave and Karst Studies, v. 88, no. 1/2, p. 29-37. DOI: 10.4311/2024MB0117

ENVIRONMENTAL DNA METABARCODING OF FUNGI ASSOCIATED WITH BAT GUANO IN WANG BURMA CAVE (PERLIS, PENINSULAR MALAYSIA)

Sanjeef Kumr Subramaniam[1,2,3], Nur Muhammad Taufiq-Makmor[4], Tan Weng Hui[4], Mohammed Rizman-Idid[1,2], Hasmahzaiti Omar[4], Abiramy Krishnan[5], and Siti Aisyah Alias[1,2,C]

Abstract

Discoveries of unique, undescribed cave-dwelling species exhibiting extreme endemism demonstrate their biodiversity richness and specialization to such exclusive environments. Studies on fungi in caves enable understanding of their diversity, distribution, evolution, and physiology, and also facilitate the discovery of harmful pathogens or beneficial species. We hypothesize that Ascomycota would be the dominant phylum associated with bat guano samples, consistent with previous findings from Asian cave systems. This study is the first to document cave fungi species in Peninsular Malaysia through environmental DNA metabarcoding, specifically to identify the species composition of fungi within bat guano samples from Wang Burma Cave, Perlis. Thirty-two distinct amplicon sequence variants were detected among 380,856 sequence reads, revealing Ascomycota as the dominant fungal phylum (>99.99%). Thirteen species were identified, including five new records for Malaysia: *Aspergillus caninus*, *A. chlamydosporus*, *A. phialosimplex*, *Candida palmioleophila*, and *Mortierella rhinolophicola. Penicillium simplicissimum* was the most dominant species (67%) across all sampling sites. This study provides the first molecular record of cave-associated fungi in Peninsular Malaysia and highlights the ecological and conservation significance of subterranean fungal communities as indicators of cave ecosystem health.

INTRODUCTION

Fungi are incredibly diverse and have crucial ecological functions worldwide (Tedersoo et al., 2014; Powell and Rillig, 2018). Fungi can be found in a variety of forms in cave environments; each one adapted to the special circumstances present in these subterranean habitats. A specific collection of environmental factors that affect the growth and development of fungi is present in caves (Farda et al., 2022). These conditions include low light levels, high humidity, stable temperatures, and limited nutrient availability (Ren et al., 2021; Mammola et al., 2022). As a result, cave fungi have evolved fascinating adaptations to thrive in such harsh conditions.

Cave fungi refer to the various species of fungi that are specifically adapted to and found within cave environments. Cave fungi are sometimes also known as troglobitic fungi, and the term “troglobitic” is derived from the Greek words “troglos” (cave) and “bios” (life), indicating their specialized adaptation to cave habitats (Saikia and Ruedi, 2021). Strict definition of troglobitic fungi would refer to a species or population that is bound to a subterranean habitat strictly, in other words, true cave life (Sket, 2008). Real obligate troglobitic fungi imply a cave origin and evolution. However, most of the currently discovered fungi from caves were known from other environments (Vanderwolf et al., 2013; Zhang et al., 2017). Zhang et al. (2017) suggested that cave fungi may have an origin from outside the cave environment. Cave fungi have unique characteristics and adaptations that allow them to thrive in the challenging conditions found within caves. These fungi play important ecological roles within cave ecosystems. They often act as decomposers, breaking down organic matter such as bat guano, decaying plant material, or animal remains and recycling nutrients back into the cave ecosystem (Nieves-Rivera et al., 2009; Karkun et al., 2012; Out et al., 2016). In fact, one of the most excellent substrates for the development and reproduction of cave fungi is bat guano (Ogórek et al., 2016; Dimkić et al., 2021). The diet (frugivorous, insectivorous, or sanguivorous) of the bat may have an impact on the nutrient content of its guano (Emerson and Roark, 2007; Cunha et al., 2020). Studying cave fungi requires specialized methods and techniques due to their unique habitat and adaptations. Once collected, cave fungal specimens are examined and identified by mycologists using morphological, microscopic, and molecular techniques (Alsohaili and Bani-Hasan, 2018). Morphological characteristics, such as spore shape, size, and color, along with the presence or absence of specific structures, are examined under microscopes.

Research has revealed diverse fungal communities, with species belonging to common genera like *Aspergillus*, *Penicillium*, and *Cladosporium* (Docampo et al., 2011; Cunha et al., 2020). These examples represent a glimpse into the research conducted on cave fungi in Asia. Research on cave fungi in Asia has yielded valuable insights into the

[1]Institute of Ocean and Earth Sciences, Advanced Studies Complex, Universiti Malaya, 50603 Kuala Lumpur, Malaysia
[2]National Antarctic Research Centre, Advanced Studies Complex, Universiti Malaya, 50603 Kuala Lumpur, Malaysia
[3]Institute for Advanced Studies, Universiti Malaya, 50603 Kuala Lumpur, Malaysia
[4]Institute of Biological Sciences, Faculty of Science, Universiti Malaya, 50603 Kuala Lumpur, Malaysia
[5]MAHSA University Malaysia, Bandar Saujana Putra, 42610 Jenjarom, Selangor, Malaysia
[C]Corresponding author: saa@um.edu.my.

biodiversity, ecology, and adaptations of these unique cave-dwelling fungi. Asian countries with extensive cave systems, such as China, Thailand, Cambodia, Vietnam, and Malaysia, have been significant focal points for such studies (Duringer et al., 2012). In China, studies have documented several new species and provided insights into their taxonomy, distribution, and ecological roles. For instance, research in Guangxi and Guizhou provinces revealed diverse fungal communities in caves, including species from genera like *Aspergillus*, *Penicillium*, and *Trichoderma* (Man et al., 2015; Huang et al., 2021; Zhang et al., 2021). In the northern region of Thailand, investigation of cave fungal diversity and physiology reported the occurrence of the genera *Fusarium*, *Aspergillus*, and *Penicillium*, among others (Cyske et al., 2021: Suphaphimol et al., 2022). While, in Cambodia and Vietnam, investigations have been conducted in caves across different regions, including the famous Bayon temple sandstone of Angkor Thom and Phong Nha-Ke Bang National Park, respectively (Lan et al., 2010; Trinh et al., 2018). Researchers have discovered new cave fungal species and examined their phylogenetic relationships. Studies have also explored the potential biotechnological applications of cave fungi, such as their production of enzymes with industrial relevance (Tavares et al., 2018; Paula et al., 2019; Fernández-Remacha et al., 2022).

Cave fungi in Malaysia have been the subject of scientific research, particularly in the cave-rich regions of Sarawak and Sabah on the island of Borneo (Hunt et al., 2007; Wasti et al., 2020). Although the richness of fungal species in caves is well established, this study uniquely documents fungi associated with bat guano within Wang Burma Cave, contributing novel records for Peninsular Malaysia. Existing published research on cave fungi in Malaysia has only employed the extraction of DNA and alignment of nucleotide sequences from pure isolates. Environmental DNA (eDNA) metabarcoding is used to determine the evolutionary relationships and species boundaries of the collected fungi. Cave fungi are often challenging to cultivate in the laboratory due to their specialized adaptations and nutrient requirements. However, researchers may attempt eDNA metabarcoding approaches to study the fungal diversity by sequencing of amplicons (Hamad et al., 2017). Therefore, the present study will be the first to employ eDNA metabarcoding for the identification of fungi and the analysis of fungal diversity in a cave in Peninsular Malaysia. The chosen cave for this study is known as Wang Burma Cave, located in the pristine limestone karst landscape of Perlis State Park in northern Peninsular Malaysia. Although the cave is a prominent natural heritage site under UNESCO with conservation efforts on charismatic cave species, such as bats and rare invertebrates, the cave's microbial biodiversity—particularly fungi—remains largely overlooked. Thus, studying the fungal communities associated with bat guano from this cave through eDNA metabarcoding will contribute toward Malaysia's cave fungal species diversity checklist.

MATERIALS AND METHODS

Study Site and Location of the Cave

The study was conducted at Wang Burma 1 Cave, which is a totally dark and dry cave (Anuwar et al., 2020). The Wang Burma 1 Cave is a part of the permanently reserved forest of Perlis State Park, Perlis, Peninsular Malaysia (6°41'51"N 100°11'53"E), and is accessible to guided visitors. Three bat guano sample collection sites (designated as WBA, WBB and WBC) were established within the middle chamber, approximately 100 m from the entrance, with WBA and WBB located 5 m apart and WBC located near the sidewall. A schematic cave map indicating sampling sites is included in Figure 1. Each of the collection sites was fixed at least 5 m apart from one another.

The sampling sites had bat inhabitants roosting on the cave ceiling (Fig. 2), with an estimated bat count ranging between 120 and 150 individuals in the chamber. Bat guano substrates were also observed on the ground. The guano samples appeared moist to semi-dry, light brown, and heterogeneous in texture, containing fine particulates of digested insect remains. Although no bat identification survey was performed during sampling, observational data suggest the colony consisted predominantly of *Hipposideros* spp. and *Rhinolophus* spp., which are commonly recorded in Peninsular Malaysian caves (Nordin et al., 2021; Hazrizal Fuad et al., 2024). Both bat genera consist of insectivores, which may be attributed to the characteristics of the bat guano sampled across the three sampling sites.

There were not many distinct characteristics between the bat guano substrates of WBA and WBB, while WBC had some dead insects and litter (small organic debris and detritus). Surface temperature of bat guano measured using a Testo 925 digital thermocouple thermometer (±0.5 °C accuracy) revealed similar temperatures for all three collection sites (25 °C). This temperature is within the range of values reported by other studies of caves in Malaysia (Baharim et al., 2018; Rajasegaran et al., 2018; Wasti et al., 2021).

Collection of Bat Guano Samples

Triplicates of 10 g of bat guano samples were collected randomly from each site at a depth of 5–10 cm from the surface. All sampling in this study adhered to safety protocols. The collected guano samples were then transferred into a 100 mL Falcon tube. The nine guano samples were kept cold in ice to slow down the metabolism of microscopic fungi (microfungi), referring to filamentous and yeast-like fungi in the samples, and transported to Universiti Malaya. Guano samples

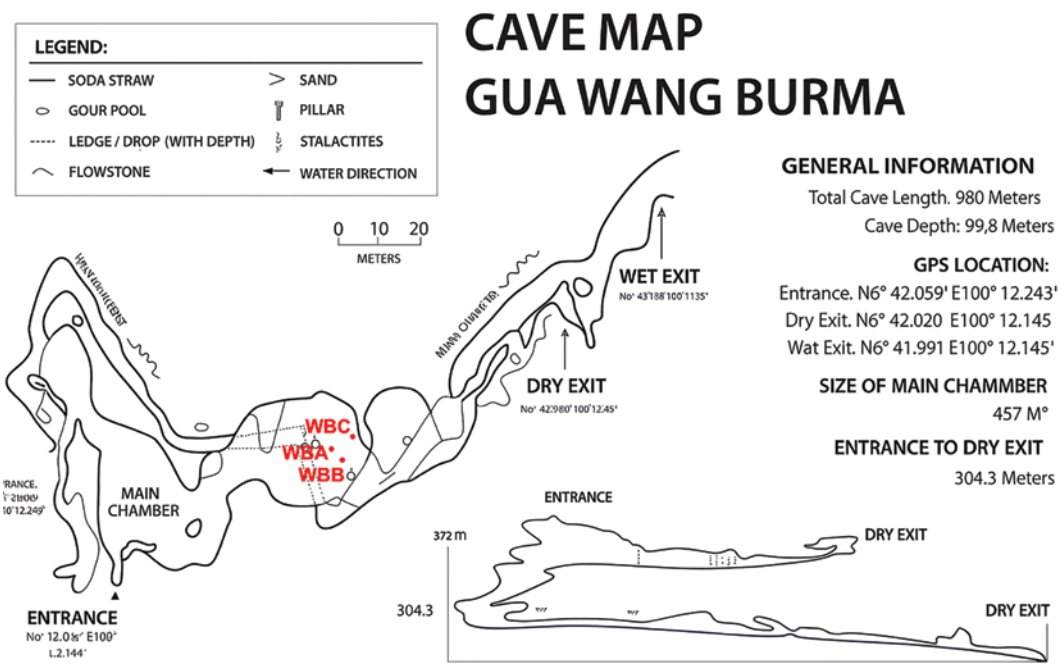

Figure 1. Schematic map of Wang Burma Cave taken on site. Locations for collection points (WBA, WBB, and WBC) are indicated with dots on the map.

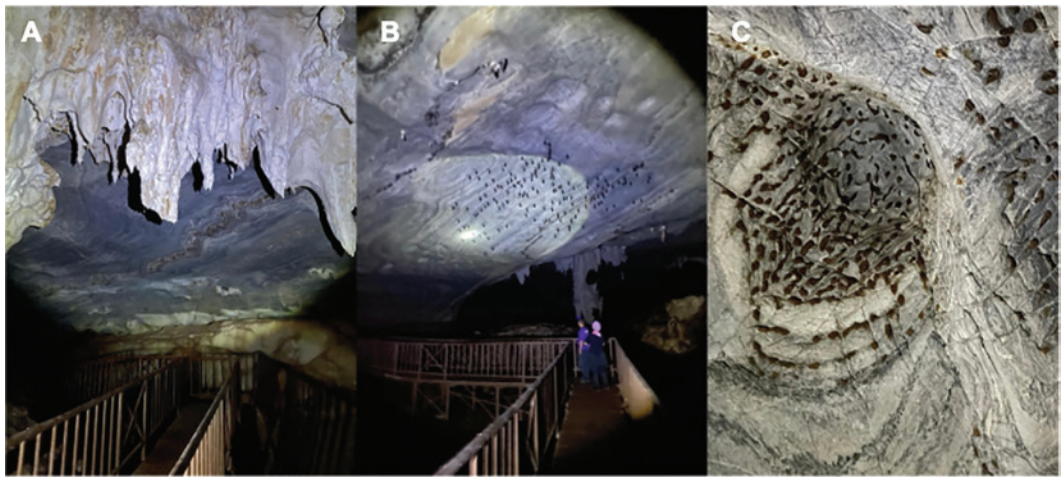

Figure 2. (a) Interior of Wang Burma Cave I; (b) bats roosting on the cave ceiling; (c) bats roosting on the cave ceiling 100 m from the entrance of the cave.

were kept frozen at 0 °C for long-term storage until needed for molecular genetics work.

DNA Extraction and Gel Electrophoresis

Total genomic DNA (gDNA) from the bat guano samples was extracted using NucleoSpin© Soil Kit according to the manufacturer's conditions (Vautier et al., 2020) with modifications. This involved a double extraction procedure of the same samples to maximize the yield of extracted gDNA from bat guano. Then, 1% TAE (Tris-acetate-EDTA) agarose gel electrophoresis was run and visualized to check the quality of the eluted gDNA. The concentration of gDNA was determined using NanoDrop and fulfilled the criterion of ≥20 ng/μL as good quality DNA. The gDNA samples were then stored at −20 °C until needed for amplicon sequencing.

Polymerase Chain Reaction

Polymerase chain reaction (PCR) of the fungal internal transcribed spacer 1 (ITS1) region was performed using the gDNA templates, including the forward primer ITS1F (5′-GGAAGTAAAAGTCGTAACAAGG-3′) (Gardes and Bruns, 1993) and the reverse primer ITS2 (5′-GCTGCGTTCTTCATCGATGC-3′) (White et al., 1990). Each 25 μL PCR comprised of 12.5 μL of 2× REDiant 2× PCR Master Mix (1st BASE), 0.5 μL of each primer (10 μM), 1–2 μL of template DNA (~10 ng), and nuclease-free water to volume. Thermocycling conditions were as follows: initial denaturation at 95 °C for 3 min; followed by 30 cycles of denaturation at 98 °C for 20 s, annealing at 55 °C for 30 s, and extension at 72 °C for 30 s; with a final extension at 72 °C for 5 min. Successful amplification and visualization of PCR products were confirmed using 1% TAE agarose gel electrophoresis.

Library Construction and Amplicon Sequencing

The first library construction was performed through amplification of the fungal ITS1 regions with KOD-Multi & Epi-® (Toyobo) using locus-specific sequence primers with forward (5′-TCGTCGGCAGCGTCAGATGTGTATAAGAGACAG-3′) and reverse (5′-GTCTCGTGGGCTCGGAGATGTGTATAAGAGACAG-3′) overhang adapters. For the second part of library construction, dual indices were attached to the amplicon PCR with the use of the Illumina Nextera XT Index

Kit v2 in accordance with the manufacturer's protocols. The Agilent Bioanalyzer 2100 System, with the Agilent DNA 1000 Kit, was used to measure the quality of libraries, whereas the Helixyte Green™ Quantifying Reagent was used to perform fluorometric quantification. Next, the libraries were normalized and pooled as prescribed by Illumina and were sequenced using the MiSeq platform (2 × 300 bp) with 300 bp paired-end (PE) according to the standard protocol. Library preparation and quality control were performed by Apical Scientific following the authors' initial extraction and PCR amplification in the Universiti Malaya laboratory. Sequencing was carried out by Apical Scientific Sdn. Bhd., generating raw paired-end reads in FASTQ format.

Assignment of Amplicon Sequence Variants

Raw reads obtained were demultiplexed and processed using the DADA2 plugin in QIIME 2 (version 2024.10.1). Quality filtering, denoising, paired-end read merging, and chimera removal were conducted using default parameters. The resulting high-quality sequencing data were assigned to unique amplicon sequence variants (ASVs), which represent exact biological sequences present in the samples, and were trimmed to the region amplified by the primers used in this study. Taxonomic assignment of ASVs was achieved through BLAST search of the UNITE Database (https://unite.ut.ee/). All raw reads and ASV datasets were deposited in GenBank Biosample (Submission SUB15333087) with accession number SAMN48597270.

Taxonomic Abundance and Community Composition

Taxonomic abundance and community composition were analyzed based on the ASV table generated following taxonomic assignment. Relative abundance at various taxonomic levels (phylum, class, order, family, and genus) was calculated to determine the composition of fungal communities across samples. The fungi identified were visualized using a chord diagram and compared with fungal diversity reported by other studies in Malaysian caves to provide a comprehensive checklist of Malaysian cave fungi.

RESULT AND DISCUSSION

Taxonomic Abundance and Diversity

Sequencing of the ITS1 region yielded a total of 491,691 raw reads, with 380,856 reads remaining after merging, dereplication, and chimera removal. In total, 32 ASVs representing two phyla, five known classes, four known orders, five known families, five known genera, and six known species were reported (Table 1).

Phylum Ascomycota was found to be the most dominant phylum (consisting of >99.99% of the 380,856 sequence reads), similar to findings by Wasti et al. (2020, 2021).

The dominance of Ascomycota aligns with previous reports from Malaysian and Southeast Asian caves, possibly due to their adaptive capacity to nutrient-poor and oligotrophic guano environments (Cunha et al., 2020; Wasti et al., 2020). Another phylum that was identified was Mortierellomycota, which consisted of only a mere 21 sequences.

Of the 32 ASVs, 14 were identified successfully to the species level, representing six species: *Aspergillus caninus*, *A. chlamydosporus*, *A. phialosimplex*, *Candida palmioleophila*, *Mortierella rhinolophicola*, and *Penicillium simplicissimum* (Fig. 3). Seven ASVs were identified only to the genus level, and these included the genera *Aspergillus*, *Candida*, *Mortierella*, *Penicillium*, and *Sagenomella*. Some ASVs were identified only to higher taxonomic levels (e.g., family, order, class, or phylum), which may be attributed to (1) low quality of the sequence reads or (2) limitations of barcode references in repository databases. Regardless, all of these ASVs were confidently classified as the phylum Ascomycota. In addition, three species, such as *A. chlamydosporous*, *C. palmioleophila*, and *P. simplicissimum*, were recorded in samples from all three sites. The three most abundant ASVs identified were ASV4 (33.6%) and ASV5 (33.8%), which are two strains of *P. simplicissimum*, and ASV16 (15.3%), which represents a strain of *C. palmioleophila*.

Eurotiomycetes and Eurotiales (73%) were the most abundant class and order, respectively, followed by class Saccharomycetes and order Saccharomycetales (21%), and class Leotiomycetes and order Helotiales (6%) (Fig. 4). The most dominant family for all three sites was Aspergillaceae (72%), while the other family under Eurotiales found in the samples, *Trichocomaceae* (<1%), had significantly lower abundance compared to its sister family. The relative abundance of Mortierellaceae was similar to the order Mortierellales, as Mortierellaceae is a monotypic family. Myxotrichaceae was similar in abundance to the order Helotiales, thus implying that there were no other fungi of other families under this order that were present in the samples. This was also the case for the enigmatic/uncertain family under Saccharomycetales labeled as "Incertae familiae."

Under Aspergillaceae, two genera were identified, which were *Aspergillus* (<1%) and *Penicillium* (99%). *Candida* (21%) was the only genus under *incertae familiae* (Saccharomycetales) found in the samples; hence, the relative abundance was similar to its family. *Mortierella* and *Sagenomella* were also the only identified genera of their respective families; hence, their relative abundance values were also similar to those of their families.

Table 1. Relative abundance of ASVs identified based on fungal ITS1 sequences in bat guano from three sites (WBA, WBB, and WBC) in Wang Burma Cave.

		Sequence Reads (*n*)			Relative Abundance	
ASV	**Identified Taxa**	**WBA**	**WBB**	**WBC**	***N***	**%**
ASV5	*Penicillium simplicissimum*	26,413	49,105	53,226	128,744	33.80
ASV4	*Penicillium simplicissimum*	66,980	54,553	6,606	128,139	33.64
ASV16	*Candida palmioleophila*	19,228	1,284	37,897	58,409	15.34
ASV9	*Myxotrichaceae*[a]	3,846	17,606	1,951	23,403	6.14
ASV19	*Candida palmioleophila*	0	642	15,690	16,332	4.29
ASV6	*Penicillium* sp. 3[b]	0	9,569	6,050	15,619	4.10
ASV23	*Sagenomella*[b]	3,051	0	123	3,174	0.83
ASV27	*Aspergillus caninus*	1,444	0	0	1,444	0.38
ASV14	*Candida palmioleophila*	673	60	496	1,229	0.32
ASV7	*Lecanoromycetes*[c]	0	0	1,077	1,077	0.28
ASV25	*Aspergillus* sp. 1[b]	1,045	0	0	1,045	0.27
ASV26	*Aspergillus chlamydosporus*	429	261	43	733	0.19
ASV21	*Ascomycota*[d]	0	315	7	322	0.085
ASV22	*Ascomycota*[d]	57	172	0	229	0.06
ASV18	*Candida palmioleophila*	0	26	180	206	0.05
ASV28	*Aspergillus phialosimplex*	200	0	0	200	0.05
ASV8	*Lecanoromycetes*[c]	0	0	123	123	0.03
ASV24	*Eurotiales*[e]	0	121	0	121	0.03
ASV29	*Penicillium* sp. 4[b]	41	28	0	69	0.02
ASV11	*Lecanoromycetes*[c]	42	0	0	42	0.01
ASV30	*Penicillium* sp. 5[c]	0	0	33	33	<0.01
ASV32	*Penicillium* sp. 6[c]	28	0	0	28	<0.01
ASV1	*Penicillium simplicissimum*	0	25	0	25	<0.01
ASV31	*Penicillium simplicissimum*	0	0	23	23	<0.01
ASV2	*Penicillium* sp. 1[b]	0	19	0	19	<0.01
ASV12	*Mortierella rhinolophicola*	0	0	16	16	<0.01
ASV15	*Candida palmioleophila*	0	0	16	16	<0.01
ASV10	*Myxotrichaceae*[a]	0	10	0	10	<0.01
ASV17	*Candida palmioleophila*	0	0	10	10	<0.01
ASV3	*Penicillium* sp. 2[b]	6	0	0	6	<0.01
ASV13	*Mortierella rhinolophicola*	0	5	0	5	<0.01
ASV20	*Candida palmioleophila*	0	0	5	5	<0.01
		123,483	133,801	123,572	380,856	100

[a]ASV9 and ASV10 can only be identified up to the family level.
[b]ASV2, ASV3, ASV6, ASV25, ASV29, ASV30, and ASV32 can only be identified up to the genus level.
[c]ASV7, ASV8, and ASV11 can only be identified up to the class level.
[d]ASV21 and ASV22 can only be identified up to the phylum level.
[e]ASV24 can only be identified up to the order level.

Insights into the Identified Fungi Associated with Bat Guano

The fungal community profiles across the three sampling sites (WBA, WBB, and WBC) revealed clear dominance patterns, as well as site-specific fluctuations in several medically relevant taxa. The most abundant species overall was *Penicillium simplicissimum*, which consistently represented the largest proportion of ASVs across all samples (up to 67%). This strong and uniform dominance suggests that *P. simplicissimum* is a core and persistent component of the cave mycobiome. Although non-pathogenic, some strains of this species are known to function as plant growth-promoting fungi and have been explored for use as biofertilizers (Shimizu et al., 2013), indicating ecological versatility rather than pathogenic relevance within this cave environment.

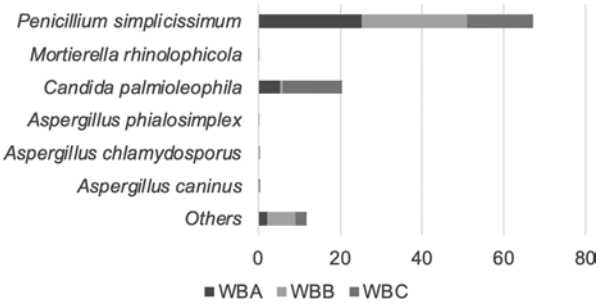

Figure 3. Relative abundance (%) of fungal species identified across three sampling sites (WBA, WBB, and WBC) based on ASV proportions.

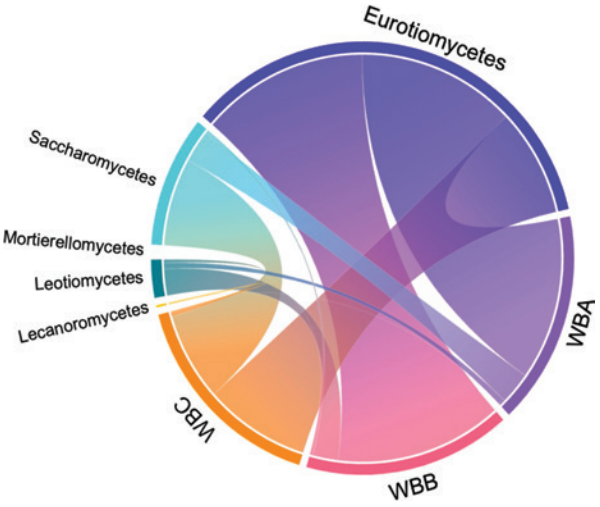

Figure 4. Chord diagram showing major identified fungal classes associated with bat guano identified from three sites (WBBA, WBB, and WBC) in Wang Burma Cave.

In contrast, *Candida palmioleophila* exhibited marked variability in relative abundance among sites, approximately 16% in WBA, 2% in WBB, and 44% in WBC, making it the second most prominent taxon in the dataset and the only species demonstrating strong spatial heterogeneity. *C. palmioleophila* is an ascomycetous yeast with documented opportunistic pathogenicity, particularly in immunocompromised patients, where it is associated with candidemia and severe complications including dermal infections, respiratory failure, and fatal systemic infections (Jensen and Arendrup, 2011; Pierantoni et al., 2020). Its uneven distribution across the cave sites may therefore indicate microhabitat-driven niche suitability rather than widespread establishment.

The detection of *Mortierella rhinolophicola*, although occurring at negligible abundances across all sites, represents a noteworthy finding. This species was first described from bat carcasses in a cave in Yunnan, China (Karunarathna et al., 2020) and may include cave-adapted or host-associated strains. Members of *Mortierella* are generally non-pathogenic, and no evidence exists thus far to suggest pathogenic potential in *M. rhinolophicola*. Its minimal presence in our samples is consistent with both its rarity in global mycobiome reports and the possibility of a specialized ecological niche within cave ecosystems.

Among the *Aspergillus* species detected (including *A. caninus*, *A. phialosimplex*, and *A. chlamydosporus*), all occurred only at trace proportions in the ASV dataset. *Aspergillus caninus* is of particular interest due to its ability to cause severe infections in canines (Kano et al., 2019; Yang et al., 2020). While the other detected *Aspergillus* species have not been associated with significant human pathogenicity, the genus as a whole contains several major agents of invasive fungal infections in immunocompromised individuals (Beck-Sagué and Jarvis, 1993). Notably, *A. fumigatus*, the primary etiological agent of aspergillosis (a lung disease), was absent from all cave samples, aligning with previous studies in Malaysian caves, where *A. fumigatus* has similarly never been documented. Instead, prior cave studies in Malaysia have reported other pathogenic *Aspergillus* species such as *A. flavus*, *A. niger*, and *A. nomius* (Marr et al., 2002; Caira et al., 2012; Wasti and Seelan, 2019; Wasti et al., 2020). The low abundance of *Aspergillus* taxa in the current dataset therefore suggests limited representation of this genus within Gua Wang Burma compared to other Malaysian cave systems.

Overall, the combination of highly dominant non-pathogenic taxa (e.g., *P. simplicissimum*), heterogeneous but medically relevant yeasts (e.g., *C. palmioleophila*), and rare occurrence of specialized or low-pathogenicity species (e.g., *Mortierella* spp. and *Aspergillus* spp.) reflects a fungal community possibly shaped by both microhabitat variation and the unique ecological constraints of the cave environment.

Diversity of Cave Fungi in Malaysia

To provide a more comprehensive analysis of available baseline data on cave fungi associated with bat guano in Malaysia, we have compiled a checklist of 34 cave fungal species reported in the present study and two previous studies conducted in Sabah caves (Table 2; Wasti et al., 2020, 2021). The present study contributes five new records, including *Aspergillus caninus*, *A. chlamydosporus*, *A. phialosimplex*, *Candida palmioleophila*, and *Mortierella rhinolophicola.* The addition of these five previously unreported bat guano-associated fungi from Peninsular Malaysia suggests that Malaysian cave mycobiomes may harbor regionally distinct assemblages shaped by local environmental gradients, guano chemistry, and bat species composition.

CONCLUSION

This study highlighted the cave fungi associated with bat guano in Wang Burma Cave, Perlis. eDNA metabarcoding analysis revealed the diverse fungal community, some of which have potential applications in biotechnology and conservation efforts. Understanding these microbial interactions will contribute to better conservation management of cave ecosystems and their associated biodiversity.

Table 2. Occurrence of fungi associated with bat guano in caves of Malaysia.

Species	Wang Burma Cave (Present Study)	Madai Cave, Sabah (Wasti et al., 2021)	Gomantong Cave, Sabah (Wasti et al., 2020)
Annulohypoxylon nitens		[a]	
Aspergillus aculeatus		[a]	
Aspergillus caninus	[a,b]		
Aspergillus chlamydosporus	[a,b]		
Aspergillus flavus			[a]
Aspergillus niger		[a]	
Aspergillus nomius		[a]	
Aspergillus ochraceus			[a]
Aspergillus phialosimplex	[a,b]		
Aspergillus restrictus			[a]
Aspergillus sp. 1	[a]	[a]	
Aspergillus fumigatus			
Blastobotrys malaysiensis			
Candida palmioleophila	[a,b]		
Cladosporium cladosporioides		[a]	
Curvularia lunata		[a]	
Mortierella rhinolophicola	[a,b]		
Paecilomyces variotii		[a]	
Penicillium citrinum			[a]
Penicillium paxilli		[a]	[a]
Penicillium simplicissimum	[a]	[a]	
Penicillium sp. 1	[a]	[a]	
Penicillium sp. 2	[a]	[a]	
Penicillium sp. 3	[a]		
Penicillium sp. 4	[a]		
Penicillium sp. 5	[a]		
Penicillium sp. 6	[a]		
Pestalotiopsis sp.			[a]
Pochonia chlamydosporia		[a]	
Purpureocillium lilacinum		[a]	
Talaromyces minioluteus		[a]	
Trichoderma asperellum		[a]	
Trichoderma paraviridescens		[a]	
Xylaria feejeensis			[a]
Total	13	17	7

[a]Fungi from bat guano.
[b]New records of identified species.

ACKNOWLEDGMENTS

The authors would like to thank the Ministry of Higher Education (MOHE) for its funding program—Higher Institution Centre of Excellence (HiCoE) (Grant No. IOES-2014G) and the Wang Burma Rangers and the Perlis Forestry Department for their assistance in the field.

AUTHOR CONTRIBUTION STATEMENT

SAA and MR-I conceived the idea for the project. NMT-M and TWH collected bat guano samples and carried out DNA extraction and metabarcoding analysis. SKS and NMT-M analyzed and discussed the metabarcoding results. AK assisted with fungal isolation and identification. SAA and MR-I supervised the findings of this work and verified the

analytical methods and results from the metabarcoding analysis. HO consulted on bat guano as a substrate for cave fungi. All authors discussed the results and contributed to the final manuscript.

REFERENCES

Alsohaili, S.A., and Bani-Hasan, B.M., 2018, Morphological and molecular identification of fungi isolated from different environmental sources in the Northern Eastern desert of Jordan: Jordan Journal of Biological Sciences, v. 11, no. 3, p. 329–337.

Anuwar, N.A.A., Sobri, S.A., Hermawan, A., Hambali, K.A., Ismail, W.O.A.S.W., and Amini, M.H.M., 2020, The potential of eco-tourism: A narrative case study of Perlis State Park, Malaysia: Journal of Critical Reviews, v. 7, no. 15, p. 3070–3077.

Baharim, N.B., Muhammad, R.F., and Yusoff, I., 2018, Hydrogeochemical evolution in a tropical cave system; Batu Caves, Peninsular Malaysia: Journal of Sustainability Science and Management, v. 13, no. 1, p. 77–92.

Beck-Sagué, C.M., and Jarvis, W.R., 1993, Secular trends in the epidemiology of nosocomial fungal infections in the United States, 1980–1990. National Nosocomial Infections Surveillance System: Journal of Infectious Diseases, v. 167, no. 5, p. 1247–1251.

Caira, M., Posteraro, B., Sanguinetti, M., De Carolis, E., Leone, G., and Pagano, L., 2012, First case of breakthrough pneumonia due to *Aspergillus nomius* in a patient with acute myeloid leukemia: Medical Mycology, v. 50, no. 7, p. 746–750.

Cunha, A.O., Bezerra, J.D., Oliveira, T.G., Barbier, E., Bernard, E., Machado, A.R., and Souza-Motta, C.M., 2020, Living in the dark: Bat caves as hotspots of fungal diversity: PLos One, v. 15, no. 12, p. e0243494.

Cyske, Z., Jaroszewicz, W., Żabińska, M., Lorenc, P., Sochocka, M., Bielańska, P., Grabowski, Ł., Gaffke, L., Pierzynowska, K., and Węgrzyn, G., 2021, Unexplored potential: Biologically active compounds produced by microorganisms from hard-to-reach environments and their applications: Acta Biochimica Polonica, v. 68, no. 4, p. 565–574.

Dimkić, I., Fira, D., Janakiev, T., Kabić, J., Stupar, M., Nenadić, M., Unković, N., and Grbić, M.L., 2021, The microbiome of bat guano: For what is this knowledge important?: Applied Microbiology and Biotechnology, v. 105, no. 4, p. 1407–1419.

Docampo, S., Trigo, M.M., Recio, M., Melgar, M., García-Sánchez, J., and Cabezudo, B., 2011, Fungal spore content of the atmosphere of the Cave of Nerja (southern Spain): Diversity and origin: Science of the Total Environment, v. 409, no. 4, p. 835–843.

Duringer, P., Bacon, A.M., Sayavongkhamdy, T., and Nguyen, T.K.T., 2012, Karst development, breccias history, and mammalian assemblages in Southeast Asia: A brief review: Comptes Rendus Palevol, v. 11, no. 2–3, p. 133–157.

Emerson, J.K., and Roark, A.M., 2007, Composition of guano produced by frugivorous, sanguivorous, and insectivorous bats: Acta Chiropterologica, v. 9, no. 1, p. 261–267.

Farda, B., Djebaili, R., Vaccarelli, I., Del Gallo, M., and Pellegrini, M., 2022, Actinomycetes from caves: An overview of their diversity, biotechnological properties, and insights for their use in soil environments: Microorganisms, v. 10, no. 2, p. 453.

Fernández-Remacha, D., González-Riancho, C., Lastra Osua, M., González Arce, A., Montánchez, I., García-Lobo, J.M., Estrada-Tejedor, R., and Kaberdin, V.R., 2022, Analysis of laccase-like enzymes secreted by fungi isolated from a Cave in Northern Spain: MicrobiologyOpen, v. 11, no. 2, p. e1279.

Hasrizal Fuad, A.B., Halmi, N.Z., Yazid, H., Arifuddin, M., Mukri, I., Azidi, S.N.Z., Anak Chuat, J.C., Nurul Hafiz, M.I., A. Rahman, N.N., Nizam, K., Zoo, S., Pooi Har, F., Appalasamy, S., and Vijaya Kumaran, J., 2024, Bat species diversity in the Merapoh rich limestone-rich area within Lipis National Geopark, Malaysia: Biodiversity Data Journal, v. 12, p. e125875.

Gardes, M., and Bruns, T.D., 1993, ITS primers with enhanced specificity for basidiomycetes—Application to the identification of mycorrhizae and rusts: Molecular Ecology, v. 2, p. 113–118.

Hamad, I., Ranque, S., Azhar, E.I., Yasir, M., Jiman-Fatani, A.A., Tissot-Dupont, H., Raoult, D., and Bittar, F., 2017, Culturomics and amplicon-based metagenomic approaches for the study of fungal population in human gut microbiota: Scientific Reports, v. 7, no. 1, p. 16788.

Huang, S., Wei, G., Wang, H., Liu, W., Bedos, A., Deharveng, L., and Tian, M., 2021, Ganxiao Dong: A hotspot of cave biodiversity in northern Guangxi, China: Diversity, v. 13, no. 8, p. 355.

Hunt, C.O., Gilbertson, D.D., and Rushworth, G., 2007, Modern humans in Sarawak, Malaysian Borneo, during Oxygen Isotope Stage 3: Palaeoenvironmental evidence from the Great Cave of Niah: Journal of Archaeological Science, v. 34, p. 1878–1894.

Jensen, R.H., and Arendrup, M.C., 2011, *Candida palmioleophila*: Characterization of a previously overlooked pathogen and its unique susceptibility profile in comparison with five related species: Journal of Clinical Microbiology, v. 49, no. 2, p. 549–556.

Kano, R., Sakai, M., Hiyama, M., and Tani, K., 2019, Isolation of *Aspergillus caninus* (synonym: *Phialosimplex caninus*) from a canine iliac lymph node: Mycopathologia, v. 184, no. 2, p. 335–339.

Karkun, A., Tiwari, K.L., and Jadhav, S.K., 2012, Fungal diversity of Mandeepkhol cave in Chhattisgarh, India: Advances in Bioresearch, v. 3, no. 2, p. 119–123.

Karunarathna, S.C., Dong, Y., Karasaki, S., Tibpromma, S., Hyde, K.D., Lumyong, S., Xu, J., Sheng, J., and Mortimer, P.E., 2020, Discovery of novel fungal species and pathogens on bat carcasses in a cave in Yunnan Province, China: Emerging Microbes & Infections, v. 9, no. 1, p. 1554–1566.

Lan, W., Li, H., Wang, W.D., Katayama, Y., and Gu, J.D., 2010, Microbial community analysis of fresh and old microbial biofilms on Bayon temple sandstone of Angkor Thom, Cambodia: Microbial Ecology, v. 60, p. 105–115.

Mammola, S., Frigo, I., and Cardoso, P., 2022, Life in the darkness of caves: Frontiers for Young Minds, v. 10, p. 657265.

Man, B., Wang, H., Xiang, X., Wang, R., Yun, Y., and Gong, L., 2015, Phylogenetic diversity of culturable fungi in the Heshang Cave, Central China: Frontiers in Microbiology, v. 6, p. 1158.

Marr, K. A., Patterson, T., and Denning, D., 2002, Aspergillosis. Pathogenesis, clinical manifestations, and therapy. Infect Dis Clin North Am, v. 16, p. 875–894.

Nieves-Rivera, Á.M., Santos-Flores, C.J., Dugan, F.M., and Miller, T.E., 2009, *Guanophilic fungi* in three caves of southwestern Puerto Rico: International Journal of Speleology, v. 38, no. 1, p. 61–70.

Nordin, J., Chew, T.H., Lim, L.S., and Shamsir, M.S., 2021, Temporal changes of bat diversity in the urban habitat island of Batu Caves, Malaysia: IOP Conference Series: Earth and Environmental Science, v. 736, no. 1, p. 012051.

Ogórek, R., Dyląg, M., Kozak, B., Višňovská, Z., Tančinová, D., and Lejman, A., 2016, Fungi isolated and quantified from bat guano and air in Harmanecka and Driny caves (Slovakia): Journal of Cave & Karst Studies, v. 78, no. 1, p. 41–49.

Out, B., Boyle, S., and Cheeptham, N., 2016, Identification of fungi from soil in the Nakimu caves of Glacier National Park: Journal of Experimental Microbiology & Immunology, v. 2, p. 26–32.

Paula, C.C.D., Montoya, Q.V., Meirelles, L.A., Farinas, C.S., Rodrigues, A., and Seleghim, M.H., 2019, High cellulolytic activities in filamentous fungi isolated from an extreme oligotrophic subterranean environment (Catão cave) in Brazil: Anais da Academia Brasileira de Ciências, v. 91, no. 3, p. e20180583.

Pierantoni, D.C., Bernardo, M., Mallardo, E., Carannante, N., Attanasio, V., Corte, L., Roscini, L., Di Fiore, L., Tascini, C., and Cardinali, G., 2020, *Candida palmioleophila* isolation in Italy from two cases of systemic infection, after a CHROMagar and Vitek system mis-identification as *C. albicans*: The New Microbiologica, v. 43, no. 1, p. 47–50.

Powell, J.R., and Rillig, M.C., 2018, Biodiversity of arbuscular mycorrhizal fungi and ecosystem function: New Phytologist, v. 220, no. 4, p. 1059–1075.

Rajasegaran, P., Shazali, N., and Khan, F.A.A., 2018, Microclimate and physiological effects in the roosts of cave dwelling bats: Implications in roost selection and conservation in Sarawak, Malaysian Borneo: Zoological Science, v. 35, no. 6, p. 521–527.

Ren, H., Wang, F., Ye, W., Zhang, Q., Han, T., Huang, Y., Chu, G., Hui, D., and Guo, Q., 2021, Bryophyte diversity is related to vascular plant diversity and microhabitat under disturbance in karst caves: Ecological Indicators, v. 120, p. 106947.

Saikia, U., and Ruedi, M., 2021, Beauties beneath: The cave bats of Meghalaya: Resonance, v. 26, no. 6, p. 829–840.

Shimizu, K., Hossain, M.M., Kato, K., Kubota, M., and Hyakumachi, M., 2013, Induction of defense responses in cucumber plants by using the cell-free filtrate of the plant growth-promoting fungus *Penicillium simplicissimum* GP17-2: Journal of Oleo Science, v. 62, no. 8, p. 613–621.

Sket, B., 2008, Can we agree on an ecological classification of subterranean animals? Journal of Natural History, v. 42, no. 21–22, p. 1549–1563.

Suphaphimol, N., Suwannarach, N., Purahong, W., Jaikang, C., Pengpat, K., Semakul, N., Yimklan, S., Jongjitngam, S., Jindasu, S., Thiangtham, S., Chantawannakul, P., and Disayathanoowat, T., 2022, Identification of microorganisms dwelling on the 19th century Lanna mural paintings from Northern Thailand using culture-dependent and independent approaches: Biology, v. 11, no. 2, p. 228.

Tavares, D.G., Barbosa, B.V.L., Ferreira, R.L., Duarte, W.F., and Cardoso, P.G., 2018, Antioxidant activity and phenolic compounds of the extract from pigment-producing fungi isolated from Brazilian caves: Biocatalysis and Agricultural Biotechnology, v. 16, p. 148–154.

Tedersoo, L., Bahram, M., Põlme, S., Kõljalg, U., Yorou, N.S., Wijesundera, R., Ruiz, L.V., Vasco-Palacios, A.M., Thu, P.Q., Suija, A., Smith, M.E., Sharp, C., Saluveer, E., Saitta, A., Rosas, M., Riit, T., Ratkowsky, D., Pritsch, K., Põldmaa, K., Piepenbring, M., Phosri, C., Peterson, M., Parts, K., Pärtel, K., Otsing, E., Nouhra, E., Njouonkou, A.L., Nilsson, R.H., Morgado, L.N., Mayor, J., May, T.W., Majuakim, L., Lodge, D.J., Lee, S.S., Larsson, K.-H., Kohout, P., Hosaka, K., Hiiesalu, I., Henkel, T.W., Harend, H., Guo, L.-d., Greslebin, A., Grelet, G., Geml, J., Gates, G., Dunstan, W., Dunk, C., Drenkhan, R., Dearnaley, J., De Kesel, A., Dang, T., Chen, X., Buegger, F., Brearley, F.Q., Bonito, G., Anslan, S., Abell, S., and Abarenkov, K., 2014, Global diversity and geography of soil fungi: Science, v. 346, no. 6213, p. 1256688.

Trinh, D.A., Trinh, Q.H., Tran, N., Guinea, J.G., and Mattey, D., 2018, Eco-friendly remediation of lamp enflora on speleothems in tropical karst caves: Journal of Cave and Karst Studies, v. 80, no. 1, p. 1–12.

Vanderwolf, K., Malloch, D., McAlpine, D.F., and Forbes, G.J., 2013, A world review on fungi, yeasts, and slime molds in caves. International Journal of Speleology, v. 42, no. 1, p. 77–96.

Vautier, M., Vasselon, V., Chardon, C., Rimet, F., Bouchez, A., and Domaizon, I., 2020, DNA extraction from environmental biofilm using the NucleoSpin® Soil kit: (MACHEREY NAGEL): protocols.io, version 1.

Wasti, I., Fui, F.S., Zhi, T.Q., Mun, C.W., Hafiz Syukri Kassim, M., Mohd Dawood, M., Haliza Hasan, N., Subbiah, V.K., Ali Anwarali Khan, F., and Seelan Sathiya Seelan, J., 2020, Fungi from dead arthropods and bats of Gomantong Cave, Northern Borneo, Sabah (Malaysia): Journal of Cave and Karst Studies, v. 82, no. 4, p. 261–275.

Wasti, I.G., and Seelan, J.S.S., 2019, The fungal diversity of Madai Cave: Sabah, Malaysia, *in* Saudi, N.S., Mohamed, H.A., Pinjaman, S., and Zahari, H. eds., Langkawi International Multidisciplinary Academic Conference 2019: Selangor, Asian Scholars Network, p. 264–274.

Wasti, I.G., Khan, F.A.A., Bernard, H., Hassan, N.H., Fayle, T., and Seelan, J.S.S., 2021, Fungal communities in bat guano, speleothem surfaces, and cavern water in Madai Cave, Northern Borneo (Malaysia): Mycology, v. 12, no. 3, p. 188–202.

White, T.J., Bruns, T., Lee, S.J.W.T., and Taylor, J., 1990, Amplification and direct sequencing of fungal ribosomal RNA genes for phylogenetics, *in* Innis, M.A., Gelfand, D.H., Sninsky, J.J., and White, T.J. eds., PCR Protocols: A Guide to Methods and Applications: New York, Academic Press, p. 315–322.

Yang, W., Jones, B.R., Rossi, G., Stephens, N., Arthur, I., Merritt, A., Reese, S., and Langner, K.F.A., 2020, First case of a dog infected with *Aspergillus* (Phialosimplex) *caninus* in Australasia: New Zealand Veterinary Journal, v. 68, no. 4, p. 231–237.

Zhang, J.F., Liu, J.K., Hyde, K.D., Chen, Y.Y., Liu, Y.X., and Liu, Z.Y., 2017, Two new species of Dyfrolomyces (Dyfrolomycetaceae, Dothideomycetes) from karst landforms: Phytotaxa, v. 313, no. 3, p. 267–277.

Zhang, Z.-F., Zhou, S.-Y., Eurwilaichitr, L., Ingsriswang, S., Raza, M., Chen, Q., Zhao, P., Liu, F., and Cai, L., 2021, Culturable mycobiota from karst caves in China II, with descriptions of 33 new species: Fungal Diversity, v. 106, no. 1, p. 29–136.

Julian J. Lewis and Michael E. Slay. Description of *Lirceus fousheensis,* n. sp., the first troglomorphic isopod of the genus *Lirceus (Hoppinellus)* from the Ozarks (Crustacea: Isopoda: Asellidae). *Journal of Cave and Karst Studies,* v. 88, no. 1/2 p. 38-44. DOI: 10.4311/2025LSC0102

DESCRIPTION OF *LIRCEUS FOUSHEENSIS,* N. SP., THE FIRST TROGLOMORPHIC ISOPOD OF THE GENUS *LIRCEUS* (*HOPPINELLUS*) FROM THE OZARKS (CRUSTACEA: ISOPODA: ASELLIDAE)

Julian J. Lewis[1,C] and Michael E. Slay[2]

Abstract

Troglomorphic, stygobiontic asellid isopods of the genera *Caecidotea* and *Conasellus* are widespread in the Ozark physiographic province of the central United States. In contrast, numerous species of *Lirceus* are common in springs and seeps where groundwaters emerge, but none are particularly morphologically adapted to caves. Herein, we describe and figure *Lirceus fousheensis*, the first troglomorphic (and presumably stygobiontic) species of the genus in the Ozarks, from Foushee Cave, Independence County, Arkansas. It is a species of the *Lirceus bicuspidatus* clade and is viewed as an isolated cave invasion arising by an adaptive shift from a common spring-dwelling species. Compared with seven cavernicolous species of *Lirceus* from southwestern Virginia caves, *Lirceus fousheensis* is intermediate in the degree of troglomorphism.

INTRODUCTION

Among the asellid isopods of North America, there are many species believed to be widespread. In some cases, like *Lirceus louisianae*, the validity of the broad range was re-affirmed by genetic sequencing of far-flung populations that demonstrated minimal divergence (Lewis et al., 2023). That species occurs in a variety of aquatic habitats, although its wide range is probably attributable to not being particularly restricted to any of them. In contrast, it is becoming increasingly apparent that many of the purportedly widespread species associated with karst habitats, particularly caves and springs, are revealed by genetic sequencing to be complexes of cryptic species. As a case in point, *Lirceus hargeri* Hubricht and Mackin (1949) was discovered to be such a complex. Rather than a single species, it is now characterized as a subgenus (*Hargerellus*) of 18 described species spanning an area from southwestern Virginia to northern Georgia, with more taxa awaiting description (Lewis et al., 2023).

In the Interior Highlands region, Hubricht and Mackin (1949) described *Lirceus bicuspidatus* from springs spanning the southern Ozarks as well as the Ouachita Mountains, a range essentially encompassing all the Arkansas uplands. The initial sampling for molecular analysis in this region demonstrated that southern populations of *Lirceus bicuspidatus* in the Ouachitas were genetically divergent, which were described as *Lirceus robisoni* (Lewis and Lewis, 2023).

Herein, we separate and describe a second new species within the *Lirceus bicuspidatus* clade, the first troglomorphic *Lirceus* discovered in the Ozarks.

SYSTEMATICS

Lirceus (Hoppinellus) fousheensis, New Species

Lirceus bicuspidatus—McDaniel and Smith, 1976: 58; Graening, 2003: 195; Graening et al., 2011: 159, 175; Lewis and Lewis, 2023: 97–98.

Material examined.—ARKANSAS: Independence County: Foushee Cave, M. Slay, 14 Jun 2011, 7♂8♀; same locality, M. Slay, P. Ardapple, J. Baxter, 25 Feb 2020, 30♂♀.

The holotype is a 6.1 mm ♂ collected from Foushee Cave on 25 February 2020, and the other specimens from this locality are designated paratypes. The specimens were deposited in the collection of the National Museum of Natural History, Smithsonian Institution, Washington, DC.

Material for molecular analysis.—ARKANSAS: Independence County: Foushee Cave 3♂♀ (site code: FOUCHECA); deposition of material and analysis at Université Lyon 1, Lyon, France. All metadata associated with molecular analyses are stored in the World Asellidae Database (Saclier et al., 2024).

Diagnosis.—*Lirceus fousheensis* is most closely related to *Lirceus bicuspidatus*, which occurs in springs and small streams in the Ozark Boston Mountains and the adjacent Springfield Plateau in northern Arkansas. *Lirceus fousheensis* is separable from *L. bicuspidatus* by its small size, the longest specimen is 8.2 mm compared to 18 mm for *L. bicuspidatus* (Hubricht and Mackin, 1949); the marked depigmentation of the body in dorsal view; and the presence of a

[1]Lewis and Associates, Biological Consulting, Borden, IN 47106
[2]Arkansas Field Office, The Nature Conservancy, Little Rock, AR 72205
[C]Corresponding author: lewisbioconsult@gmail.com.

Figure 1. *Lirceus fousheensis*, n. sp., from Foushee Cave, Independence County, Arkansas (photograph by Michael Slay).

single small triangular process on the palmar margin of the propodus of the first pereopod, as opposed to two prominent bicuspate processes as the name implies for *L. bicuspidatus*.

Description.—Length of males is 6.6 mm, the longest female is 8.2 mm, and the body is about 2.5× as long as wide. Eyes present and well formed, dorsal pigmentation reduced, light brown or tan, present on the head and longitudinal midline of pereonites, and pleotelson. Lateral margins of pereonites depigmented, pleotelson with pigment granular in appearance (Fig. 1).

Head broad, about 2.5× as wide as long, anterior margin with medial–lateral carinae broadly rounded, about equal in height with medial carina, lateral margin entire, post-mandibular lobes, and lateral incisions not apparent (Fig. 2). Lateral margins of head, pereonites, and pleotelson moderately setose and spinose. Antenna 1 short, reaching to about midlength of penultimate article of antenna 2 peduncle, flagellum with 5 articles, with aesthetes on distal 4 articles. Antenna 2, flagellum with about 45 articles. Mandible with 3-merous palp, setose on all articles.

Pereopod 1 of male, propodus about 1.7× as long as wide, palmar margin with one large and one smaller stout proximal spines, medial process small, subtriangular; dactyl flexor margin with stout subungual spine, plus about 12 smaller spines descending in size toward the propodus. Female pereopod 1, sexual dimorphism present, propodus about 2.6× as long as wide, palmar margin flat, 3 stout proximal spines present, processes absent, comb spines in row along margin. Pereopod 4, carpus of male 2.2× as long as wide, dactyl flexor margin with stout subungual spine, plus 3 smaller stout spines. Pereopod 4 of female, sexual dimorphism present, carpus 2.6× as long as wide, dactyl flexor margin with stout subungual spine, plus 3 smaller stout spines.

Pleotelson widest anteriorly, tapering distally, about 1.1× wider than long, caudomedial lobe broadly rounded, uropodal sinuses slightly produced. Pleopod 1 (Fig. 3) protopod mesial margin with 2 retinaculae and 1 small seta; exopod about 1.7× as long as wide, 1.2× length of protopod, and lateral and distolateral setae longer than apical setae. Pleopod 2, protopod without setae; exopod, proximal article without setae; distal article trapezoidal, about 1.1× longer than proximal article, about 1.6× as long as wide, with about 6 elongate setae along the proximolateral margin, 5 longer setae along the apical margin; endopod tip with cannula extending across the axis of the endopod, cylindrical, arising from the base of broad, digitiform, dentate, and scalloped lateral process, with shelf extending to a broadly rounded mesial process; caudal margin of endopod broadly rounded, sclerotized. Pleopod 3 exopod, anterior surface moderately setose, and lateral and apical margins densely setose. Pleopod 4 exopod, lateral margin setose, setae formula 30–14–11. Pleopod 5 exopod, proximolateral margin with 2 elongate setae.

Total length of male uropod is about 0.55× the length of the pleotelson in ventral view, in dorsal view extending about 0.5× the length of pleotelson; protopod flattened, about 0.7× of the length extending beyond the margin of the pleotelson; exopod and endopod slightly flattened; exopod about 0.8× the length of endopod; and endopod about 1.4× longer than protopod.

Etymology.—This species is named after the type-locality, Foushee Cave. Suggested vernacular name is the Foushee cave isopod.

Habitat and range.—*Lirceus fousheensis* is known only from Foushee Cave, where the isopods occur in the cave stream. McDaniel and Smith (1976) first noted the presence of what they characterized as a troglobitic “unpigmented and minutely eyed isopod” from Foshee [sic] Cave and reported the same species from Hell Creek Cave, Stone County, Arkansas. As to the latter, the junior author has entered Hell Creek Cave on numerous occasions and has not seen any *Lirceus*, nor have we been able to locate specimens or other references in unpublished reports or the literature. McDaniel and Smith cited the late Thomas E. Bowman as identifying their specimens, but we have been unable to locate the Stone County material in the collection of the Smithsonian Institution, where Dr. Bowman worked for his entire career.

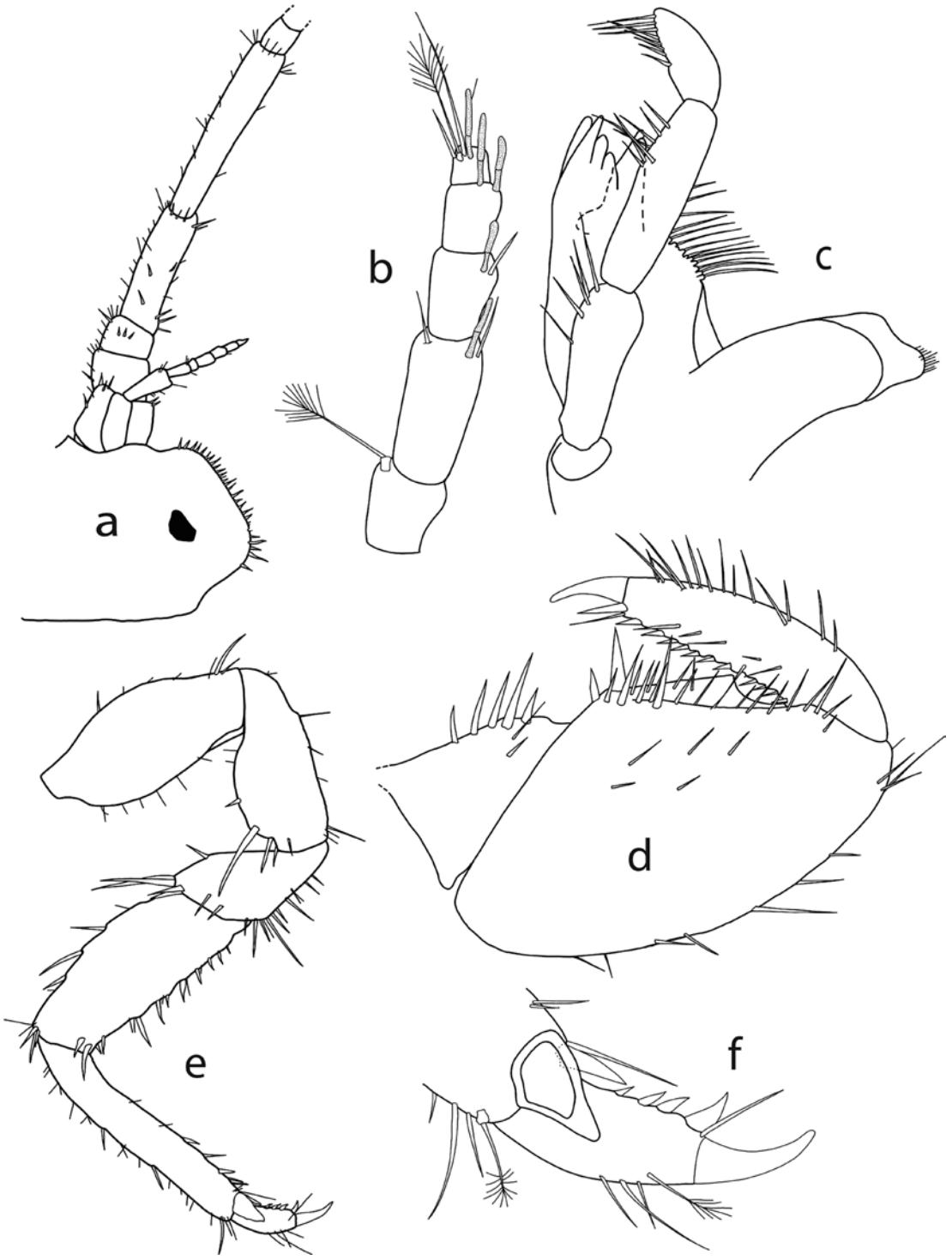

Figure 2. *Lirceus fousheensis*, n. sp., male paratype from Foushee Cave, Independence County, Arkansas: (a) head, antenna 1 and peduncle of antenna 2, pigmentation omitted; (b) distal articles of antenna 1; (c) mandible; (d) pereopod 1, distal articles; (e) pereopod 4; and (f) same, dactylus.

The location of Foushee Cave is indicated on the U.S. Geological Survey Concord quadrangle 7.5-min topographic map as Blowing Cave. The cave is gated, and permission from the Arkansas Natural Heritage Commission is required for entry. Foushee Cave was formed in a narrow band of Mississippian limestone in the Springfield Plateau along the eastern part of the Ozark physiographic province in Arkansas (Fig. 4).

Relationships and evolution.—From a morphological standpoint, the most obvious differences separating *Lirceus fousheensis* from *L. bicuspidatus* are troglomorphisms, notably the pronounced depigmentation. Certain considerations

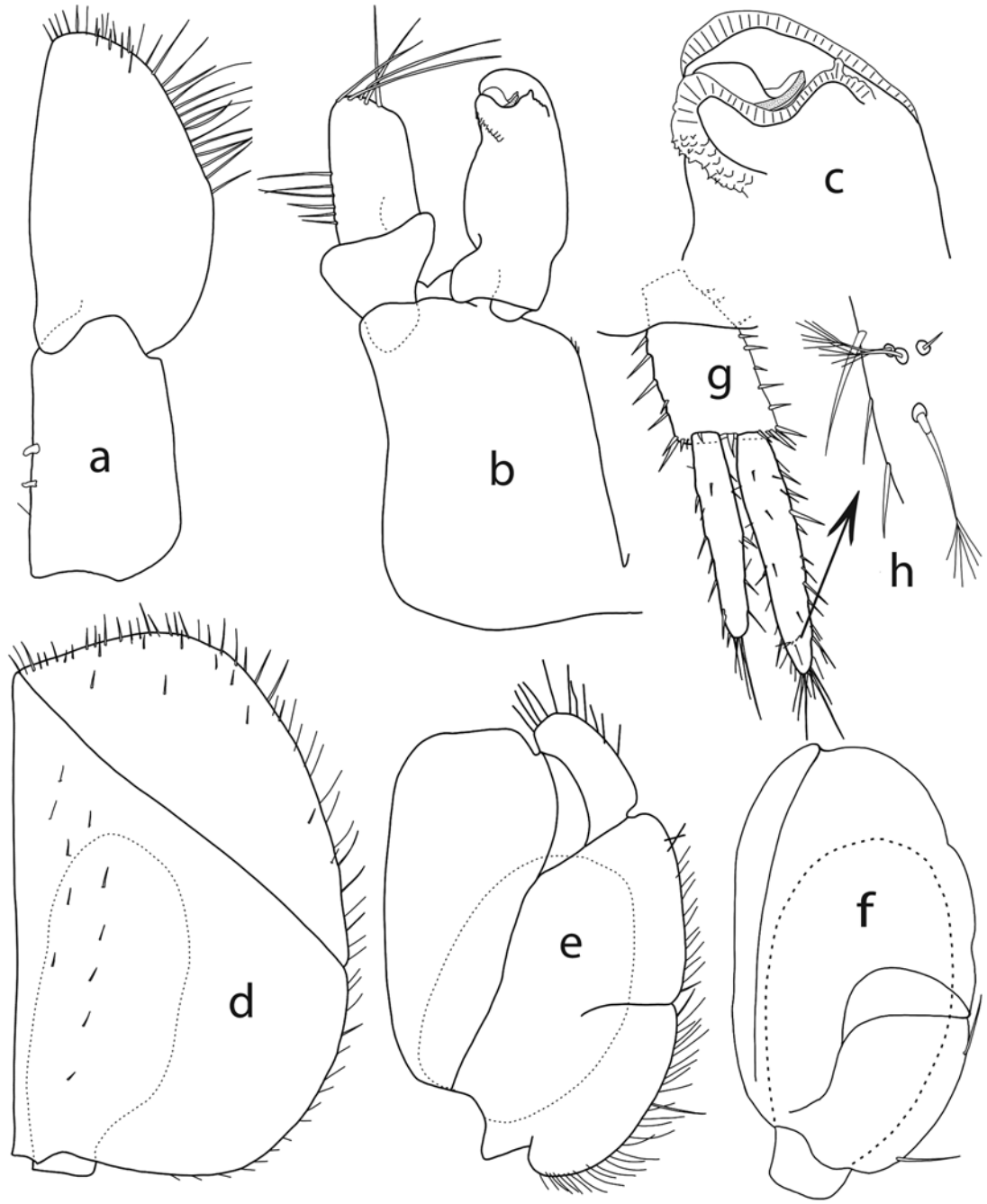

Figure 3. *Lirceus fousheensis*, n. sp., male paratype from Foushee Cave, Independence County, Arkansas: (a) pleopod 1, (b) pleopod 2, (c) same, endopodite tip, (d) pleopod 3, (e) pleopod 4, (f) pleopod 5, (g) uropod, and (h) uropod endopodite detail of row of plumose setae.

must be taken when using troglomorphisms for taxonomic separation of species. Among asellids of eastern North America, in species of the genus *Conasellus,* there is significant plasticity in the presence or absence of eyes and pigmentation. For example, the shallow groundwater species *Conasellus hobsoni* exhibits morphs that range from eyed and pigmented to eyeless and unpigmented, with no discernible genetic divergence nor other morphological differentiation (Lewis et al., 2023).

In contrast, seven troglomorphic species of *Lirceus* were reported by Lewis et al. (2023) and in each the presence of troglomorphisms was linked with speciation through independent means, e.g., other morphological differences and genetic sequencing. Likewise, changes in pigmentation were equally important among the epigean, spring-dwelling species of *Lirceus* in Virginia and Tennessee. The presence of changes in pigmentation patterns, including troglomorphisms, appears to be important as a taxonomic characteristic in *Lirceus*. This was first noted by Hubricht and Mackin

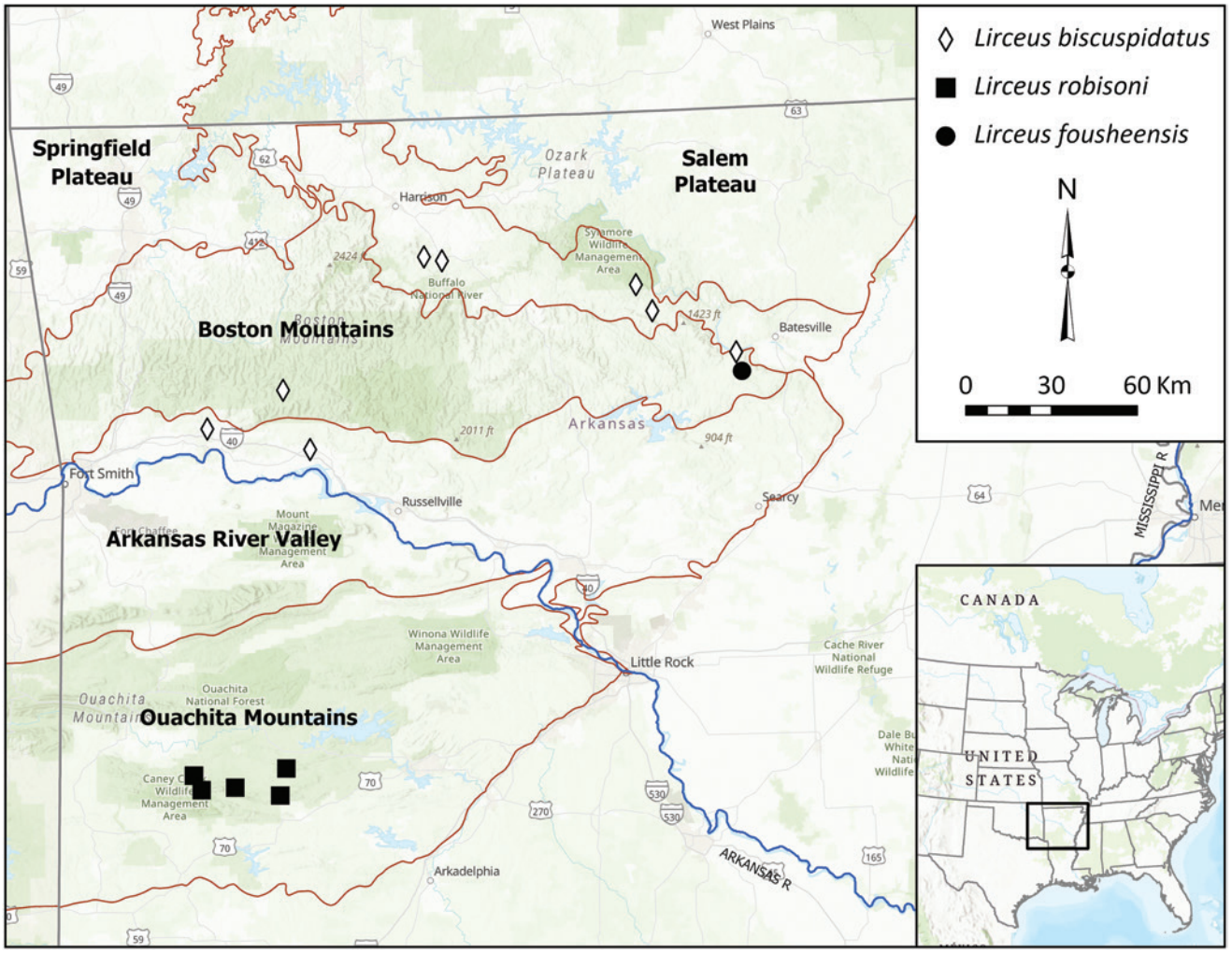

Figure 4. Distribution of species of the *Lirceus bicuspidatus* clade.

(1949), although their assessment that "the differences are difficult to describe and must be seen to be really understood" falls short of being helpful.

Lirceus fousheensis joins an assemblage of seven Appalachian species (Lewis et al., 2023), where a continuum of troglomorphisms is exhibited (Fig. 5). Of these, *Lirceus fousheensis* most closely resembles *L. bisetus*, a species endemic to Lane Cave, in Scott County, Virginia, in its degree of troglomorphism (Fig. 6).

Another morphological phenomenon associated with troglomorphic *Lirceus* species is paedomorphism, particularly in secondary sexual characteristics. This is seen most obviously in the propodus of the first pereopod, which in males of *Lirceus bicuspidatus* is bulbous and displays large, bicuspid processes along the palmar margin. In *Lirceus fousheensis*, the prominent processes are reduced to a single small subtriangular process.

From an ecological perspective, *Lirceus fousheensis* has undergone an adaptive shift from the epigean ancestor inhabiting spring streams to those in Foushee Cave, which is now a reproducing population that is abundant in the dark zone of the cave. The presence of a presumed stygobiontic *Lirceus* in Foushee Cave is unique among the cave communities of the southern Ozarks, the result of an isolated cave invasion.

The speciation of *Lirceus fousheensis* may be in part attributable to its isolation in the karst of the eastern edge of the Springfield Plateau, where it is largely separated from other populations of *L. bicuspidatus* from which it was derived. This endemism is shared with the aquatic cavesnail *Amnicola cora*, another stygobiontic species known only from Foushee Cave.

Concerning molecular genetic analysis, we have sequence data of the mitochondrial 16S gene from nine samples of isopods of the *Lirceus bicuspidatus* clade. Five of these samples were provided through collections made by Dr. Henry Robison and were referable to populations of *Lirceus robisoni* in the Ouachita Mountains (Lewis and Lewis, 2023). The other four were collected from populations in the southern Ozarks: (1) Foushee Cave; (2) the spring stream below the

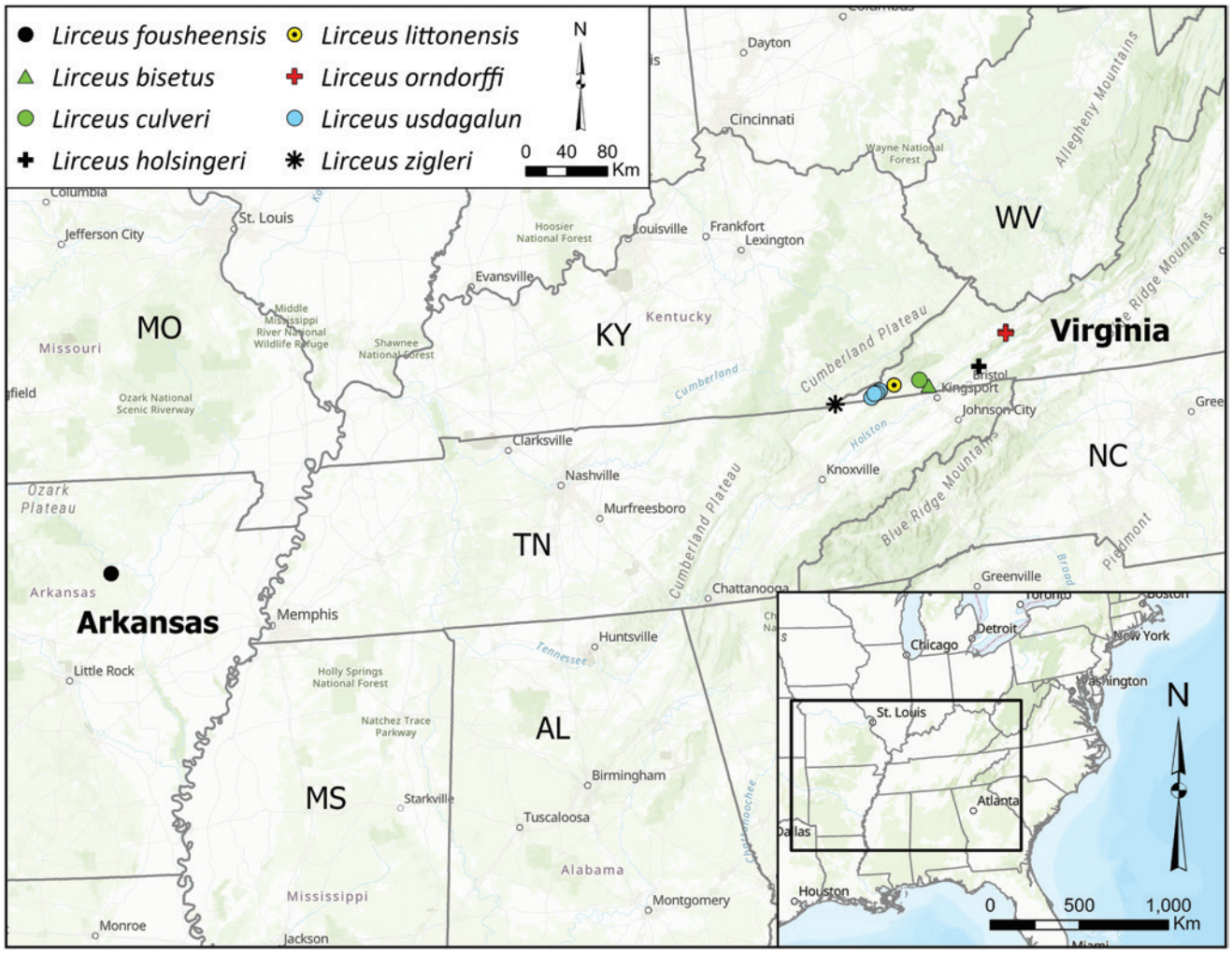

Figure 5. Distribution of troglomorphic *Lirceus* in the eastern United States.

Figure 6. Examples of pigmentation patterns and troglomorphism in isopods of the genus *Lirceus*, from left to right: *Lirceus bicuspidatus*, Johnson County, Arkansas; *Lirceus fousheensis*, Foushee Cave, Independence County, Arkansas; *Lirceus bisetus*, Scott County, Virginia; *Lirceus orndorffi*, Tazewell County, Virginia; and *Lirceus littonensis*, Lee County, Virginia.

entrance of Foushee Cave; (3) the type-locality of *Lirceus bicuspidatus* from a spring in Clarksville, Johnson County, Arkansas; and (4) a spring near Yardelle, Newton County, Arkansas. The sequence data are sparse, but the most significant result was that the troglomorphic isopods in Foushee Cave occur in a separate clade from the fully pigmented specimens taken from the spring stream flowing from the cave.

ACKNOWLEDGMENTS

We would like to thank Ms. Krista Estep, Illustrator, for digital rendering of the drawings of *Lirceus fousheensis*. We acknowledge significant support provided for molecular phylogenetic analysis by Dr. Florian Malard, Prof. Christophe J. Douady, and Ms. Lara Konecny-Dupré of the Laboratoire d'Ecologie des Hydrosystèmes Naturels et Anthropisés (LEHNA), Université Lyon 1, Villeurbanne, France. Funding for the preparation of the description of *Lirceus fousheensis* was provided by the Arkansas Natural Heritage Commission.

REFERENCES

Graening, G.O., 2003, Subterranean biodiversity of Arkansas, Part 2: Status update of the Foushee cavesnail, *Amnicola cora* Hubricht, 1979 (Mollusca: Gastropoda: Hydrobiidae): Journal of the Arkansas Academy of Science, v. 57, p. 195–196.

Graening, G.O., Fenolio, D.B., and Slay, M.E., 2011, *Cave life of Oklahoma and Arkansas*: Norman, University of Oklahoma Press, 226 p.

Hubricht, L., and Mackin, J.G., 1949, The freshwater isopods of the genus *Lirceus* (Asellota: Asellidae): American Midland Naturalist, v. 42, no. 2, p. 334−349, https://doi.org/10.2307/2422012.

Lewis, J.J., and Lewis, S.L., 2023, Freshwater isopods of the genus *Lirceus* from caves and springs of the Interior Highlands, USA, with descriptions of three new species (Isopoda: Asellidae): Journal of Cave and Karst Studies, v. 85, no. 3/4, p. 86–101, https://doi.org/10.4311/2022LSC0113.

Lewis, J.J., Lewis, S.L., Orndorff, W., Orndorff, Z., Malard, F., Konecny-Dupré, L., Saclier, N., and Douady, C., 2023, The groundwater isopods of Virginia (Isopoda: Asellidae and Cirolanidae), Virginia Museum of Natural History: Special Publication 19, 214 p.

McDaniel, V.R., and Smith, K.L., 1976, Cave fauna of Arkansas: Selected invertebrate taxa: Arkansas Academy of Science Proceedings, v. 30, p. 57–60.

Saclier, N., Duchemin, L., Konecny-Dupré, L., Grison, P., Eme, D., Martin, C., Callou, C., Lefébure, T., François, C., Issartel, C., Lewis, J.J., Stoch, F., Sket, B., Gottstein, S., Delić, T., Zagmajster, M., Grabowski, M., Weber, D., Reboleira, A.S.P.S., Palatov, D., Paragamian, K., Knight, L.R.F.D., Michel, G., Lefebvre, F., Hosseini, M.-J.M., Camacho, A.I., De Bikuña, B.G., Taleb, A., Belaidi, N., Tuekam Kayo, R.P., Galassi, D.M.P., Moldovan, O.T., Douady, C.J., and Malard, F., 2024, A collaborative backbone resource for comparative studies of subterranean evolution: The World Asellidae database: Molecular Ecology Resources, v. 24, no. 1, p. e13882, https://doi.org/10.1111/1755-0998.13882.

GUIDE TO AUTHORS

The *Journal of Cave and Karst Studies* is a multidisciplinary journal devoted to cave and karst research. The Journal is seeking original, unpublished manuscripts concerning the scientific study of caves or other karst features. Authors do not need to be members of the National Speleological Society, but preference is given to manuscripts of importance to North American speleology.

LANGUAGES: The *Journal of Cave and Karst Studies* uses American-style English as its standard language and spelling style. A second abstract in another language will be considered when room allows and is determined necessary. In the case of proper names, the Journal tries to accommodate other spellings and punctuation styles. In cases where the Editor-in-Chief finds it appropriate to use non-English words outside of proper names (generally where no equivalent English word exist), the Journal italicizes them. Common abbreviations, i.e., e.g., et al., etc. should appear in normal text. Authors are encouraged to write for our combined professional and amateur readerships. Spell out first use of acronyms.

CONTENT: Each paper will contain a title, the authors' names and addresses, an abstract, and the text of the paper, including a summary or conclusions section. Acknowledgments and references are to follow the text. Manuscripts should be limited to 6,000 words and no more than 10 figures and 5 tables. Larger manuscripts may be considered, but the Journal reserves the right to charge processing fees for larger submissions.

ABSTRACTS: An abstract stating the essential points and results is required. The abstract is to be a summary, not a promise of what topics are covered in the paper.

STYLE: The *Journal* consults The Chicago Manual of Style on most general style issues.

REFERENCES: References to previously published work should be followed by the relevant author's name and date in parentheses. All cited references are to be listed alphabetical at the end of the manuscript with senior author's last name first, followed by date of publication, title, publisher, volume, and page numbers. Geological Society of America format should be used (see http://www.geosociety.org/gsa/gsa/pubs/Ref-Guide-Examples). Please do not abbreviate periodical titles. Web references are acceptable when deemed appropriate. The references should follow the style of: Author (or publisher), year, Webpage title: Publisher (if a specific author is available), full URL (e.g., http://www.usgs. gov/citguide.html), and the date the website was accessed in brackets. If there are specific authors given, use their name and list the responsible organization as publisher. Citations within the text should read: (Author, Year).

SUBMISSION: Manuscripts are to be submitted via the PeerTrack submission system at https://www.editorialmanager.com/jcks. Additional instructions are provided at that address. You will be prompted to establish a login and password, after which you will enter information about your manuscript and upload your manuscript, tables, and figure files. Manuscript files can be uploaded as DOC, WPD, RTF, TXT, or LaTeX. Note: LaTeX files should not use any unusual style files; a LaTeX template and BiBTeX file may be obtained from the Editor-in-Chief. Table files can be uploaded as DOC, WPD, RTF, TXT, XLS, or LaTeX files and figure files can be uploaded as TIFF, AI, EPS, or CDR files. The including of supplementary materials should be minimized. Supplemental data or other materials (e.g. video clips) may be placed on the Journal's website at the discretion of the Editor-in-Chief. The data used within a paper must be made available upon request during the review process.

FIGURES: Figures and lettering must be neat and legible. A list of figures and their captions should be provided at the end of the text or as a separate document and not within the figure. Figures should be numbered in sequence and referred to in the text by inserting (Fig. x). Most figures will be reduced; hence, the lettering should be large. Photographs must be sharp and high contrast. Figures must have a minimum resolution of 300 dpi for acceptance. Please minimize the use of JPEG images.

TABLES: See https://caves.org/wp-content/uploads/2022/01/JCKS_Tables.pdf. for table layout guidelines.

MEASUREMENTS: All measurements will be in the International System of Units (SI or metric) except when quoting historical references. Other units will be allowed where necessary if placed in parentheses following the SI units.

DISCUSSIONS: Critical discussions of papers previously published in the Journal are welcome. Authors will be given an opportunity to reply. Discussions and replies must be limited to a maximum of 1000 words and discussions will be subject to review before publication. Discussions must be within 12 months after the original article appears.

COPYRIGHT AND AUTHOR'S RESPONSIBILITIES: The submitted work should represent original work of the author(s) that has not been previously published. It is the author's responsibility to clear any copyright or acknowledgement matters concerning text, tables, or figures used from others. Authors should address sensitive or legal issues such as landowner and land manager concerns or policies, verify that the work was conducted using necessary permissions and permits, and minimize the disclosure of sensitive features and cave locations.

PROCESS: Submitted manuscripts are assigned to the appropriate Associate Editor and sent out to at least two experts in the field for review. Reviewed manuscripts are then returned to the author for consideration of the referees' remarks and revision, where appropriate. Revised manuscripts are returned to the Associate Editor who then recommends acceptance or rejection. The Editor-in-Chief makes final decisions regarding publication. Upon acceptance, the senior author will be sent one set of PDF proofs for review prior to publication.

Journal of Cave and Karst Studies

Volume 88 Number 1-2 June 2026

CONTENTS